Nucl. Fusion **47** (2007) S337–S384 doi:10.1088/0029-5515/47/6/S07

Chapter 7: Diagnostics

A.J.H. Donné[1,a], A.E. Costley[2], R. Barnsley[2], H. Bindslev[3], R. Boivin[4] G. Conway[5], R. Fisher[4], R. Giannella[6], H. Hartfuss[7], M.G. von Hellermann[1], E. Hodgson[8], L.C. Ingesson[1,9], K. Itami[10], D. Johnson[11], Y. Kawano[10], T. Kondoh[10], A. Krasilnikov[12], Y. Kusama[10], A. Litnovsky[13], P. Lotte[14], P. Nielsen[15], T. Nishitani[10], F. Orsitto[16], B.J. Peterson[17], G. Razdobarin[18], J. Sanchez[8], M. Sasao[19], T. Sugie[10], G. Vayakis[2], V. Voitsenya[20], K. Vukolov[21], C. Walker[2], K. Young[11] and the ITPA Topical Group on Diagnostics

[1] FOM-Institute for Plasma Physics Rijnhuizen, Association EURATOM-FOM, Partner in the Trilateral Euregio Cluster, PO Box 1207, 3430 BE Nieuwegein, The Netherlands
[2] ITER Cadarache JWS, Cadarache Centre, 13108 St Paul-Les-Durance, France
[3] EURATOM-Risø National Laboratory, 4000 Roskilde, Denmark
[4] General Atomics, San Diego, USA
[5] Max-Planck-Institute for Plasma Physics, Boltmannstrasse 2, D-85748 Garching, Germany
[6] European Commission, Directorate-General for Research, Rue Montoyer 75, B-1050 Bruxelles, Belgium
[7] Max-Planck-Institute for Plasma Physics, Wendelsteinstrasse, 17491 Greifswald, Germany
[8] Laboratorio Nacional de Fusión, EURATOM-CIEMAT, 28040 Madrid, Spain
[9] EFDA CSU Garching, Boltzmannstrasse 2, D-85748 Garching, Germany
[10] Japan Atomic Energy Agency, Naka, Ibaraki-ken, 311-0193, Japan
[11] Princeton Plasma Physics Laboratory, Princeton, NJ 08543, USA
[12] SRC RF TRINITI, Troitsk, Russian Federation
[13] Institut für Plasmaphysik, Forschungszentrum Jülich GmbH, Association EURATOM-FZJ, Partner in the Trilateral Euregio Cluster, D-52425 Jülich, Germany
[14] Association Euratom-CEA, DSM/DRFC, CEN Cadarache, 13108 St Paul-Les-Durance, France
[15] Consorzio RFX, Associazione EURATOM-ENEA sulla Fusione, Padova, Italy
[16] ENEA, Via Enrico Fermi 45, 00044 Frascati, Italy
[17] National Institute for Fusion Science (NIFS), 322-6 Oroshi, Toki, Gifu 509-5292, Japan
[18] Ioffe Physico-Technical Institute, 26 Polytekhnicheskaya St., St Petersburg, Russia
[19] Department of Quantum Science and Energy Engineering, Tohoku University, Sendai 980-8579, Japan
[20] Institute of Plasma Physics of NSC Kharkov Institute of Physics and Technology, 61108 Kharkov, Ukraine
[21] Nuclear Fusion Institute, RRC, 'Kurchatov Institute', 123182 Moscow, Russian Federation

E-mail: donne@rijnh.nl.

Received 25 February 2006, accepted for publication 5 February 2007
Published 1 June 2007
Online at stacks.iop.org/NF/47/S337

Abstract

In order to support the operation of ITER and the planned experimental programme an extensive set of plasma and first wall measurements will be required. The number and type of required measurements will be similar to those made on the present-day large tokamaks while the specification of the measurements—time and spatial resolutions, etc—will in some cases be more stringent. Many of the measurements will be used in the real time control of the plasma driving a requirement for very high reliability in the systems (diagnostics) that provide the measurements.

The implementation of diagnostic systems on ITER is a substantial challenge. Because of the harsh environment (high levels of neutron and gamma fluxes, neutron heating, particle bombardment) diagnostic system selection and design has to cope with a range of phenomena not previously encountered in diagnostic design. Extensive design and R&D is needed to prepare the systems. In some cases the environmental difficulties are so severe that new diagnostic techniques are required.

[a] Author to whom any correspondence should be addressed.

The starting point in the development of diagnostics for ITER is to define the measurement requirements and develop their justification. It is necessary to include all the plasma parameters needed to support the basic and advanced operation (including active control) of the device, machine protection and also those needed to support the physics programme. Once the requirements are defined, the appropriate (combination of) diagnostic techniques can be selected and their implementation onto the tokamak can be developed. The selected list of diagnostics is an important guideline for identifying dedicated research and development needs in the area of ITER diagnostics.

This paper gives a comprehensive overview of recent progress in the field of ITER diagnostics with emphasis on the implementation issues. After a discussion of the measurement requirements for plasma parameters in ITER and their justifications, recent progress in the field of diagnostics to measure a selected set of plasma parameters is presented. The integration of the various diagnostic systems onto the ITER tokamak is described. Generic research and development in the field of irradiation effects on materials and environmental effects on first mirrors are briefly presented. The paper ends with an assessment of the measurement capability for ITER and a forward of what will be gained from operation of the various diagnostic systems on ITER in preparation for the machines that will follow ITER.

PACS numbers: 52.70.−m, 28.52.−s

(Some figures in this article are in colour only in the electronic version)

Contents

1. Introduction
2. Requirements for plasma measurements
   2.1. Role of plasma measurements
   2.2. Detailed measurement requirements
3. Basis for plasma measurements
   3.1. Magnetic measurements
   3.2. Fusion product measurements
   3.3. Measurements of T_e and n_e
   3.4. Measurement of ion temperatures
   3.5. Measurements of impurities
   3.6. Measurements of radiated power
   3.7. Measurements of the q-profile
   3.8. Operational parameters
4. R&D needed for diagnostics
   4.1. Development of diagnostic components and new concept diagnostic techniques
   4.2. R&D programme on radiation effects on materials
   4.3. R&D programme on mirrors
5. Integration in the tokamak
6. Summary of progress in key issues identified in the ITER Physics Basis
7. Assessment of measurement capability for ITER
8. What can be learnt from operation on ITER
9. Summary

1. Introduction

It is an established fact that the knowledge gained with and the performance of present fusion machines is directly linked to its diagnostic capability. This will also be the case for ITER. For this reason and because the application of diagnostics to ITER is by far not as straightforward as that on present devices, it is a necessity to include the diagnostics in all steps of the design of the machine.

The difficulties of implementing diagnostics on ITER arise mainly from the environmental aspects and especially the relatively high levels of neutron flux and fluence that will be experienced by some diagnostic components [1–3]. In consequence, many phenomena new to diagnostic design can occur and have to be taken into account in diagnostic system design; for example, phenomena such as radiation induced conductivity (RIC) and radiation induced EMF (RIEMF) in cables, and radiation induced absorption and luminescence in optical materials. At least ten different environmentally induced phenomena that can potentially play a role have been identified. The phenomena can have several deleterious effects: for example, they can change the physical properties

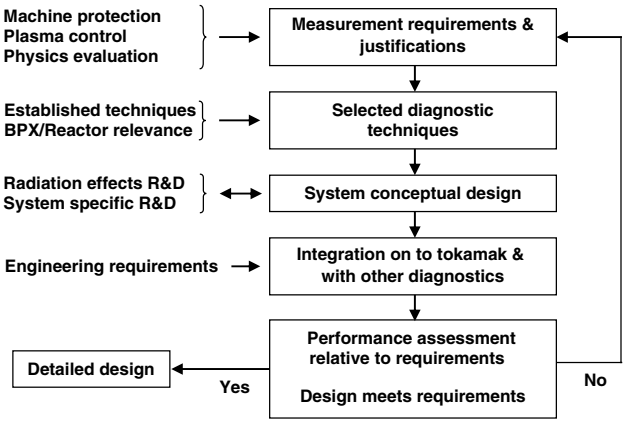

Figure 1. Schematic flow diagram of the design approach for diagnostics developed for ITER.

of the material of the component/sensor and thereby change its performance; they can generate spurious signals and they can cause damage that limits the lifetime. In some cases, the material itself can be changed permanently through transmutation. The effects may only exist during the plasma pulse (prompt), or they can be accumulative.

In addition, the nuclear environment sets stringent demands on the engineering of the diagnostic systems: for example, the diagnostic systems must meet the strict ITER requirements for containment of Tritium and vacuum integrity; they must be able to withstand high pressures that can potentially occur under accident scenarios; activation must be minimized and it must be possible to maintain and replace those components that are activated with the ITER remote handling equipment.

A systematic approach to diagnostic design is required which incorporates many elements that are new with respect to the design of diagnostic systems for present-day machines. The design approach developed for ITER is shown schematically in figure 1. The starting point is to identify and develop the requirements and the justification for the measurements for the large range of parameters that have to be measured [4–6]. The measurement requirements are in general the same or more stringent than on present-day devices. Moreover, in view of the key role many of the measurements will play in real-time control of the plasma (e.g. in the stabilization of neoclassical tearing and resistive wall modes, and active control of the presence and properties of internal transport barriers), a high level of reliability and robustness is required. The precise measurement requirements are determined by the needs for machine protection, plasma control and evaluating and understanding the performance of the plasma (physics evaluation). Diagnostic systems require space on the machine, and cost and complexity and so the requirements for measurement must be individually justified. This also makes clear what would be lost if certain parameters cannot be measured to the specified level and this helps in setting priorities for space and resource allocation. The measurement requirements and their justification will be described in detail in section 2.

After the measurement requirements and justifications have been defined one can select the diagnostic techniques. Implementation of existing diagnostic techniques on ITER implies substantial design and in many cases dedicated R&D. Some plasma parameters cannot be measured by existing techniques under ITER conditions and therefore new techniques are needed. In section 3 the present status of diagnostics for measuring a number of key parameters in ITER are briefly presented along with some results of diagnostic specific R&D that is related to the conceptual design of these systems. The more generic R&D on radiation effects and on first mirrors is discussed in section 4.

Following the selection of appropriate diagnostic techniques, their design and implementation on ITER can be developed, including integration with other machine and/or diagnostic components. The diagnostic integration aspects for ITER are described in section 5. The progress in the field since the publication of the ITER Physics Basis [7] is discussed in section 6.

The last step in the iteration process is to assess whether the selected diagnostics are suitable to measure all plasma and machine parameters to the specified requirements. If this is the case, then one can start the detailed engineering design of the (combination of) diagnostics. However, if the requirements are not met it is necessary to go back to the beginning of the loop to judge whether the requirements are too stringent and can be relaxed or, if this is not possible, whether alternative or improved diagnostics (e.g. new techniques, more sightlines, higher accuracy) should be implemented. The assessment of the current measurement capability for ITER is presented in section 7.

In section 8 a first survey is made of measurements that are—at the present level of understanding—likely to be needed for a DEMO reactor. A summary is given of what information will be gained from the operation of the various diagnostic systems on ITER in preparation for the machines that will follow ITER. The paper concludes with a brief summary.

2. Requirements for plasma measurements

2.1. Role of plasma measurements

As on existing machines, first wall and plasma measurements will be required on ITER for machine protection, plasma control and physics evaluation. The measurements of some parameters may contribute to all the three roles although the requirements on the measurements (accuracies, resolutions, etc) may be different. In order to meet the needs for these three roles it is expected that about 45 different parameters will have to be measured [8, 9].

2.1.1. Measurements required for machine protection. Key parameters which must be measured at a very high level of reliability for machine protection are the gap between the plasma edge and the first wall, first wall temperature, line-average density and disruption precursors (particularly the detection of locked modes). Furthermore, it is also necessary to measure the divertor plate surface temperature, fusion power, halo currents, and edge localized mode (ELM) type. The motivation for these measurements was presented in the ITER

Physics Basis [7] and remains essentially the same. However, for ITER, the specific limits have changed.

2.1.2. Measurements needed for plasma control and evaluation. The measurements needed for plasma control and evaluation are naturally directly linked to the experimental programme, and particularly to the operating phase (i.e. H, D or D/T) and the operating scenario (H-mode, hybrid, etc). Since there is expected to be a phased introduction of powerful operation and advanced scenarios, the demands on the measurements will rise during the experimental programme [10]. The plans for the ITER programme have been developed [10] as well as the corresponding needs for plasma measurements [11].

The first phase of operation will be a hydrogen, non-nuclear phase, mainly intended for full commissioning of the tokamak systems in a non-nuclear environment. The main elements of the full DT phase reference operation, such as plasma current initiation, current ramp-up, formation of a divertor configuration and current ramp-down will be developed in this phase. Plasma operation will be inductive, mainly L-mode with some limited operation in H-mode, probably at reduced toroidal magnetic field, $B_{\rm tor}$. Plasma measurements will be required to support the control and operation of the plasma and to evaluate the performance achieved. The principal measurements required for control are the plasma shape and position, plasma current, $I_{\rm p}$, loop voltage, $V_{\rm loop}$, vertical speed and line-averaged density. Identification of magnetohydrodynamic (MHD) modes, particularly modes that may lock, will be necessary to minimize the number of disruptions. Measurement of the surface temperature of the divertor plates and first wall will be required and used in the protection of these components. Key measurements for performance evaluation will include the core electron density and temperature profiles, $n_{\rm e}(r)$ and $T_{\rm e}(r)$, the core ion temperature, $T_{\rm i}$, and the radiated power from the core, $P_{\rm rad}$. A full list of the required measurements is shown in table 1.

The next operational phase will be a deuterium phase in which fusion reactions will occur for the first time. The operating mode will be the baseline, inductive, ELMy H-mode. The additional control measurements will be the ELM type and occurrence, and indicators of divertor detachment. The fusion power, $P_{\rm fus}$, will be low but measurements of it will be required for evaluation purposes. Additional evaluation measurements include $n_{\rm e}(r)$ and $T_{\rm e}(r)$ at the edge, and $P_{\rm rad}(r)$ (table 1).

The high power D/T phase will follow the deuterium phase. The primary operating mode will be the baseline inductive ELMy H-mode. Fusion burn times of $\geqslant 300$ s, $\beta_{\rm N}$ values of 1.5–2 and fusion powers of 400 MW are expected. Some of the measurements required in the H and D phases for evaluation will be brought into the control loops, for example measurements of $P_{\rm rad}$ and $P_{\rm fus}$. Some additional measurements will be required for control, in particular measurements of the core $T_{\rm e}$ and $T_{\rm i}$, the helium density profile, $n_{\rm He}(r)$, the tritium/deuterium density ratio, $n_{\rm T}/n_{\rm D}$, the rotation velocities in toroidal and poloidal direction, $v_{\rm tor}$ and $v_{\rm pol}$ and the position of the divertor ionization front.

At high values of normalized beta, $\beta_{\rm N}$ ($\geqslant$ 2) active stabilization of neoclassical tearing modes (NTMs) may be necessary to avoid deterioration of the plasma confinement or the occurrence of disruptions. NTMs occur around the rational q-surfaces $q = 1.5$ and $q = 2$ and they are usually observed as periodic perturbations on $T_{\rm e}$ and $n_{\rm e}$ (and also on the related soft x-ray emission) measured around these positions. They can also be clearly observed with magnetic pick-up coils. Experiments have shown that they can be stabilized by current drive at rational q surfaces, but to have ample time to stabilize the modes it is necessary to detect them when they are still at low amplitude. Measurements of the perturbations are required along with the location of the rational q surfaces.

By driving a substantial fraction of the plasma current by non-inductive current drive at reduced current the pulse duration can be significantly extended. This 'hybrid operation' offers a promising route towards true steady-state operation. In this case, measurements of the q-profile are required as well as measurements for relatively long times ($\sim$1500 s).

A complete scenario for steady-state operation at high values of Q (the ratio of fusion power from plasma to auxiliary heating power to plasma) has not yet been developed but there are a variety of candidate scenarios. Two possibilities are weak central magnetic shear and strong reversed shear operation. Both would employ reduced minor radius, reduced current (10 MA), increased elongation ($\kappa_x = 2$) and both need improved confinement ($H_{\rm H} \geqslant 1.5$) and high $\beta_{\rm N}(\geqslant 3)$. Since this is still a rapidly developing area it is not possible to be definitive about the requirements for measurements in these cases. However, it will be necessary for both to have accurate measurements of the profiles of current density and pressure. In particular, for strong reversed shear it will be important to know the location and the value of $q_{\rm min}$.

Recent experiments have shown that internal transport barriers (ITBs) can be stimulated by active profile control and can lead to enhanced performance, albeit so far only for relatively short duration. One method of stimulating an ITB is to create a region of low (or reversed) magnetic shear in the vicinity of a rational q surface by local current drive. ITBs can usually be observed as strong gradients in the electron and ion temperature profiles as well as strong shear in the poloidal and toroidal rotation profiles. Active control of ITBs is, however, not straightforward since very minute changes in the value of q (smaller than the typical measurement accuracy of present diagnostics) may lead to the creation or destruction of ITBs. More pronounced and rapid changes are observed on the electron and ion temperature profiles and on the rotation profile and so control on the gradient of these parameters may be more successful.

Resistive wall modes (RWMs) can also occur under high β conditions and are observed as low frequency, low m- and n-number modes on magnetic signals as well as periodic perturbations in $T_{\rm e}$ and $n_{\rm e}$. They can be stabilized by inducing plasma rotation. For indefinite stabilization it will be necessary to drive appropriate fields using an external coil set.

2.2. Detailed measurement requirements

The implementation of diagnostics on ITER must be carefully optimized. The available space for diagnostics will be limited and unavoidably diagnostic systems add cost and complexity. Priorities must be established with the obvious logic where those systems that provide measurements for

Table 1. Required plasma measurements for different operating scenarios.

Operating scenario	Required Measurements[a]	
	Control	Evaluation
H phase. Inductive. Ohmic L-mode. Limited H-mode	Plasma shape and position, vertical speed, B_{tor}, I_p, V_{loop}, $q(a)$, $q(95\%)$, locked modes, $m = 2$ modes, low m/n MHD modes, line-averaged density, runaway electrons, surface temperature of divertor plates and first wall.	Halo current, impurity identification and influx, $n_e(r)$ and $T_e(r)$ in core, T_i in core, P_{rad} from core, line-averaged Z_{eff}, H/L mode indicator, gas pressure and composition (divertor and duct), ELM occurrence and type.
D phase. Inductive. ELMy H-mode	Plasma shape and position, vertical speed, B_{tor}, I_p, V_{loop}, $q(a)$, $q(95\%)$, locked modes, $m = 2$ modes, low m/n MHD modes, line-averaged density, runaway electrons, surface temperature of divertor plates and first wall, **H/L mode indicator, ELM occurrence and type, divertor detachment.**	Halo current impurity identification and influx, $n_e(r)$ and $T_e(r)$ in core, T_i in core, P_{rad} from core, line-averaged Z_{eff}, gas pressure and composition (divertor and duct), **shape and position (1000 s), β, $n_e(r)$ and $T_e(r)$ at edge, P_{fus}, $P_{rad}(r)$, heat deposition profile in divertor.**
D/T phase. Inductive. ELMY H-mode	Plasma shape and position (**1000 s**), vertical speed, B_{tor}, I_p, V_{loop}, $q(a)$, $q(95\%)$, locked modes, $m = 2$ modes, low m/n MHD modes, line-averaged density, runaway electrons, surface temperature of divertor plates and first wall, H/L mode indicator, ELM occurrence and type, divertor detachment, **$T_e(r)$ in core, T_i in core, P_{rad} from core, P_{fus}, $n_{He}(r)$, n_{He} in divertor, n_T/n_D in core, divertor ionisation front position, $v_{tor}(r)$ and $v_{pol}(r)$.**	Halo current impurity identification and influx, $n_e(r)$ in core, line-averaged Z_{eff}, gas pressure and composition (divertor and duct), β, $n_e(r)$ and $T_e(r)$ at edge, $P_{rad}(r)$, heat deposition profile in divertor, **neutron and alpha source profiles, impurity profile, position of q = 1.5 and q = 2 surfaces, $T_i(r)$ in core, $Z_{eff}(r)$, D and T influx, neutral density (near wall), n_e and T_e in divertor, impurity and DT influxes in divertor with spatial resolution, alpha loss, neutron fluence, erosion of divertor tiles.**
High power D/T Phase. Inductive ELMY H mode. High β	Plasma shape and position (1000 s), vertical speed, B_{tor}, I_p, V_{loop}, $q(a)$, $q(95\%)$, locked modes, $m = 2$ modes, low m/n MHD modes, line-averaged density, runaway electrons, surface temperature of divertor plates and first wall, H/L mode indicator, ELM occurrence and type, divertor detachment, $T_e(r)$ in core, T_i in core, P_{rad} from core, P_{fus}, $n_{He}(r)$, n_{He} in divertor, n_T/n_D in core, divertor ionisation front position, $v_{tor}(r)$ and $v_{pol}(r)$, **β, position of q = 1.5 and q = 2 surfaces, high sensitivity measurements of n_e and T_e, detection and measurement of NTMs.**	Halo current impurity identification and influx, $n_e(r)$ in core, line-averaged Z_{eff}, gas pressure and composition (divertor and duct), $n_e(r)$ and $T_e(r)$ at edge, $P_{rad}(r)$, heat deposition profile in divertor, neutron and alpha source profiles, impurity profile, $T_i(r)$ in core, $Z_{eff}(r)$, D and T influx, neutral density (near wall), n_e and T_e in divertor, impurity and DT influxes in divertor with spatial resolution, alpha loss, neutron fluence, erosion of divertor tiles.
Hybrid operation	Plasma shape and position **(1500 s)**, vertical speed, B_{tor}, I_p, V_{loop}, $q(a)$, $q(95\%)$, locked modes, $m = 2$ modes, low m/n MHD modes, line-averaged density, runaway electrons, surface temperature of divertor plates and first wall, H/L mode indicator, ELM occurrence and type, divertor detachment, $T_e(r)$ in core, T_i in core, P_{rad} from core, P_{fus} $n_{He}(r)$, n_{He} in divertor, n_T/n_D in core, divertor ionisation front position, $v_{tor}(r)$ and $v_{pol}(r)$, β, position of $q = 1.5$ and $q = 2$ surfaces, high sensitivity measurements of n_e and T_e, detection and measurement of NTMs.	$q(r)$, halo current impurity identification and influx, $n_e(r)$ in core, line-averaged Z_{eff}, gas pressure and composition (divertor and duct), $n_e(r)$ and $T_e(r)$ at edge, $P_{rad}(r)$, heat deposition profile in divertor, neutron and alpha source profiles, impurity profile, $T_i(r)$ in core, $Z_{eff}(r)$, D and T influx, neutral density (near wall), n_e and T_e in divertor, impurity and DT influxes in divertor with spatial resolution, alpha loss, neutron fluence, erosion of divertor tiles.
Steady state operation	Plasma shape and position (**3600 s**), vertical speed, B_{tor}, I_p, V_{loop}, $q(a)$, $q(95\%)$, locked modes, $m = 2$ modes, low m/n MHD modes, line-averaged density, runaway electrons, surface temperature of divertor plates and first wall, H/L mode indicator, ELM occurrence and type, divertor detachment, $T_e(r)$ in core, T_i in core, P_{rad} from core, P_{fus}, $n_{He}(r)$, n_{He} in divertor, n_T/n_D in core, divertor ionization front position, $v_{tor}(r)$ and $v_{pol}(r)$, β, position of $q = 1.5$ and $q = 2$ surfaces, high sensitivity measurements of n_e and T_e, detection and measurement of NTMs shape and position (for 1000 s), **$T_i(r)$ in core, position of q_{min}, high resolution measurements of the gradient of T_e and T_i, measurement of RWMs.**	$q(r)$, halo current impurity identification and influx, $n_e(r)$ in core, line-averaged Z_{eff}, gas pressure and composition (divertor and duct), $q(95\%)$, $n_e(r)$ and $T_e(r)$ at edge, $P_{rad}(r)$, heat deposition profile in divertor, shape and position (500 s), neutron and alpha source profiles, impurity profile, $Z_{eff}(r)$, D and T influx, neutral density (near wall), n_e and T_e in divertor, impurity and DT influxes in divertor with spatial resolution, alpha loss, neutron fluence, erosion of divertor tiles.

[a] Parameters in bold font are new to the function (control or evaluation).

machine protection are given the highest priority followed by those needed for basic plasma control and then those needed for more advanced control. In many cases the measurements needed for performance evaluation and physics studies can be obtained from the same systems that are used for machine protection and plasma control, although it might be necessary to enhance the measurement specifications (resolutions, etc). In some cases dedicated measurements are needed specifically for key physics studies.

For ITER, the measurement requirements have been specified in detail on the basis of a careful consideration of the needs [7, 11]. The specifications required to meet all of the ITER operating modes are shown in table 2. In addition, for each parameter a justification has been prepared. This details why the measurement is needed and explains the specific requirements. An example is shown in table 3. Both the requirements and the justifications are constantly under review and development. The active involvement of researchers in other areas is sought in this process. The requirements and the justifications are frequently reviewed by the ITPA Topic Groups. The requirements and justifications are the main driver for diagnostic selection and design.

3. Basis for plasma measurements

3.1. Magnetic measurements

Magnetic measurements in ITER must observe a demanding specification because their performance affects margins and therefore operational flexibility near machine limits [12]. Recovering these margins by altering the machine design would imply significant costs. Furthermore, the design environment is challenging and the installation and operation conditions are harsh:

- By their nature, magnetic diagnostics interact strongly with key parts of the tokamak, such as the vacuum vessel and plasma facing components, which impose significant physical and electromagnetic constraints on the magnetic sensors.
- During *installation*, relatively fragile sensors and wiring may have to survive the assembly of multi-ton structural elements nearby.
- During *operation*, neutron and γ irradiation and plasma heat loads are significant; for a long-pulse, long-life and high fluence machine, thermal cycling and radiation damage are also important.
- Finally, maintenance of components inside the tokamak, where possible at all, is extremely difficult, time consuming and expensive.

Radiation in particular affects the sensor design in several ways: (I) In the selection of sensor parameters to avoid prompt effects on the signal due to radiation induced conductivity (RIC) and radiation induced electro-motive force (RIEMF) in the cables. (II) In the choice of materials to avoid fluence-dependent electrical and mechanical degradation, such as radiation induced thermo-electric sensitivity (RITES), radiation induced electrical degradation (RIED), swelling and cracking. (III) In the design of suitable cooling mechanisms to take away the generated heat, and so minimize temperature induced electro-motive force (TIEMF) caused by temperature gradients.

For RIC, the insulator materials and thickness have to be chosen so that the corresponding loading error is negligible. Due to space constraints, coils are affected more than loops.

An RIEMF *potential difference* between the coil winding and ground is produced due to a charge-induced voltage generation between the mineral insulated (MI) cable central conductor (core) and the outer sheath when subjected to neutron and gamma radiation. The net voltage or current measured depends on the cable and surrounding materials, the RIC in the cable insulation, and external loads. It is already well documented and can be modelled (see section 4.2). There are indications that some fraction of the RIEMF current can generate a differential voltage (that is *along* the wire) through asymmetries in the radiation field and loading. RIEMF voltage can also influence the signal through poor common mode rejection ratio of the integrator.

RITES has recently been invoked to explain the appearance of larger than expected fluence-dependent signals across the terminals of ITER-like test coils exposed to ITER-like radiation levels in fission reactors (see section 4.2). It appears to dominate over any possible RIEMF induced differential voltage for the case of coils.

Recent experiments have demonstrated that a significant differential voltage can be generated along the MI cable central conductor due to temperature differences alone along the cable (see section 4.2). This thermally induced electro-motive force (TIEMF) can produce differential voltages in the microvolt range for temperature differences in the range 10–100 °C, and is possibly the main cause of earlier unexplained in-reactor experimental results on coils.

RIED is the degradation of insulating properties in the presence of radiation. This occurs for significant electric field ($>200\,\mathrm{kV\,m^{-1}}$), at elevated temperature ($>200\,^{\circ}\mathrm{C}$), exposed to significant radiation level ($>100\,\mathrm{Gy\,s^{-1}}$) and kept in this condition for significant time ($>1000\,\mathrm{s}$). The insulator material, including impurity content, is important and even different samples of the same material can behave differently.

Of these effects, several (RIEMF, RITES, TIEMF but also thermo-magnetic effects within the sensors, connectors and wiring) can readily generate parasitic voltages in the 100 nV–10 μV range. ITER therefore will need some supplementary measurements of key equilibrium parameters that do not rely on passive inductive sensors alone.

The design of the ITER magnetic diagnostic has been evolving for some time. All the above issues affecting the ITER magnetic design and performance have had to be considered and, through ITER-specific R&D, some of the key issues have been identified for the first time. Throughout, the aim of the design activity has been to provide a design that meets a demanding specification and is qualified for the machine lifetime despite the identified constraints. Thus, as far as possible, the design

- uses proven materials and techniques for the components,
- provides generous engineering margins,
- minimizes maintenance features and relies on redundancy to improve reliability and
- is supported by relevant R&D in ITER-like environments.

Table 2. Specification for plasma measurements on ITER.

Measurement	Parameter	Condition	Range or Coverage	Resolution: Time or Freq.	Resolution: Spatial or Wave No.	Accuracy
1. Plasma current	I_p	Default	0–1 MA	1 ms	Integral	10 kA
			1–17.5 MA	1 ms	Integral	1%
		I_p Quench	20–0 MA	0.1 ms	Integral	30% + 10 kA
2. Plasma position and shape	Main plasma gaps, Δ_{sep}	$I_p > 2$ MA, full bore	—	10 ms	—	10 mm
		I_p Quench	—	10 ms	—	20 mm
	Divertor channel location (r dir.)*	Default	—	10 ms	—	10 mm
		I_p Quench	—	10 ms	—	20 mm
	dZ/dt of current centroid	Default	0–5 m s^{-1}	1 ms	—	0.05 m s^{-1} (noise) + TBD% (absolute)
3. Loop voltage	V_{loop}	Default	0–30 V	1 ms	4 locations	5 mV
		I_p Quench	0–500 V	1 ms	4 locations	10% + 5 mV
4. Plasma energy	β_p	Default	0.01–3	1 ms	Integral	5% at $\beta_p = 1$
		I_p Quench	0.01–3	1 ms	Integral	$\sim$ 30%
5. Radiated power	Main plasma P_{rad}	Default	TBD–0.3 GW	10 ms	Integral	10%
	X-point/MARFE region P_{rad}	Default	TBD–0.3 GW	10 ms	Integral	10%
	Divertor P_{rad}	Default	TBD–0.3 GW	10 ms	Integral	10%
	Total P_{rad}	Disruption	TBD–50 GW	3 ms	Integral	20%
6. Line-averaged electron density	$\int n_e dl/dl$	Default	10^{18}–4×10^{20} m^{-3}	1 ms	Integral	1%
		After killer pellet	8×10^{20}–2×10^{22} m^{-3}	1 ms	Integral	100%
7. Neutron flux and emissivity	Total neutron flux		10^{14}–5×10^{20} n s^{-1}	1 ms	Integral	10%
	Neutron/α source		10^{14}–4×10^{18} n m^{-3} s^{-1}	1 ms	$a/10$	10%
	Fusion power		TBD–1 GW	1 ms	Integral	10%
	Fusion power density		TBD–10 MW m^{-3}	1 ms	$a/10$	10%
8. Locked modes	B_r(mode)/B_p		10^{-4}–10^{-2}	1 ms	$(m, n) = (2, 1)$	30%
9. Low (m, n) MHD modes, sawteeth, disruption precursors	Mode complex amplitude at wall		TBD	DC–3 kHz	$(0, 0) < (m, n) < (10, 2)$	10%
	Mode–induced temperature fluctuation		TBD	DC–3 kHz	$(0, 0) < (m, n) < (10, 2)$ $\Delta r = a/30$	10%
	Other mode parameters TBD					
10. Plasma rotation	V_{tor}		1–200 km s^{-1}	10 ms	$a/30$	30%
	V_{pol}		1–50 km/s	10 ms	$a/30$	30%
11. Fuel ratio in plasma core	n_T/n_D	$r/a < 0.9$	0.1–10	100 ms	$a/10$	20%
12. Impurity species monitoring	Be, C rel. conc.		10^{-4}–5×10^{-2}	10 ms	Integral	10% (rel.)
	Be, C influx		4×10^{16}–2×10^{19} s^{-1}	10 ms	Integral	10% (rel.)
	Cu rel. conc.		10^{-5}–5×10^{-3}	10 ms	Integral	10% (rel.)
	Cu influx		4×10^{15}–2×10^{18} s^{-1}	10 ms	Integral	10% (rel.)
	W rel. conc.		10^{-6}–5×10^{-4}	10 ms	Integral	10% (rel.)
	W influx		4×10^{14}–2×10^{17} s^{-1}	10 ms	Integral	10% (rel.)
	Extrinsic (Ne,Ar, Kr) rel. Conc.		10^{-4}–2×10^{-2}	10 ms	Integral	10% (rel.)
	Extrinsic (Ne, Ar, Kr) influx		4×10^{16}–8×10^{18} s^{-1}	10 ms	Integral	10% (rel.)
13. Z_{eff} (line-averaged)	Z_{eff}		1–5	10 ms	Integral	20%
14. H-mode: ELMs and L–H transition indicator	ELM D_α bursts	Main plasma	—	0.1 ms	One site	—
	ELM density transient	$r/a > 0.9$	TBD	TBD	TBD	TBD
	ELM temperature transient	$r/a > 0.9$	TBD	TBD	TBD	TBD

Table 2. Continued.

Measurement	Parameter	Condition	Range or Coverage	Resolution: Time or Freq.	Resolution: Spatial or Wave No.	Accuracy
	L–H D_α step	Main plasma		0.1 ms	One site	—
	L–H pedestal formation (n_e, T_e)	$r/a > 0.9$	—	0.1 ms	—	TBD
15. Runaway electrons	E_{max}		1–100 MeV	10 ms	—	20%
	$I_{runaway}$	After thermal quench	(0.05–0.7) $\cdot I_p$	10 ms		30% rel
16. Divertor operational parameters	Max. surface temperature		200–2500 °C	2 ms	—	10%
	Erosion rate		$1–10 \times 10^{-6}$ m s^{-1}	2 s	10 mm	30%
	Net erosion		0–3 mm	Per pulse	10 mm	12×10^{-6} m
	Gas pressure		1×10^{-4}–20 Pa	50 ms	Several points	20% during pulse
	Gas composition	$A = 1–100$ $\Delta A = 0.5$	TBD	1 s	Several points	20% during pulse
	Position of the ionization front		0–TBD m	1 ms	100 mm	—
17. First wall (FW) visible image and wall temperature	FW image		TBD	100 ms	TBD	—
	FW surface temperature		200–1500 °C	10 ms	TBD	20 °C
18. Gas pressure and composition in main chamber	Gas pressure		10^{-4}–20 Pa	1 s	Several points	20% during pulse
	Gas composition	$A = 1–100$ $\Delta A = 0.5$	TBD	10 s	Several points	50% during pulse
19. Gas pressure and gas composition in ducts	Gas pressure		< 7 kPa	100 ms	Several points	20% during pulse
	Gas composition	$A = 1–100$ $\Delta A = 0.5$	TBD	1 s	Several points	20% during pulse
20. In-vessel inspection	Wall image		100% coverage of FW and divertor	—	1 mm	
21. Halo currents	Poloidal current	In disruption	0–0.2 I_p	1 ms	9 sectors	20%
22. Toroidal magnetic field	B_T		2–5.5 T	1 s	2 locations × 2 methods	0.1%
23. Electron temperature profile	Core T_e	$r/a < 0.9$	0.5–40 keV	10 ms	$a/30$	10%
	Edge T_e	$r/a > 0.9$	0.05–10 keV	10 ms	5 mm	10%
24. Electron density profile	Core n_e	$r/a < 0.9$	3×10^{19}–3×10^{20} m^{-3}	10 ms	$a/30$	5%
	Edge n_e	$r/a > 0.9$	5×10^{18}–3×10^{20} m^{-3}	10 ms	5 mm	5%
25. Current profile	$q^{(r)}$	Physics study	0.5–5	10 ms	$a/20$	10%
			5–TBD	10 ms	$a/20$	0.5
	$r(q = 1.5, 2)/a$	NTM feedback	0.3–0.9	10 ms	—	50 mm/a
	$r(q_{min})/a$	Reverse shear control	0.3–0.7	1 s	—	50 mm/a
26. Z_{eff} profile	Z_{eff}	Default	1–5	100 ms	$a/10$	10%
		Transients	1–5	10 ms	$a/10$	20%
27. High frequency macro instabilities (fishbones, TAEs)	Fishbone-induced perturbations in B, T, n		TBD	0.1–10 kHz	$(m, n) = (1, 1)$	—
	TAE mode-induced perturbations in B, T, n		TBD	30–300 kHz	$n = 10–50$	—
28. Ion temperature profile	Core T_i	$r/a < 0.9$	0.5–40 keV	100 ms	$a/10$	10%
	Edge T_i	$r/a > 0.9$	0.05–10 keV	100 ms	TBD	10%

Table 2. Continued.

Measurement	Parameter	Condition	Range or Coverage	Resolution: Time or Freq.	Resolution: Spatial or Wave No.	Accuracy
29. Core He density	n_{He}/n_e	$r/a < 0.9$	1–20%	100 ms	$a/10$	10%
30. Confined alphas	Energy spectrum	Energy resolution TBD	(0.1–3.5) MeV	100 ms	$a/10$	20%
	Density profile		(0.1–2) $\times 10^{18}$ m^{-3}	100 ms	$a/10$	20%
31. Escaping alphas	First wall flux	Default	TBD–2 MW m^{-3}	100 ms	$a/10$ (along poloidal direction)	10%
		Transients	TBD–20 MW m^{-3}	10 ms	TBD	30%
32. Impurity density profile	Fractional content, $Z \leqslant 10$	$r/a < 0.9$	0.5–20%	100 ms	$a/10$	20%
		$r/a > 0.9$	0.5–20%	100 ms	50 mm	20%
	Fractional content, $Z > 10$	$r/a < 0.9$	0.01–0.3%	100 ms	$a/10$	20%
		$r/a > 0.9$	0.01–0.3%	100 ms	50 mm	20%
33. Fuel ratio in the edge	n_T/n_D	$r/a > 0.9$	0.1–10	100 ms	Radial integral	20%
	n_H/n_D	$r/a > 0.9$	0.01–0.1	100 ms	Radial integral	20%
34. Neutron fluence	First wall fluence		0.1–1 MWy m^{-2}	10 s	TBD	10%
35. Impurity and D,T influx in the divertor	Γ_{Be}, Γ_C, Γ_W		10^{17}–10^{22} at s^{-1}	1 ms	50 mm	30%
	Γ_D, Γ_T		10^{19}–10^{25} at s^{-1}	1 ms	50 mm	30%
36. Plasma parameters at the divertor targets	Ion flux		10^{19}–10^{25} ions s^{-1}	1 ms	3 mm	30%
	n_e		10^{18}–10^{22} m^{-3}	1 ms	3 mm	30%
	T_e		1 eV–1 keV	1 ms	3 mm	30%
37. Radiation profile	Main plasma P_{rad}		0.01–1 MW m^{-3}	10 ms	$a/15$	20%
	X-point/MARFE region P_{rad}		TBD–300 MW/m^3	10 ms	$a/15$	20%
	Divertor P_{rad}		TBD–100 MW/m^3	10 ms	50 mm	30%
38. Heat loading profile in the divertor	Surface temperature		200–1000 °C	2 ms	3 mm	10%
			1000–2500,°C	20×10^{-6} s	3 mm	10%
	Power load	Default	TBD–25 MW m^{-2}	2 ms	3 mm	10%
		Disruption	TBD–5 GW m^{-2}	0.1 ms	TBD	20%
39. Divertor helium density	n_{He}		10^{17}–10^{21} m^{-3}	1 ms	—	20%
40. Fuel ratio in the divertor	n_T/n_D		0.1–10	100 ms	integral	20%
	n_H/n_D		0.01–0.1	100 ms	integral	20%
41. Divertor electron parameters	n_e		10^{19}–10^{22} m^{-3}	1 ms	50 mm along leg, 3 mm across leg	20%
	T_e		0.3–200 eV	1 ms	50 mm along leg, 3 mm across leg	20%
42. Ion temperature in the divertor	T_i		0.3–200 eV	1 ms	50 mm along leg, 3 mm across leg	20%
43. Divertor plasma flow	V_p		TBD–10^5 m s^{-1}	1 ms	100 mm along leg, 3 mm across leg	20%
44. n_H/n_D ratio in the plasma core	n_H/n_D		0.01–0.1	100 ms	$a/10$	20%
45. Neutral density between plasma and first wall	D/T influx in main chamber		10^{18}–10^{20} at m^{-2} s^{-1}	100 ms	Several poloidal and toroidal locations	30%

* Strike point location perpendicular to the separatrix.

Table 3. Example of justification: T_e measurements.

The electron temperature profile is a major indicator of plasma performance and a key component of transport analyses. The profile is key information in instability analyses. Steep transport barriers are observed inside the plasma core and electron temperature pedestals at the edge play a role in analysis of the transport. A time resolution of 10 ms is short compared with times of interest and allows for the study of MHD. For kinetic control of the stored energy or ITB gradient, 10 ms time resolution is expected to be sufficient since this is much faster than the typical core confinement times and of the same order as the actuator (heating) response time. The core temperature should be measured with 10% accuracy or better to enable a useful determination of the stored energy and to support useful analysis of plasma performance with transport codes. To resolve fine structure on the profile such as internal transport barriers it should be measured at 30 locations across the profile. The edge, with much steeper gradients should be measured with only 0.5 cm between measurements at about 20 locations.

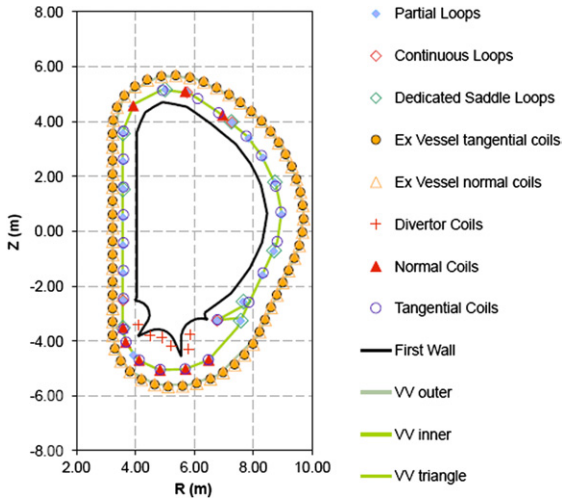

Figure 2. Poloidal distribution of the magnetic sensors (the diamagnetic loops and external Rogowski coils are not shown).

In order to meet the measurement requirements (specifically those for measurements 1–4, 8–9, 21–22 and 27 listed in table 2), magnetic diagnostics for ITER comprise several subsystems. The distribution of some of these systems poloidally and toroidally is indicated in figure 2 and figure 3, respectively. Figure 4 gives a three-dimensional view of the coil distribution around the vessel.

The *inner vessel sensors* are distributed behind the blanket modules and the divertor coils are mounted on instrumented divertor cassettes. Apart from the specialized high frequency coils, they are conventional designs based on MI cable. The coils are the most critical design element, because their effective area is constrained to be rather small (0.3 m^2) so they cannot tolerate parasitic voltages $>$ 500 nV for long-pulse operation. At the same time their extended size means they are more difficult to cool.

A removable divertor is featured in ITER, as is the need for good control of the X-point, which in turn requires sensors placed near it. In ITER these *divertor coils* have the highest exposure to radiation and additionally have to use an automatic connector to the outside so are the most likely to experience problems, although they are the easiest to maintain.

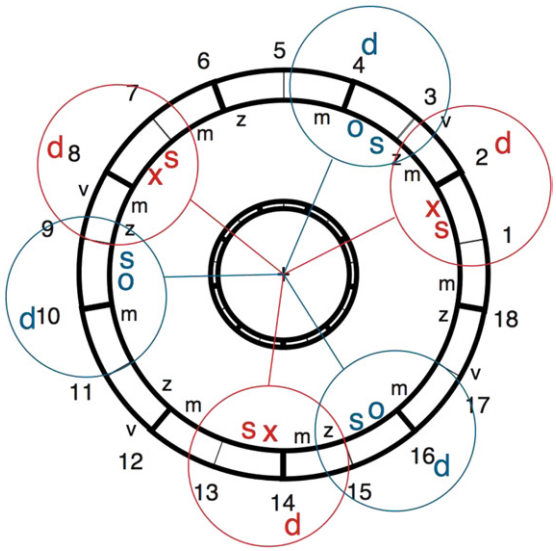

Figure 3. Schematic toroidal layout of key equilibrium inner vessel and outer vessel systems. The nine assembly sectors and two vacuum vessel skins are marked in bold lines. Key: (x) hardwired coil set, (o) replaceable coil set, (s) saddle set, (z) HF coil set, (m) MHD saddles, (v) outer vessel set, (d) divertor set. Three groups of sensors (separated toroidally by 120°) are summed for each equilibrium input set. Figure taken from [12].

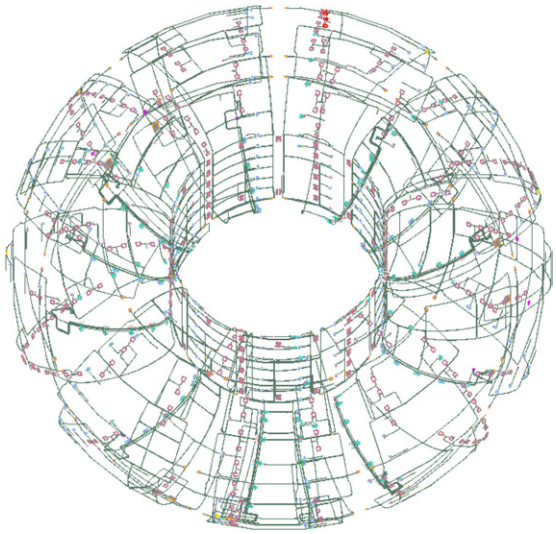

Figure 4. Top view of the complete in-vessel magnetics set on ITER.

The *outer vessel sensors* are mounted on the outside surface of the vacuum vessel. The environment there is much more benign (radiation levels, temperature range, peak field change rate) so there is more design freedom for the sensors. A number (over 60) of tangential and radial coils of 2 m^2 effective area are planned. It appears that suitable Hall effect sensors can also be installed if R&D to extend their temperature to ~140°C is successful [13, 14]. These sensors will provide supplementary information to guard against drift for long pulses.

An extensive array of *halo current sensors* is planned to cover a significant fraction of the first wall blanket modules

and divertor cassettes. Features in the halo current toroidal distribution with widths down to 40° can be observed through four 18-fold Rogowski toroidal arrays and there are six fully instrumented (all blanket and all divertor cassette elements) poloidal sectors.

A set of *diamagnetic loops* with in- and ex-vessel compensation coils and some dedicated saddle loops for local vertical field measurement is also included. The extensive set of in-vessel blanket cooling and support structures means that the diamagnetic loops have to be manufactured as matched mirror image pairs (around obstacles). The long-vessel timescale (0.3 s) means that in-vessel compensation for the loop is essential to meet the measurement requirements, and is provided by special coils of high ($\sim$30 m^2) effective area.

Ex-vessel *continuous Rogowski coils* are also included. The large size of the machine and big changes in machine component temperature for different phases of operation mean that, if the Rogowski coils are not to increase their radial build, they have to be at least in part embedded in a machine component (in this case the toroidal field coil casing).

Using all these systems, it is expected that the measurement specifications for parameters 1–4, 8–9, 21–22 and 27 in table 2 will be met for standard-length ITER pulses [15], provided that the sensors are constructed to withstand the environmental constraints. By far the most serious challenge has been to adapt the design to the irradiation environment by a careful choice of materials, construction and sensor location.

For RIC and RIED the choice of insulator type and thickness can ensure that they do not affect the reliability of the measurement. The effects depend on the ambient temperature, hence, temperature control is also important. In ITER, the coils are most sensitive to RIC. By using suitable thickness of Al_2O_3 insulation <0.2% error is expected from this source. ITER magnetics has been designed to be below threshold for RIED by placing the coils in a shielded area (<100 Gy s^{-1}) and sizing the insulation for low electric fields <150 kV m^{-1}. In addition, the expected duration of high voltages on the sensors is rather low, < 200 s, occurring in short events, such as disruptions of all kinds and edge localised modes (ELMs). The highest temperature of the inner vessel tangential coils (240 °C) could be an issue so an improvement in the coil cooling may be required.

For RIEMF, conductor and sheath materials, radiation field uniformity and integrator specification are the important parameters. From the currents observed in ITER-like coils in fission reactors [16], the maximum RIEMF current is about 1 μA and this, into a load resistance of 1 kΩ, would generate a common mode voltage of 1 mV and require a common mode rejection ratio of 2000 or better for the integrator. Integrators presently available that can meet the ITER pulse length requirements [15] need further work to achieve this. The resulting RIEMF voltage would be about 100 nV for the expected asymmetry of order 10%. This is tolerable, so it appears that an acceptable specification can be found for the ITER coils for long-pulse applications remaining compatible with fast equilibrium reconstruction.

For RITES, conductor material, radiation field uniformity and temperature control all play a role. For the equilibrium coils already designed for ITER it is expected that RITES will contribute $\sim$1 μV to the coil output and therefore, together with TIEMF, could be the dominant sources of error at the coil and in the flux measurements for timescales in excess of a few hundred seconds. More R&D is required on cable performance under irradiation, but presently it appears that specialized coils for long pulses with better cooling characteristics and, almost certainly, poorer frequency response will have to be added to the design. It may also prove necessary to relocate these coils near the middle of the blanket module from the present location near the edge.

In most aspects of the ITER magnetic diagnostic, design feasibility has been shown, even for extended pulse operation. The remaining uncertainty is confined to the better determination of parasitic voltages and further improvements in integrator technology. The design is still evolving, in particular to take account of ongoing R&D developments in this area. As a further safeguard, additional systems exist in the ITER design for the verification of key magnetics measurements for long pulses: a reflectometer for plasma position (see section 3.3) for the four main plasma control gaps, as well as sets of divertor thermocouples and an infrared (IR) thermography system (see section 3.8) for the long-term identification of the average strike-point location. It is expected that the party providing the magnetics will, together with the ITER International Team and in consultation with all users, provide the final specification for this system.

3.2. Fusion product measurements

In order to demonstrate fusion power generation in a future controlled nuclear fusion project, such as ITER, the total neutron source strength should be measured with high accuracy and high reliability. Measurements of the distributions in space and velocity of the confined alpha particles are needed because collective effects and alpha particle–plasma interactions can affect the ignition physics [17]. The neutron fluence on the first wall and the loss location of alpha particles are important parameters to be measured for protection of the device and for the design of future thermonuclear reactors.

To measure all these required parameters, it is planned to develop six neutron diagnostics, *internal* and *external neutron flux monitors*, a *radial* and a *vertical neutron camera*, *neutron activation systems*, *neutron spectrometers*, as well as *lost alpha detectors*. Several other methods including *fast-ion collective Thomson scattering* and *charge-exchange recombination spectroscopy* are proposed for the measurement of confined alpha particles. Overviews of neutron and confined/escaping alpha diagnostics for ITER have been recently published [18, 19].

The aim of the *neutron flux monitors* (NFM) is the time-resolved measurement of the total neutron source strength and the neutron fluence on the first wall. The NFMs will provide the signals necessary for real time control of the ITER fusion power. Each of them consists of detectors, blank reference detectors, a moderator and a housing [20–22] and is designed to meet the ITER requirements of time-resolved measurements of the neutron source strength (parameter 7 in table 2) in a wide dynamic range from 10^{14} to 5×10^{20} neutrons s^{-1} with a temporal resolution of 1 ms. A measurement accuracy of

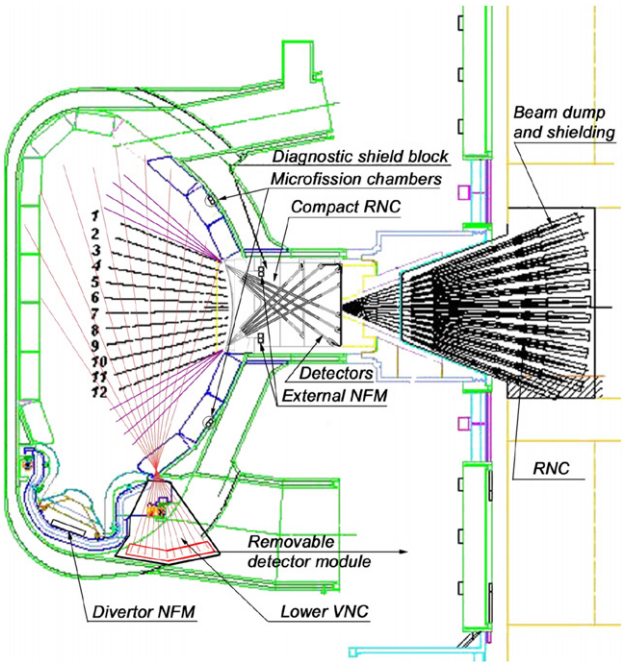

Figure 5. Geometry of the radial and the proposed lower vertical neutron camera (RNC and LVNC) for ITER.

10% can be achieved by using an activation system for cross calibration.

A *radial neutron camera* (RNC) is designed to measure the neutron emission profile. Furthermore, it will improve the accuracy in the measurement of the total neutron source strength. Because of the length of the equatorial port, only the core region of $-0.5 \leqslant r/a \leqslant 0.5$ would be covered by an ex-vessel RNC. Therefore, an extended RNC with additional compact in-plug cameras (two sets of collimators and detectors) has been designed [22]. With the extended RNC the neutron emission profile can be measured for $-0.9 \leqslant r/a \leqslant 0.9$.

Recent JET results [23–25] have clearly demonstrated the influence of non-uniform fast particle populations on the neutron emission profile. During ion cyclotron resonance heating, neutral beam injection, sawtooth oscillations, Alfvén eigenmodes and other instabilities it was observed that the neutron emission profile is not constant on magnetic flux surfaces. Under these conditions both a RNC and VNC are needed to reliably measure the neutron source profile in JET. If similar asymmetries would occur in ITER a *vertical neutron camera* (VNC) would be needed. A lower vertical neutron Camera (LVNC) is presently proposed for ITER [22]. As shown in figure 5, ten collimators of the LVNC are arranged inside a shielding block of stainless steel plus water, attached to the vacuum chamber on the divertor level. The plasma is viewed through a locally widened vertical gap between blanket modules. The collimators are arranged so as to provide a plasma coverage of $-0.7 < r/a < 0.75$.

Compact *neutron spectrometers* (diamond, stilbene and NE-213 detectors) placed inside each collimator of the RNC and VNC are planned to yield a line-integrated measurement that is strongly weighted to the region of highest temperature. An additional high resolution spectrometer with an energy resolution of <3% behind the central chord of RNC is foreseen to measure the ion temperature from the Doppler width of the 14.1 MeV neutron emission. In addition, it is proposed to obtain the fuel ion isotope ratio, n_d/n_t, in the core by measuring the spectrum in the DD neutron energy region (2.5 MeV) [26,27]. Proton recoil and time-of-flight techniques are under consideration for these measurements.

Neutron activation systems are needed for making robust measurements of the fusion output under all plasma conditions, as well as to absolutely calibrate all other neutron diagnostics [28]. One system is based on the pneumatic transfer of a set of encapsulated activation samples from the irradiation station to remote counting stations, where gamma rays from the induced radioactivity will be measured. The irradiation stations will be located inside some of the permanent filler modules and view the plasma through a gap between neighbouring blanket modules. A detailed analysis using the Monte-Carlo neutron particle (MCNP) transport code will be used to establish the relation between total neutron yield and the neutron fluence and spectrum at the points of irradiation. A second, time-resolved, neutron activation system based on flowing water is being designed [29].

A strategy for the *absolute calibration* of the neutron diagnostic systems has been developed. It includes absolute calibration of all detectors at the manufacturer as well as at an on-site neutron radiation facility. The absolute calibration of the most sensitive RNC, VNC and NFM detectors will be done *in situ*, after their installation on ITER, using a moveable DT neutron generator inside the vacuum vessel. This also involves a detailed MCNP analysis. The least sensitive detectors are cross-calibrated against the more sensitive (directly calibrated) detectors by using the plasma as the source. The neutron activation system will be used to check for any changes of the calibration factors during ITER operation.

The measurement of the confined alpha particles is one of the most difficult diagnostic challenges in ITER. Several measurement methods have been proposed and the feasibility of their implementation has been studied. An important issue is to achieve a spatial resolution that is good enough to support studies of transport, ITBs, and alpha particle-driven and/or pressure-driven instabilities. A measurement of the velocity distribution of the alpha particles is also important for analyses of Alfvén instabilities.

A technique that can potentially meet the ITER measurement requirements for the confined alphas is *collective Thomson scattering*. Several approaches have been proposed (60 GHz, 170 GHz, 3 THz and 28 THz) and some of them are being tested on present devices [30–33]. For ITER, the 60 GHz option is the most attractive because it combines the expectation of a good S/N ratio with the minimum required technological developments [34]. The system would be robust against density variations and mechanical disturbances. However, for a given source, the technique does have a magnetic field limitation and for 60 GHz this will be $B > 3$ T. This is not expected to be a serious limitation since high fusion performance on ITER will mostly be achieved at high field. A collective Thomson scattering system for measuring confined fast alpha particles on ITER based on the 60 GHz option has been designed and integrated into one of the ITER ports [35]. Implementation of the system appears feasible

although some key interface details need to be worked through. Detailed calculations have demonstrated that the system can in principle separate the isotropic alpha population from the energetic ions originating from the deuterium beams [36]. In addition, studies of a 28 THz option utilizing a high repetition CO_2 laser have been conducted. In supporting R&D, a 28 GHz laser with a pulse energy of 17 J operating at a repetition rate of 15 Hz in single-mode has been achieved [37]. The system will be applied as source in a far-forward collective Thomson scattering set-up at JT-60U. The design and R&D work currently in progress, including the experimental work on current tokamaks (JT-60U, TEXTOR and ASDEX-UG), will enable a decision to be taken for the ITER system, on the basis of experience, in the near future.

Several ideas for diagnosing alpha particles are based on *charge exchange recombination spectroscopy* (CXRS). A method that uses one of the ITER heating beams could be applied for the measurement of high energy (0.8–2.4 MeV) alpha particles moving in a direction close to that of the heating beam [38, 39]. The expected signal to background ratio is, however, quite low. CXRS on the diagnostic neutral beam (DNB) might be considered for studying thermalized alpha particles [38]. Due to the strong beam attenuation, the measurement range is limited to $r/a > 0.6$. Charge exchange neutralization with high energy neutral beams was proposed [40]. This method uses a tangential ^{3}He beam with an energy of 0.8–1.5 MeV. Intense beam development is required for this method [41, 42].

Alpha knock-on neutron tail measurements are an indirect method using elastic scattering between alpha particles and fuel ions producing energetic deuterons or tritons. One proposal, which has been successfully tested on JET [43], is to measure the high energy neutron tail produced by alpha knock-on energetic ions. This tail can potentially be measured using a neutron spectrometer, such as a magnetic proton recoil spectrometer, [43], a bubble detector [44, 45] or a nuclear emulsion track detector [46]. The discrimination of the alpha knock-on neutrons from beam particle knock-on neutrons is a potential problem that needs to be addressed. One potential solution is to view neutrons that are emitted in the opposite toroidal direction from the injected beams. A related idea is to measure knock-on ions neutralized by the 1 MeV D^0 heating beams or by electron capture from intrinsic impurities [47]. In both methods, fast neutrals are analysed by a neutral particle analyser (NPA). By observing charge-exchange neutrals with energies greater than the beam energy, the beam particle knock-on ions can be avoided. By also measuring the He^+ ions created in the stripping foil, it should be possible to separate energetic D^+ from He^{2+}-ion signals.

Alpha particle measurements are also possible by means of *gamma-ray spectroscopy* using the ^{9}Be(α,nγ)^{12}C and/or ^{10}B(α,pγ)^{13}C reactions [48, 49]. This is a passive method. For a proper interpretation of the measurements it is necessary to know the radial distribution of Be and/or B from another (spectroscopic) diagnostic. The technique can provide information on the spatial profile of the alpha particles with relatively coarse energy resolution, albeit in a limited operational range (relatively high level of impurities). Modifications are in progress at JET to make the gamma-ray spectrometer more radiation hard by the application of LiH filters [50].

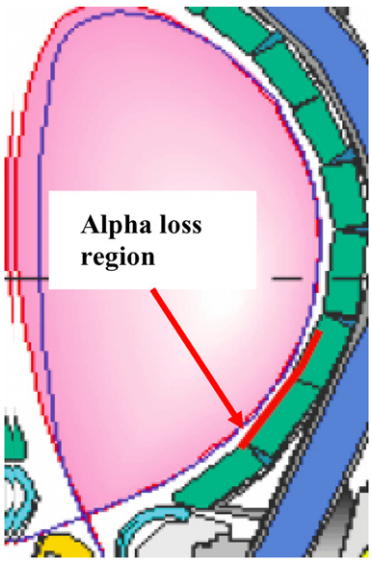

Figure 6. The region where escaping alpha particles will impact on the first wall.

With regard to the measurement of escaping alpha particles, it is important not only to monitor the bombardment location (loss imaging) for machine protection but also to measure the pitch angle and energy distribution of the escaping alpha particles as well as their temporal behaviour during MHD to understand the underlying physics. The loss location is predicted to be between 200° and 240° in poloidal angle, as shown in figure 6, with a toroidal enhancement between adjacent toroidal field coils [51]. An *infrared (IR) camera and/or a band-filtered camera for ceramic scintillators* on the first wall can be used for loss imaging [52]. Diagnostics under development on current machines for time-resolved pitch angle and energy measurement of escaping alphas include Faraday cup and scintillator probes. On ITER, the scintillators would need to be actively cooled since they would be exposed to temperatures above 300 °C. Furthermore, for Faraday cups and scintillators, radiation induced effects such as RIC and RIEMF might be problematic for current measurement in the nA range (see section 4.2). Therefore, new techniques, better suited to the ITER environment, need to be developed for the measurement of escaping alpha particles (see section 4.1).

3.3. *Measurements of T_e and n_e*

Accurate measurements of the electron temperature and density throughout the plasma are important for operating ITER. The accuracy and time resolution required varies with the region of the plasma and with the operating mode [53] (see table 2). Generally speaking we can divide the plasma into three regions with different requirements:

(a) The central plasma with the highest temperatures and the main burning region. The spatial resolution required here is <10 cm ($\sim a/30$) and in general a modest time resolution (10 Hz) is needed. The electron temperature may be measured by Thomson scattering and electron cyclotron emission (ECE), whereas Thomson scattering in conjunction with interferometry can diagnose the electron density.

(b) In order to measure the profiles at the plasma edge during H-mode operation a much higher spatial resolution is required, defined as $\Delta r \sim 0.5$ cm at the equatorial plane with a repetition rate of 100 Hz. Thomson scattering and reflectometry are the main measurement techniques.

(c) The divertor region is particularly difficult. Generally the requirements are for a very high spatial *and* temporal resolution of both the inner and outer divertor leg. The measurement techniques are the same as above. The difficulty is generally associated with access and survivability of optical components that have to be placed in the vicinity of this region. A two-dimensional mapping is not possible and even making a scanning system may prove difficult.

On ITER a *LIDAR Thomson scattering system* [54–56] will provide the basic equatorial core measurements. A key advantage of a light detection and ranging (LIDAR) system over a conventional system is the single port access and the automatic alignment between the laser beam and the detection system. Inside the port plug the same optical elements are used for both the laser beam and for the collected scattered light. As a result these elements do not require remote alignment. The first optical mirror is indented deep into the port plug, thus minimizing the degradation caused by plasma deposition and erosion. Using two different lasers a trade off can be made between time and spatial resolution. One laser ($t = 300$ ps) could provide about 7 cm resolution ($a/30$) at moderate time rate (10 Hz), while the second laser ($t = 1$ ns) would allow for a faster measurement rate (100 Hz) with a more coarse spatial resolution (20 cm).

For a spatial resolution of 6–7 cm detectors would be required with response time better than 300 ps and large spectral bandwidth (T_e in ITER could reach values above 30–40 keV, leading to a very broad scattering spectrum). Such detectors, based on GaAs photocathodes, have recently been developed for JET [57,58]. As a complementary tool, titanium sapphire lasers with 300 ps pulses and high repetition rate can be available (custom made) from industry.

Electron cyclotron emission (ECE) would provide an additional T_e measurement which would be less sensitive to first-mirror degradation because of the long wavelength (about 1000 times longer than that of Thomson scattering). Therefore, stainless steel mirrors with modest optical quality requirements can be used. The diagnostic will provide T_e with a large bandwidth (>10 kHz). The high temperatures foreseen in ITER (30–40 keV) will affect the spatial resolution, due to the larger relativistic and Doppler broadening, which will lead to a widening of the radial extension from which a given frequency in the ECE spectrum is emitted. The target of $a/30$ would be possible only in regions with a low enough value of T_e (typically $r/a > 0.5$ for $T_e(0) = 30$ keV on ITER) [59–61]. The relativistic downshift at the high temperatures in ITER is substantial and will strongly limit the access to the plasma (see figure 7) [62].

It is important to remark that the high temperature scenarios considered for ITER ($T_e(0)$ up to 40 keV) would degrade the spatial resolution of T_e due to a further widening of the emission layer. In the case of LIDAR the very wide spectrum will reduce the accuracy of T_e and n_e at the highest temperatures but not affect the spatial resolution.

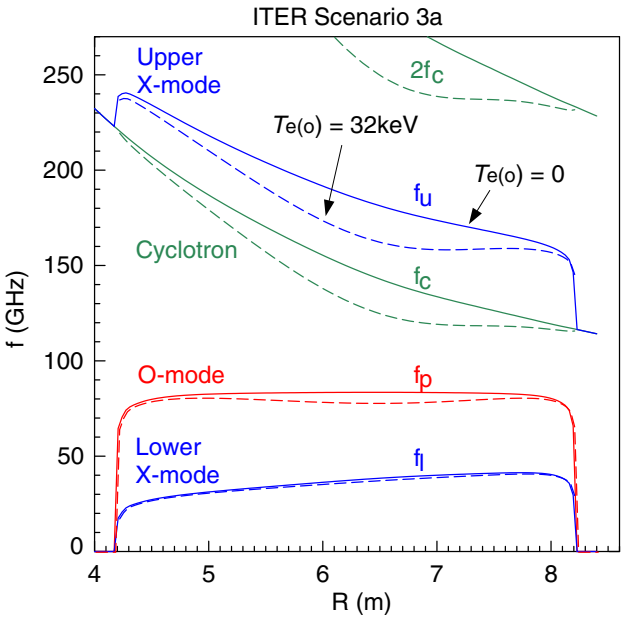

Figure 7. Cutoffs and resonances for the ITER standard 3a scenario (hybrid 13.8 MA, 0.93×10^{19} m^{-3} and 32 keV) with non-relativistic ($T_e = 0$) and relativistic correction ($T_e = 32$ keV).

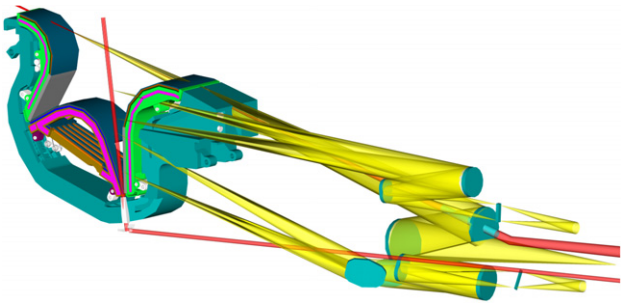

Figure 8. Outer leg and X-point divertor Thomson scattering. Layout of laser lines and observation geometry.

In scenarios with strong additional heating (radio frequency, neutral beam and possibly alpha heating), deformations of the electron distribution function can occur and might lead to apparent discrepancies in the different measurements of temperature by Thomson scattering [63], ECE, etc (possibly by more than 20%) [64]. In such cases, there is no single value of the 'temperature' and temperature ceases to be a useful parameter—a description of the velocity distribution is needed. Both ECE and Thomson scattering will be affected by such distortions but differently. Having two independent diagnostics that sample the velocity distribution in different ways is a great advantage in this situation since it makes it obvious that such distortions are present. Simultaneous observation of several ECE harmonics and (if access restrictions allow for) oblique ECE observation may provide information on the velocity distribution and this is something that is being investigated in current work.

Significant effort has been focused on developing Thomson scattering for the difficult to access divertor area [65–67]. Resolutions of 5 cm along the leg and 3 mm across the leg seem to be achievable on ITER (see figure 8). The remaining limitations are the limited spatial coverage, the low

time resolution (20 Hz) and the lower T_e limit (at very low T_e, the Thomson scattering spectrum is narrow and remains very close to the laser wavelength. This makes the separation of the scattered light and the laser stray light by using filters difficult, leading to a lower T_e limit of 1 eV) [68]. On this last point, newly developed grating polychromators [69] would allow the suppression of laser stray light while allowing a narrow scattering spectrum to be recorded, thus lowering the T_e limit to 0.3 eV.

LIDAR systems, operating with a laser line tilted to the flux surfaces, are also considered to provide measurements adjacent to the X-point with a 0.5 cm effective radial resolution at 20 Hz. A similar technique (LIDAR or conventional Thomson scattering measurements with the laser line tilted to the flux surfaces for an enhanced effective radial resolution) may also be used for edge T_e and n_e measurements in the main plasma. The technique has been extensively tested in JET [70] where edge profiles are measured with 1 cm resolution at a low frequency ($\gg$ 1 Hz) and reduced radial extension ($\gg a/10$).

To meet the ITER requirements of having a spatial resolution of 5 mm in the edge region, a conventional Thomson scattering system is foreseen in one of the upper ports [71]. The system is used to monitor the plasma in the top region of the plasma where the flux surfaces are expanded. This leads to a higher effective spatial resolution when the measurements are mapped to the midplane. The candidate laser system is a 5 J Nd : YAG laser operating at 100 Hz and at the fundamental wavelength of 1064 nm [72]. Conventional filter polychromators are foreseen for detection. The optical design gives a 60 cm field depth and this satisfies the requirement for a measurement for the equivalent region of $r/a > 0.9$ at the midplane. There is a strong incentive to extend the high resolution measurements deeper into the plasma, perhaps to an r/a of 0.8 for edge pedestal studies. This will probably have significant consequences for the design of the measurement system and could mean that the first mirror will be subject to enhanced environmental damage because it will have to be closer to the plasma. At JT-60U a laser system has been developed delivering pulses of 7.46 J at 50 Hz, approaching the performance required for ITER [72, 73]. In this system, a phase conjugation mirror based on stimulated Brillouin scattering (SBS-PCM) is employed to compensate the wavefront distortion induced by thermal lensing in the high power amplifying laser rods [74].

One of the pending problems for Thomson scattering systems on ITER is related to the survivability of the first mirrors. The recent progress on this issue, which is generic to many diagnostics, will be discussed in detail in section 4.3.

The basic measurement of the n_e-profile can be achieved by means of a *toroidal interferometer/polarimeter*. Because the toroidal magnetic field is well known, the n_e information can be unfolded from the polarimetry measurements. The concept has been extensively tested at JT-60U [75], where at a wavelength of 10.6 μm an accuracy of $\sim 0.01^\circ$ has been achieved in the Faraday rotation angle at a time resolution of $\sim$1 ms with a dual CO_2 laser interferometer/polarimeter ($\lambda = 10.6\,\mu$m, 9.27 μm). ITER plans to use a system with five CO_2 lines ($\lambda = 10.6\,\mu$m). For vibration compensation of the interferometer, collinear HeNe lines [7] ($\lambda = 3.39\,\mu$m) or CO lines [76] ($\lambda = 5.3\,\mu$m) were originally proposed. However, based on the robust and reliable operation of a dual CO_2 laser interferometer [77], it is thought that CO_2 lines ($\lambda = 9.27\,\mu$m) are better candidates for vibration compensation [78]. Additionally, a combination of the isotope CO_2 lasers: $^{14}C^{16}O_2$ ($\lambda = 12.1\,\mu$m) and $^{12}C^{18}O_2$ ($\lambda = 9.0\,\mu$m) was demonstrated to be an attractive option to achieve both a good reliability and a high resolution [78]. The combined use of phase and Faraday rotation will give a very reliable line-integral measurement. (According to the requirements, not more than one pulse per year should be lost due to failures in the system). Of course, recent studies [79] on the effects of T_e in interferometry and polarimetry should be considered in order to assess the 1% accuracy required for this system (especially for the high values of $T_e > 30$ keV). The density profile in ITER will also be measured as a by-product of the *poloidal polarimeter* system. This system will yield the density in two ways: by standard interferometry and by using the Cotton–Mouton effect. As the main function of the instrument, however, is the measurement of the q-profile, it is described in section 3.7.

Another approach to determine the line average density (even with some information about profile flatness) comes from *time delay refractometry* [80], based on the measurement of the time delay of pulses launched across the plasma (with frequencies slightly above the cut-off frequency). The technique uses robust mirrors (like ECE and reflectometry) and in principle is free from fringe loss effects, which are typical for phase interferometers. The available frequency window is the x-mode propagation window above the lower x-mode cut-off and below the absorption from the first electron cyclotron harmonic. The typical operational range depends on density, magnetic field and aspect ratio. In ITER, the high T_e scenarios (>40 keV) would only allow the operation of this system in the range 50–80 GHz.

Reflectometry will be used to measure density profiles, density fluctuations and plasma position (understood as the position for a given density layer). As it happens with ECE, reflectometry will provide a high bandwidth (up to MHz) n_e measurement, which will also have the strategic advantage of using plasma/radiation resilient launchers (typically stainless steel mirrors with modest optical requirements).

One of the main achievements of reflectometry during the last five years has been its transition from a diagnostic under test status to a routine density profile diagnostic. Machines such as ASDEX-Upgrade [81–83], DIII-D [84, 85], Tore Supra [86], TJ-II [87] and others have operated density profile reflectometers with > 90% data availability which provide routine input to the data analysis systems. Also, successful experiments on plasma position monitoring (reflectometry/magnetics comparison) have been performed in ASDEX Upgrade in the relevant frequency range [88]. Access to the plasma edge would not be a problem (O-mode can be used, with frequencies between 15 and 100 GHz typically). Despite the progress in the development of the technique it is still not possible to produce density profiles in real time and so feedback control on this parameter cannot yet be attempted, although in principle it is thought to be feasible to monitor the gap between the last-closed magnetic flux surface and the vacuum vessel with a time resolution of about 10 ms [62].

Access to the core will be limited to scenarios with peaked density and will be strongly restricted for H-mode plasmas with

a flat n_e-profile. In this case, only the lower cut-off x-mode observed from the high field side will offer the possibility to reach the plasma centre (see figure 7), by using frequencies in the range 30–60 GHz. A significant effort has been devoted to the design and test of waveguides able to carry the signal to the high field side through the narrow spaces available on ITER [89].

Divertor reflectometry has been subject to extensive analysis and simulation work given the lack of experience in existing machines. Simulations and waveguide studies show the technical feasibility to operate from 15 up to 300 GHz (peak $n_e = 10^{21}\,m^{-3}$), but propagation above this density would require to operate in the range 300–1000 GHz, which offers poor possibilities on sources and detectors and would require a specific set of several waveguides. Interferometry (CO_2) is considered as a more robust candidate system for that density range. The only available experience on *divertor interferometry* is still related to experiments carried out during the 1990s at relatively low frequencies: 130/200 GHz for JET [90] and 183/217 GHz for JT-60U [91]. Although the experience gained with those systems is very important, their use for the high density divertor of ITER might be of limited interest (cut-off frequencies >300 GHz).

Observation of *line ratios in the He emission* from the plasma has been used as a diagnostic for n_e in JET [92] and in the divertor plasma of JT-60U [93] with encouraging results. The technique also has prospects for T_e-measurements, albeit that the results are very preliminary.

3.4. Measurement of ion temperatures

Accurate data on ion temperatures play a key role for plasma control, modelling of tokamak physics and serves as pivotal input for global consistency checks. For example, in the case of the prediction of thermal and non-thermal neutron rates, precise radial profiles of ion temperatures, ion densities and plasma rotation are required. Experiments on internal transport barriers with enhanced core confinement need accurate assessments, or even real-time control of local ion temperature gradients. This has led to a challenging specification of required accuracies both in terms of absolute values and also radial and temporal resolution (see table 2). Other characteristic examples for consistency checks linked directly to ion temperatures are kinetic plasma energy (the sum of ion and electron pressure (see figure 9)).

In view of the prime importance of high quality ion temperature profiles two main methods have been considered as complementary approaches for ITER. The first is *active beam spectroscopy* promising highly resolved radial profiles, and the second approach is passive emission spectroscopy, e.g. *high resolution x-ray spectroscopy*. Other methods e.g. neutron spectroscopy will, in principle, also provide data on ion temperatures (see section 3.2).

Active beam spectroscopy requires a powerful diagnostic neutral beam (H^0 or D^0), that is sufficiently energetic to allow penetration into the plasma centre. A charge capture process between beam neutrals and fully stripped plasma ions such as He^{2+}, C^{6+} or Be^{4+} leads to excitation of CX emission lines in the visible spectral range. For hot fusion plasma experiments with dimensions like ITER the intersection of a pencil-like

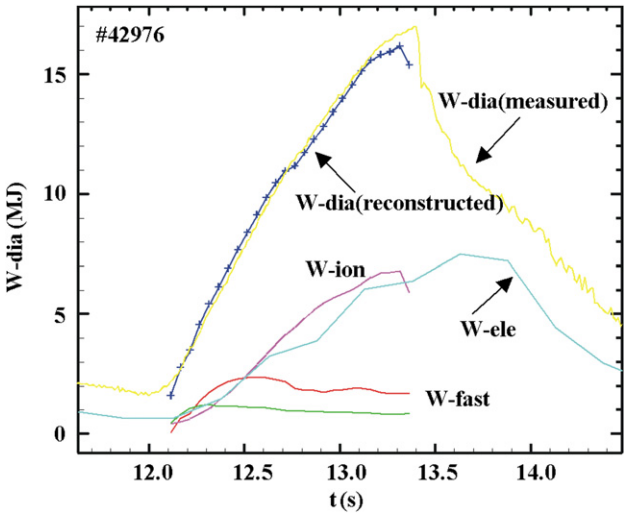

Figure 9. Illustration of global data consistency check for JET DT pulse #42976 of diamagnetic plasma energy and sum of electron and ion kinetic energy as reconstructed from T_e, n_e (LIDAR and DCN-interferometry) and T_i, n_i (CXRS), respectively. Typical ion local temperature errors are below 5%. The error of the bulk ion density is essentially determined by the uncertainty in electron density, since $Z_{eff} < 2$ for high performance plasmas.

neutral diagnostic beam and an array of viewing lines provide highly localized measurements. Hence the name 'active beam spectroscopy' in contrast to 'passive emission spectroscopy', where localization has to be established indirectly, e.g. making use of a considerable number of observation lines and a subsequent tomographic reconstruction of local values and radial profiles.

Modelling studies (cf [94]) have shown that an active beam diagnostic system would provide a feasible solution for ITER, promising adequate radial resolution and the means of measuring ion temperatures, plasma rotation and the densities of the main intrinsic impurity ions as well as the density of the bulk ions. In fact, CXRS has been recognized as the sole approach to direct measurement of thermal helium ash densities.

In this context it needs to be emphasized that a comprehensive evaluation of CX spectra implies ultimately the consistency of temperature, rotation, ion densities and continuum radiation all quantities derived from the same local active spectrum. Following this philosophy, or concept of integrated data evaluation, the requirement for reliable helium ash measurements is inseparable from the issue of accurate ion temperatures and plasma rotation measurements.

For the ITER CXRS diagnostic a dedicated diagnostic neutral beam (DNB) with energy of 100 keV amu^{-1} and a power of 2.2 MW injected radially into the plasma will be used [95]. Two observation ports are envisaged incorporating three periscope systems aligned onto the diagnostic beam. Each line of observation representing one point along the outer minor radius of the plasma will be imaged onto multi-species spectrometers tuned to characteristic wavelength regimes thus covering the main ions in the plasma. Details of the diagnostic and performance studies are published in several papers, [94, 96–99].

The substantial attenuation of the injected neutral beam along its path to the plasma centre has been a critical concern

for the feasibility of a CXRS diagnostic for ITER [100]. However, ion temperatures will rely on the evaluation of the CVI charge-exchange spectrum, where carbon is an intrinsic impurity with concentrations of the order of 1% of the electron density, and spectral signal-to-noise numbers in excess of 30 are expected even close to the magnetic axis with a local electron density of $10^{20}\,\mathrm{m}^{-3}$. The signal-to-noise numbers are extrapolated from existing JET CX data, in particular, data confirming the photon statistics of the signal representing the underlying continuum radiation.

Recently a variation of the CXRS technique was tested on JT-60U. This system has an enhanced spatial resolution to measure the profiles of ion temperature and plasma rotation in the region of an internal transport barrier [101]. The measurement points are scanned along the neutral beam line by means of a collection lens with a piezo stage, which is installed in front of the optical fibres. This effectively increases the available number of viewing channels by one order of magnitude.

The technical advantage of using line emission in the visible range for CXRS and its relative ease of combining a great number of optical lines of sight fed to high resolution spectrometers placed beyond a biological wall is linked to a very critical issue: this is the survival and lifetime of optical components close to the plasma boundary. In fact, the survival of the 'first mirror' is a common critical concern for all optical diagnostics (continuum radiation, D-alpha emission line, etc, see section 4.3). Intensive studies on coating effects and also active schemes including shutters and on-line calibration techniques are currently undertaken and explored.

High resolution x-ray crystal spectroscopy of impurities offers Doppler measurements of T_i, v_{tor} and v_{pol} and line-ratio measurement of T_e. To date, most tokamaks have been equipped with at least a central-chord high resolution x-ray crystal spectrometer, and in some cases with up to five chords. However, it has been prohibitively expensive and complex to install a sufficient number of discrete spectrometers to give continuous spatial resolution. To overcome this limitation, and to put crystal spectroscopy on a par with other space-resolving diagnostics, there is now a successful worldwide effort to demonstrate space-resolving high resolution x-ray crystal spectrometers [102–105]. This has been aided by recent advances in fast, 2D x-ray solid-state [106] and gas-filled [107] detectors. During the next two or three years, radially resolved Doppler measurements from such instruments can be expected to become routine.

The present design for ITER [108] is based on this recent progress. The plasma radial profile is viewed by several imaging crystal spectrometers shared between an equatorial (figure 10) and an upper (figure 11) port. The plasma between $\sim 0.75 < r/a < 0.9$ cannot be viewed directly with the present ITER port design, and is accessed via graphite reflectors. Design work is continuing to minimize or eliminate this region. To maximize reliability, maintainability and upgradeability, the incorporation of any components inside the port plugs has been avoided. In the few cases where in-port components were unavoidable, the performance of the diagnostic was reduced rather than the in-port complexity increased.

The impurity line and continuum emission for ITER reference H-mode and ITB plasmas has been modelled using

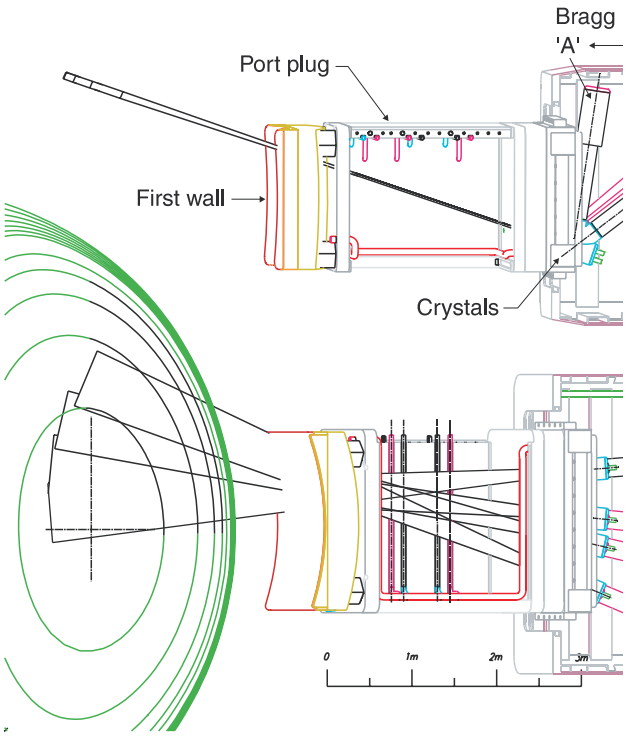

Figure 10. Schematic of the equatorial port array of imaging spectrometers.

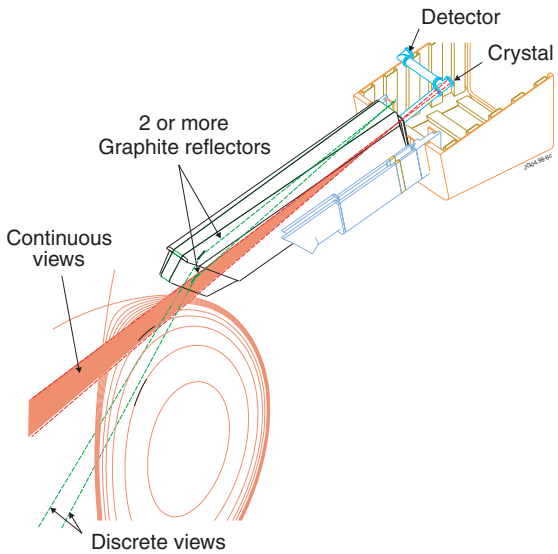

Figure 11. Schematic of the imaging x-ray crystal spectrometer in the upper port.

the ADAS atomic database [109] and the SANCO impurity transport code [110]. Using the instrument sensitivity for a spatially resolving crystal spectrometer array with double-curved crystals and 2D detectors, signals and signal-to-noise ratios were calculated for impurities including argon, iron and krypton. These were shown to have lines suitable for the measurement of the ion temperature (0.5–30 keV) and the rotation over almost the entire plasma minor radius. The main contribution to the signal-to-noise ratio is the plasma continuum radiation on which the lines are superimposed. The main limitation to the allowed impurity concentration is not

the contribution to $Z_{\rm eff}$, but the impurity radiated power, there being a broad operating range between about 100 kW and 10 MW. Helium-like krypton has been the prime candidate for core Doppler spectroscopy on ITER, due to its almost ideal ionization balance and ease of injection. Precision wavelengths have been measured [111] and Kr has been injected into a tokamak for preliminary studies [112]. The ITER system has been designed primarily for Kr, but is also able to observe Fe with better signal-to-noise ratio.

Detector background measurements obtained during D–T experiments at JET indicate that solid-state gas-filled and micro-channel plate detectors can be adequately shielded from the background radiation expected behind an ITER port plug [113, 114].

A quasi-tomographic technique to reconstruct the $T_{\rm i}$ and rotation profiles [115], has been applied to various viewing options that separate the toroidal and poloidal rotation components. The line-integral nature of the measurement can be mitigated by careful choice of observed impurities. The He-like Kr and H-like Fe ionization stages are suitable for the core, while He-like Fe and H-like Ar are more suited for the outer plasma. The ITER measurement requirements can broadly be met with impurity concentrations of $\sim 10^{-5} n_{\rm e}$, corresponding to incremental radiated powers $\Delta P_{\rm rad} \sim 500$ kW.

Measurement of the ion temperature in the divertor plasma is challenging. It has been shown in JT-60U that ion temperatures in the divertor plasma can be deduced from the Doppler broadening of the ($n = 6$–7) visible CIV line [116]. The spectral profile of this line was found to be composed of two Doppler broadening components. An impurity transport code (IMPMC) indicated that the broader component corresponded to the C^{3+} temperature at the common flux region (SOL) and the narrower component to the C^{3+} temperature at the private flux region, and that the temperature relaxation time of C^{3+} and D^{+} was shorter than the ionization time of C^{3+}. Hence the broader component of the CIV line corresponds to the D^{+} temperature at the common flux region (50–150 eV) and the narrower component to that at the private flux region (~20 eV). A similar technique could provide the measurement of the ion temperature in the ITER divertor plasma, albeit that its feasibility needs to be studied.

3.5. Measurements of impurities

Impurities can be intrinsically produced in the plasma as fusion reaction ash, they can be generated by plasma wall interaction on the solid surfaces surrounding the discharge or they can be injected or puffed into the plasma for performance optimization or diagnostic purposes. Impurities can play an important role in all regions of the tokamak from the core plasma to the scrape-off layer and the divertor plasma. Measurements of their concentration, ionization and kinetic state in the discharge can be performed by passive and active spectroscopy of continuum and line radiation, in a wavelength domain ranging approximately from 0.05 to 1000 nm.

Expected impurities include a wide range of elements with nuclear charge, Z, ranging from above 70 (as tungsten will probably be used as a constituent material of plasma facing components) and down to 1 (as the mass-1 isotope of hydrogen is a fusion product that cannot be considered as fuel). Active charge exchange on hydrogenic isotopes, i.e. protons, deuterons and tritons allows potentially the measurement of local fuel mixture ratios in the confined plasma area [117]. Alternatively, methods based on experimental NPA data have been described recently which lead to local D/T ratios [118].

The ratio of the $Z = 1$ contaminant, ^{1}H, to that of deuterium and tritium will be measured at the plasma periphery by *H-alpha spectroscopy*. In particular this diagnostic will supply local values of the influxes of the three hydrogenic isotopes. Because the hydrogenic sources are asymmetric it is important to include several viewing fans with multiple lines of sight aiming at different positions at the periphery of the main plasma, e.g. as proposed for the ITER monitoring system [119]. The first mirror will be the most critical element of the spectroscopic system and much research is devoted to study and mitigate all effects that degrade the mirror performance (see section 4.3). Regular monitoring of the calibration factors (wavelength dependent optical throughput) needs to be incorporated into the diagnostic design.

The effective ion charge, $Z_{\rm eff}$, is usually derived from measurements of *visible continuum emission* by filter arrays observing in a narrow spectral range (about $\lambda = 523$ nm) [120] that is free from spectroscopic line emission. Most spectrally resolved observations in many confinement devices have confirmed that this wavelength region is indeed totally free from apparent line radiation, even during special events such as MARFES or disruptions. However, it is not uncommon that inconsistent results are found for different lines of sight. Indeed it has been observed that, contrary to previous indications [121], reflection from the vessel walls may yield light intensities that are comparable to those emitted by the plasma [122, 123]. Furthermore, direct observation of puffed gases has shown evidence of molecular emission around 523 nm [124]. These findings suggest a necessity of using other spectral intervals together with the one mentioned above and of including at least a limited number of spatial channels featuring a good spectral resolution to confirm that the wavelength intervals used are indeed free of line emission.

The *charge-exchange recombination spectroscopy* on ITER will be based on a dedicated diagnostic neutral beam (see section 3.4). This diagnostic yields local values of the relative concentrations ($n_Z/n_{\rm e}$) of the main low Z contaminants (He, Be, C) in their fully ionized states in the main plasma. The measurement is based on determining the intensity ratio between lines emitted by the plasma impurities as a result of the charge-exchange processes and lines emitted by the beam atoms as a result of the electron impact excitation [38]. The resulting uncertainties will only depend on the local plasma parameters, the relative calibration of different spectral channels and on atomic physics models. They will not depend on beam attenuation calculations, absolute calibration or on the transmission properties of the optical transmission system [98]. Feasibility and conceptual design studies for ITER have shown that the use of high throughput optics, 'vertical' observation of the beam and optimization of the detection system will result in typical signal-to-noise ratios of the order of 10 or higher for helium, beryllium, carbon (as well as deuterium or tritium) [39, 125]. A self-consistent evaluation of the local impurity ion densities gained by CXRS will lead to radially resolved profiles of the effective ion charge $Z_{\rm eff}$ and can be

cross-checked against line-of-sight averaged values of $\langle Z_{\rm eff}\rangle$ gained from visible bremsstrahlung.

Most of the line radiation emitted by the plasma will be in the vacuum ultraviolet and soft x-ray regions. Therefore, much emphasis is put on the design of two classes of vacuum-coupled systems: *vacuum ultraviolet (VUV) spectroscopic diagnostics*, mainly using gratings as dispersing elements, and arrays of *x-ray crystal spectrometers*. The detection and monitoring of core impurities require medium-resolution spectroscopy over a broad band between about 0.1 and 160 nm. The design for ITER x-ray/VUV spectroscopic diagnostics has been developed over the last decade and was incorporated into the ITER-98 design description document DDD [126]. Subsequently, the design has been developed and adapted to the current ITER.

As transmission of VUV radiation does not allow the use of any windows, these systems will need to be themselves extensions of the plasma main chamber vacuum and be included in the ITER tritium circuit [127, 128]. Shielding of detectors and matching of the spectrometer apertures with the divergence of the light beams is possible by employing focussing mirrors under a grazing angle. Beam partitioning and multiplexing between VUV instruments in a tritium-compatible vacuum system covering different ranges and/or with different spectral resolving power will be achieved with various kinds of reflectors, as demonstrated during recent trace tritium experiments in JET [129]. Based on this, and on a 4-channel VUV spectrometer developed for W7-X [130] a 6-channel system covering the spectrum between 2.3 and 160 nm is proposed for impurity monitoring in the main plasma of ITER [131]. An imaging VUV spectrometer has also been designed, to view the outer plasma from an upper port for profile reconstruction in the edge and scrape-off layer (SOL). A two-channel VUV spectrometer design has been developed for the measurement of tungsten spectra in the divertor region [131].

The soft x-ray spectrum between 0.1 and 10 nm contains strong $\Delta n = 1$ transitions of all impurities with $Z \geqslant 4$ (Be). These lines and their associated continuum can be monitored by *x-ray crystal spectrometers*, with high sensitivity and stable calibration. Excellent signal-to-noise ratio is provided by photon-counting, energy-resolving detectors. The JET x-ray survey spectrometer, a scanning monochromator with input collimator, uses flat crystals and multilayer mirrors to monitor the band between 0.1 and 10 nm [132]. It was the only JET D–T compatible survey spectrometer of all core impurities [133] until the VUV spectrometer was made D–T compatible. The use of multi-channel systems exploring the plasma with several neighbouring lines of sight [134] and/or of imaging systems [135] employing position-sensitive detectors will deliver spatially and spectrally resolved information on-line radiation from He- and/or H-like states of such impurities. Tomographic processing of such information will make it possible to reconstruct the one-dimensionally space-resolved emission (as well as ion temperature and toroidal velocity) profiles [115] and hence the concentration of the emitting impurities (see section 3.4).

Because of the complex geometry of the divertor its observation with absolutely calibrated spectrally resolving instruments is a particularly challenging task. The ITER *divertor impurity monitor* [136, 137] will use a multiplicity of sight lines from upper and equatorial ports as well as from a divertor port. Filter spectrometers (with about 300 spatial channels each) will be employed to monitor 12 emission lines, while low- and high-resolution spectrometers will supply information on influxes, localization (e.g. ionization fronts) radiation, ionization state and temperature of impurities and of fuel components.

The survivability of plasma facing optics will be a most serious problem for this diagnostic in particular, as mirrors will need to be located inside the vacuum vessel. Molybdenum or tungsten mirrors (to reduce adverse effects due to sputtering) protected by baffles to reduce particle bombardment [138] will probably be part of the technical solution, but a final satisfactory solution is far from being available now and considerable progress from the ongoing ITER-oriented research is still required.

Inferring local physical parameters from line-integrated signals supplied by these diagnostics will require, to some extent, integrating the measured intensities with geometric and physical data supplied by other diagnostics and modelling codes. Furthermore, despite the multitude of observation points and the large number of spatial channels, tomographic reconstruction of emissivities might be problematic in many cases because of the complex geometry, incomplete coverage of some positions and possible unevenness of calibration between different channels and/or viewing fans. In any case the vast amount of information supplied by such a system will be a very stringent constraint for the validation (or the refutation) of predictions and of the interpretations of results obtained with the aid of numerical simulations.

Active spectroscopy for the divertor, in the form of *laser-induced fluorescence*, has also been proposed for ITER to measure concentrations (and temperatures) of impurities [139]. Based on a tuneable, narrow band laser, the system would primarily be devoted to measurement of neutral helium (but other populations such as Ar^{1+} are also being suggested). The approach considered in more detail so far is based on a four level scheme in the He I triplet system, which would certainly be representative of the population of the metastable state $2\,^3S$. Uncertainties remain however about the ability to make firm deductions about the total helium population in a medium where several local parameters will remain unknown or poorly known (e.g. densities of some neutral populations) and where transit times of neutral atoms across a very narrow plasma might become comparable to their lifetimes in some metastable states. A more comprehensive assessment of uncertainties arising in the specific ITER divertor environment and of possible application of this technique to other populations is presently under way.

3.6. Measurements of radiated power

The profiles of the radiated power and the total power radiated in regions of the plasma are important parameters for basic and advanced plasma control. The basis for the measurement of these parameters by *bolometers* is described in the ITER Physics Basis [7]. The aim is to derive spatially resolved profiles of the emitted power by computational tomography techniques, which requires a large number of lines of sight.

The ITER measurement requirement is a time resolution of 10 ms (3 ms during disruptions) and a spatial resolution of 20 cm for bulk-plasma profiles and 5 cm in the divertor. The required time resolution is similar to what is achieved on present-day machines, whereas the required spatial resolution is significantly higher than that achieved on present-day machines with around 100 lines of sight. Consequently, several hundreds of lines of sight are required on ITER given the two-dimensional nature of the profile reconstruction problem. At present 300–350 bolometer channels are foreseen, most of which are nearly in the same poloidal cross-section. For some purposes, such as the measurement of ELMs, a higher time resolution would be beneficial, but at present it is not clear whether this can be achieved.

In addition to the specified resolution, it is important to consider the actual phenomena that are to be diagnosed by bolometers [140]. Highly radiative plasmas ('radiative divertor' operation), to reduce the power flux to the strike points and reduce ELMs, may play an important role in ITER and are obtained routinely in existing tokamaks [141–145] with or without impurity seeding; also feedback on the radiation level in such discharges has been demonstrated. Bolometers play an important role in the characterization of radiation and detachment during such operation, and parameters derived from bolometer measurements will provide input for plasma simulation codes, including divertor, edge and bulk plasma. In addition to profile information in the bulk and divertor plasma, the total powers radiated in the divertor, X-point region and inside the last-closed flux surface are useful information. Several of these quantities are very difficult to determine accurately on present machines due to the steep gradients in emissivity [141]. Computer simulations are being performed to optimize the line-of-sight arrangement in ITER [146–148] For this purpose, sparse-data tomography reconstructions techniques are used as developed for present bolometer systems [7,149–151], which have to take into account *a priori* information about the expected emission profile to cope with the small number of lines of sight compared with tomography applications in other fields. The simulations of ITER plasmas show that many important features can be diagnosed in a way that is useful for physics analysis, but that steep gradients and quantification of spatial resolution are difficult, and that the line-of-sight arrangement can be optimized further. Conventional bolometers are also sensitive to charge-exchange neutrals. The neutral particle loss can be separated from the radiation by the reconstruction techniques if the viewing geometry is adequately chosen and the charge-exchange neutrals mainly originate in the divertor, as demonstrated in JET [152] and for ITER98 [147]. It is not expected that bolometer sensors that are insensitive to particles are feasible in the ITER environment. It has also been demonstrated that the total radiated power can be reliably and quickly determined from measurements by a neural network that has been trained on output of tomographic reconstructions [153].

In recent years significant steps have been taken towards radiation-hard bolometer sensors. The reference *resistive bolometer* type that is envisaged for ITER is based on the high temperature mica-gold miniature bolometer developed for JET [154], and before that for other machines [155]. These bolometers employ a thin mica substrate as support for a delicate gold meander electrical resistance bridge network. Mica was chosen because of the commercial availability of very thin ($\geqslant 25\,\mu$m) sheets with surface roughness considerably less than 50 nm suitable for depositing the delicate gold track. Neutron irradiation tests of such a bolometer, however, have shown several problems related to irradiation damage, including a weakening of the gold grids, possibly due to partial transmutation to mercury, detachment of the meander from the substrate possibly related to this alloy change and/or substrate swelling, as well as basic electrical contact problems following high temperature neutron irradiation [156, 157]. With the mica bolometer as the starting point, radiation-hard substrates, such as ceramics, of appropriate thickness and appropriate deposition techniques for platinum are being developed in the EU. Commercially available sheets of alumina and AlN with platinum resistance tracks have been prepared and irradiated with electrons and neutrons at high temperature in vacuum to assess the behaviour and compatibility of the materials [158–160]. While no degradation of the platinum nor the substrates was observed, electrical contact with the thin film again proved problematic. This important aspect for delicate devices in a harsh radiation environment is being examined. A prototype bolometer based on a silicon-nitride substrate and platinum resistance tracks and absorbers has been successfully demonstrated under tokamak conditions, and is now ready for radiation testing [161]. Thermal and mechanical analyses of the integration of this type of bolometer into ITER are progressing. The performance of these resistive bolometers can be improved by including a feedback on temperature [162, 163], which has recently been demonstrated on ASDEX-Upgrade. The disadvantage is a larger number of wires. To reduce the number of cables, a capacitive bolometer based on ferroelectric materials with potentially high performance has been proposed [146, 164] and is being developed further as a radiation-hard alternative to the resistive bolometers [165–168] The dielectric properties as a function of temperature (20–400 °C) and frequency (1–250 kHz) before and after neutron irradiation have been measured for different types of ferroelectric films. Irradiation and annealing measurements on $PbZrO_3$-films, a highly oriented perovskite antiferroelectric material, to a neutron fluence of 10^{22} n m^{-2} show only moderate radiation damage and thus these films are most promising for further investigations. However *in situ* measurements during ionizing radiation show marked degradation of the dielectric (capacity) properties [169]. Research and development of infrared (IR) imaging bolometers [170, 171] have also continued resulting in the *infrared imaging video bolometer* (IRVB), which, by using a single large foil, has improved sensitivity and the option of tradeoffs between sensitivity and spatial resolution [172, 173] IRVBs are operating successfully on LHD [174] and a test under reactor-relevant tokamak conditions in view of its application on ITER is under way on JT-60U [175, 176]. Because the sensitivity of the IRVB is expected to approach that of conventional resistive bolometers (see table 4), the device is radiation hard and does not require in-vessel electrical wiring, it may complement conventional bolometers on ITER with unique two-dimensional views of the plasma [175]. Also, the IRVB has been suggested as a detector for a multi-foil thermal

Table 4. Comparison of IR-imaging and resistive bolometers, existing and planned (*) in various devices considering infrared (IR) camera sensitivity, size of slit and bolometer pixel A, foil material and thickness t_f, time resolution Δt, number of channels, noise equivalent power density, η/A and signal-to-noise ratio S/N [175].

Device/type	IR camera sensitivity (mK)	Slit/pixel size, A (mm^2)	Foil metal/t_f (μm)	Δt (ms)	Number of channels	η/A (μW cm^{-2})	S/N
LHD/IRVB	120	$8 \times 8/7 \times 7$	Au/1	17	11×11	180	11–110
LHD/resistive	—	$5 \times 16/1.5 \times 4$	Au/4	5	32	60	5–20
JT-60U/IRVB*	85	$5 \times 5/5 \times 5$	Au/2.5	33	12×16	300	4–60
JT-60U/resistive	—	$4 \times 20/2.5 \times 6$	Au/5	10	32	330	2–20
ITER/IRVB*	25	$5 \times 5/5 \times 5$	Hf/10	10	12×17	190	5–100
ITER/resistive*	—	TBD/TBD	Pt/10 (TBD)	10	350 (total)	160 (JET)	6–3600

detector to be used for the measurement of energetic particle energy spectra [177].

3.7. Measurements of the q-profile

The control of the plasma current profile (or equivalently of the q-profile) is a key issue to perform the long-duration discharges and to control advanced tokamak operation scenarios in next step machines. For example, the buildup of an internal transport barrier strongly depends on the presence of a flat or reversed shear region. Also for ITER this control will be of primary importance, and two different diagnostics are presently foreseen to yield important information from the plasma centre that will be used as strong constraints in q-profile reconstruction codes: far-infrared polarimetry and a motional stark effect diagnostic.

The *far-infrared polarimeter* foreseen for ITER features nine chords that view the plasma under different angles via an equatorial port [178]. The diagnostic is an adaption of the system that was proposed for ITER-98 [179]. Additionally a total of 4–5 chords viewing the plasma from the top port is proposed to achieve a higher spatial resolution in the area where the transport barriers are most likely to occur. The beams have a double passage through the plasma and are reflected by retro-reflectors, indented about 25 cm deep in remote handling grips at the high field side. These elements, having a diameter of only 37 mm are the critical components in the set-up, as their surface roughness should stay below a certain threshold. Recent simulation experiments in which retro-reflectors were bombarded by deuterium ions from a source to a total sputtering depth equal to that of a full lifetime in ITER (5 μm sputtering from a Mo retro-reflector), have demonstrated that at the operational wavelength of 118 μm the reflection coefficient is still rather high [180]. It is therefore no longer thought that the retro-reflectors will be a potential showstopper of this diagnostic when it is operated at 118 μm. Detailed ray-tracing calculations for a single chord have been done to assess the sensitivity to misalignment. The required positional and angular tolerances can be achieved and moreover, it has been demonstrated that it is possible to automatically align the laser beam on the retro-reflector by tilting one of the mirrors in the beam line in two directions [178].

The measured Faraday rotation angle is the line-integrated product of the density and the parallel component of the poloidal magnetic field. To deduce the latter quantity and, hence, the current density profile, from the measurements the density needs to be measured by another diagnostic. Preferably this measurement needs to be done along the same viewing chords. The standard method to measure the line-integrated density via interferometry will be very vulnerable to fringe jumps, and is therefore not thought to be robust enough a technique. Another method that has the potential to yield the line-integrated density is the Cotton–Mouton effect. In ITER, at a wavelength of 118 μm, this effect is large enough to retrieve the line-integrated density. Simulation studies [178] have shown that the accuracy in the q-profile determination is almost independent whether interferometry of the Cotton–Mouton effect is used to unfold the density from the Faraday rotation measurements.

The use of the *Cotton–Mouton effect* for density measurements has been experimentally demonstrated on Wendelstein 7-AS [181]. The method is further being explored at JET [182] in a so-called complete polarimetry set-up in which the Faraday effect and the Cotton–Mouton effect are simultaneously measured to retrieve the poloidal magnetic field and the electron density. The work on the ITER polarimeter has thus far been largely devoted to the conceptual design of the optics in the port plug and not so much on the polarimetry technique itself. The future work should address the choice of a specific polarization modulation and measurement technique, whose selection must be based on consideration of accuracy and time resolution. A very suitable method to measure the poloidal magnetic field with high temporal resolution is based on simultaneous probing the plasma with two counter propagating circularly polarized waves. This method, introduced at the RTP tokamak [183] is used at the MST reversed field pinch [184] where the electron density and poloidal magnetic field can be simultaneously measured with a temporal resolution up to 4 microseconds. The same method is also used on the NSTX spherical tokamak [185]. It should be explored whether this technique can be further modified to also incorporate the measurement of the Cotton–Mouton effect. Segre ([186] and references therein) has proposed several polarimetric methods allowing the simultaneous measurement of the Faraday rotation and of the Cotton–Mouton effect by phase measurements only, which are expected to be less affected by fluctuation of the laser power and other experimental errors. One of these methods has been positively tested in the laboratory [187].

The *motional stark effect* (MSE) diagnostic, which is based on the polarization pattern of the Balmer-Alpha spectrum emitted by a fast neutral beam injected into a fully ionized plasma, is used presently at many of the operating fusion devices. Two schemes for MSE are currently used. One is the 'conventional' polarimetry measurement of the linearly

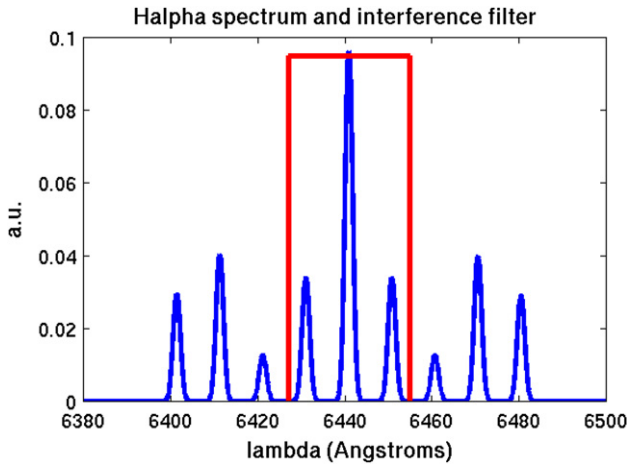

Figure 12. Typical calculated MSE spectrum for ITER showing clearly separated lines.

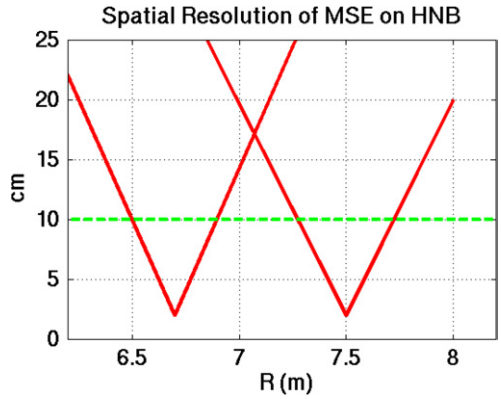

Figure 13. Spatial resolution that can be achieved with the two observation systems of the MSE diagnostic observing the HNB.

polarized σ or π components, and the other is a spectroscopy measurement of the full D_α spectrum.

MSE based on polarimetry is used on many present experiments [188–193] The method makes use of an active measurement of the orientation of one of the Stark components in the Balmer-alpha spectrum emitted by high velocity neutral beam particles passing transversely through the magnetic field. Active polarization methods make use of photo-elastic modulators followed by high étendue interference filters and fibre links. The measured signals are either processed digitally or analogue lock-in techniques are used. The signal evaluation at the modulation frequency and its harmonic yields finally the local pitch angle or ratio B_p/B_t.

Passive polarization techniques [194, 195] usually exploit the entire Stark spectrum in connection with a single polarizing element in front of the fibres. In this case the observed spectrum is evaluated by parametrizing a fully modelled synthetic spectrum and a least-square spectral fit is applied for the extraction of the pitch angle. In ITER this will be relatively straightforward since the lines are clearly separated due to the high beam energies used (see figure 12). The strength of a full spectral evaluation is the wealth of information gained in parallel to the polarization characteristics, in terms of quantitative spectral amplitudes, which are a measure of the local beam strength, a Doppler shift as a measure of the viewing geometry and hence a source for precise localization, and finally asymmetries in the MSE pattern which are a measure of a finite divergence of probing neutral beam. The draw back of a full spectral analysis is the need of suitable spectrometers, which ultimately limits the optical throughput. In contrast, the active polarization technique can make effective use of high étendue interference filters, and therefore generally speaking higher optical throughput.

New tools are also proposed for spectroscopy, as the use of tuneable birefringent filters [196]. The pitch angle can be measured from the Stark shift with these filters, which would avoid the polarization problem of mirrors. A five-stage filter is now used on NSTX. For next step devices with a low magnetic field, where the measured σ and π lines are still partially mixed, MSE combined a laser induced fluorescence technique is proposed [197].

For ITER, in principle both the proposed heating neutral beam (HNB) and the dedicated diagnostic neutral beam (DNB) can be exploited as source for a MSE diagnostic [38]. MSE on the HNB has the advantage of a good plasma core penetration, of passing very close to the magnetic axis, and to be continuous, but it will only work in neutral beam heated plasmas. MSE on the DNB is limited by a maximum duty cycle of the order of 25% but is available in all plasma scenarios. The polarimetry method is proposed to be used on the HNB [198] while the spectroscopy MSE method is proposed for the DNB [98]. *Beam emission spectroscopy* (BES) will be used in combination with CXRS on the DNB and enables the deduction of absolute ion densities from measured line-intensity ratios (see section 3.4 and 3.5) [98]. BES and CXRS use exactly the same in-port front-end optics, but different spectrometers to focus on different parts of the spectrum. BES is used to study the emission by beam ions, while CXRS is used to monitor the emission by the plasma ions. The expected signal strength is in both cases well above the underlying bremsstrahlung fluctuation level. The ITER geometry and the concept of the combined BES/CXRS system is presently being tested in a pilot experiment at TEXTOR [99].

Calculations have demonstrated that the MSE measurement at high Lorentz electric fields is possible with both the methods on the next step devices, as long as the Lorentz electric field is lower than 2×10^8 V m^{-1}. On ITER, only a slight attenuation of the neutral beam is expected due to auto-ionization of excited levels with $n > 6$. Now, with the increase in Lorentz electric field due to the higher beam energy, the influence of the radial electric field on the MSE measurements is negligible for most scenarios, and hence, it is not necessary to correct its effect. A strong constraint of MSE diagnostics is to be located close to the neutral beams so as to minimize the spatial resolution of the diagnostic. On ITER, for instance, these constraints added to a compromise with other diagnostic requirements lead to a split of the diagnostic into two systems, viewing two neutral beams (a central and an edge diagnostic). With this configuration, a full MSE profile measurement can be done with a spatial resolution better than 15 cm almost everywhere, and better than 5 cm around $\rho = 0.2$ and 0.65 (see figure 13), but for some regions lower than the ITER measurement requirement (10 cm).

In recent years advanced applications of MSE diagnostics have been developed and demonstrated. In JT-60U, a new

analytical method to evaluate the spatial and temporal changes in the current density profile directly from the MSE diagnostic has been developed [199]. With this method, a spatially localized decrease in the current density at the magnetic island location was observed. This suggests that the bootstrap current is decreased due to a flattening of the pressure profile within the magnetic island. In DIII-D, the local oscillating component of the poloidal magnetic field was successfully measured [200]. This component was associated with a resistive wall mode. Thus, the MSE diagnostic can be utilized to measure MHD instabilities. Furthermore, MSE optics were employed for beam emission spectroscopy (BES) in JT-60U [201]. Local fluctuations of the electron density associated with tearing modes and ELM activities were successfully measured by fast acquisition of the detector signal (at 1 MHz). It should be investigated whether the MSE diagnostic in ITER could be used to measure parameters in addition to the standard q-profile measurement.

The installation of a MSE diagnostic in next step devices implies new challenges arising from the much harsher environment. For instance, to minimize the neutron flux escaping from the machine, it is necessary to use at least four mirrors instead of one. As the reflections on mirrors are known to alter the initial polarization, it was necessary to prove that MSE measurements could still be done with a high accuracy. A laboratory demonstration of accurate MSE measurement using four mirrors positioned as in the ITER design has been performed [202]. Another strong difficulty with the MSE measurement will arise from layers of deposits especially on the first mirror. The modifications of the initial polarization have been simulated and measured on plasma exposed mirrors. To cope with these effects *in situ* calibrations have to be integrated in the design of the diagnostic, and real-time check-up techniques (as the simultaneous measurement of σ and π lines) are envisaged [203].

3.8. Operational parameters

The unavoidable interaction of the plasma with first wall components is an area of tokamak physics that has been steadily rising in importance, as its key role in determining overall fusion performance has become apparent. In parallel, plasma facing components (PFCs) have evolved to operate under increasingly higher loads, with lower margins for plasma contact. The plasma hours required to meet machine objectives have also become more ambitious (several thousands of hours for ITER). The resulting wear and tear on the first wall components has several unwanted consequences, including the gradual erosion of PFCs and the generation of significant debris. The difficulties of maintenance on large machines further emphasize the need to operate the tokamak first wall within its intended envelope, avoiding and/or mitigating any damaging condition. In practice, a number of diagnostics are required primarily aimed at the following:

- detection and prevention of PFC damage: infrared (IR) cameras, IR thermography, thermocouples,
- detection of runaways: IR cameras,
- proper operation of the divertor, including the attachment / detachment and pumping / fuelling cycle: Langmuir probes, pressure gauges, hydrogen monitors, residual gas analysers and erosion monitors,
- detection of potentially harmful amounts of dust and other debris (Dust monitors).

Infrared cameras can be a sensitive tool to detect the onset of localized first wall heating [204]. This can be due to unforeseen plasma–wall interaction, as well as localized heating by runaway electrons, trapped ions and escaping alphas. Ideally, all PFCs should be covered by IR observations, though this is limited in practice by access. IR cameras can also be used for the direct detection of runaway emission [205, 206]. This, in the heavily shielded high-radiation level ITER, cannot be readily detected by the usual methods of tangential bremsstrahlung or by emitted γ-ray and neutrons when they strike the first wall, due to a combination of poor tangential access and gamma background effects. They can be detected by poloidal soft x-ray arrays [207], therefore, if ITER-spurred development [208] of radiation-hard soft x-ray detectors based on vacuum photo-diodes [209, 210] succeeds, this could provide an alternative ITER-relevant measurement. With suitable views, IR cameras can also be used for detailed power deposition studies near strike points (see, e.g. [211]).

In ITER, IR cameras are able to cover 75% of the total area of the PFCs (figure 14), with a resolution of 3–30 mm, using a combination of midplane views (five locations of three views each) and upper port views (six locations). To gain coverage without excessive first wall labyrinths, they employ small (5 mm pupil; 50 mm flat first mirror) all-metal optics, starting within a few mm of the first wall. A drawback of this approach is the risk of deposition on the first mirror; specific R&D is required to address this. Only about 50% of the divertor targets are directly visible; however extensive local plasma–target interaction is expected to generate light in the divertor legs, which are well covered, and can be used to trigger mitigating action and as a guide to maintenance activities.

Poor IR camera coverage will occur for any closed divertor design with high triangularity. Divertor coverage can be supplemented by localized *IR thermography* systems. These can also be IR camera-based, though the difficulties of direct divertor views, the large étendue requirement and high radiation levels, that make the use of fibre optics at least very difficult, all favour alternative approaches. For ITER, a reverse-spectrometer is planned [212]. In this system, positioned in the divertor cassette, a grating is used to spectrally multiplex a wide field of view into a narrow exit beam. The system is designed to monitor the heat load footprint at the inner and outer target at one toroidal location with rather better resolution (3 mm) than that achieved there by the IR Camera system and with excellent time resolution (down to 20 μs). The system is intended to allow early detection of excessive local heat load that is likely to lead to unacceptable erosion rates and possibly local target damage. In addition, it will provide an estimate of the separatrix location in principle much more accurately than can be achieved by the magnetics and this can be used to correct magnetics drift for long pulses. Due to the expected high levels of re-deposition in this area, the system needs to be provided with suitable shutters; nevertheless the lifetime of its first mirror is uncertain at this time. Alternative approaches to divertor thermography on ITER, based on conventional optics, fibre optics or a combination of these are also pursued and are promising, but designs and assessment of

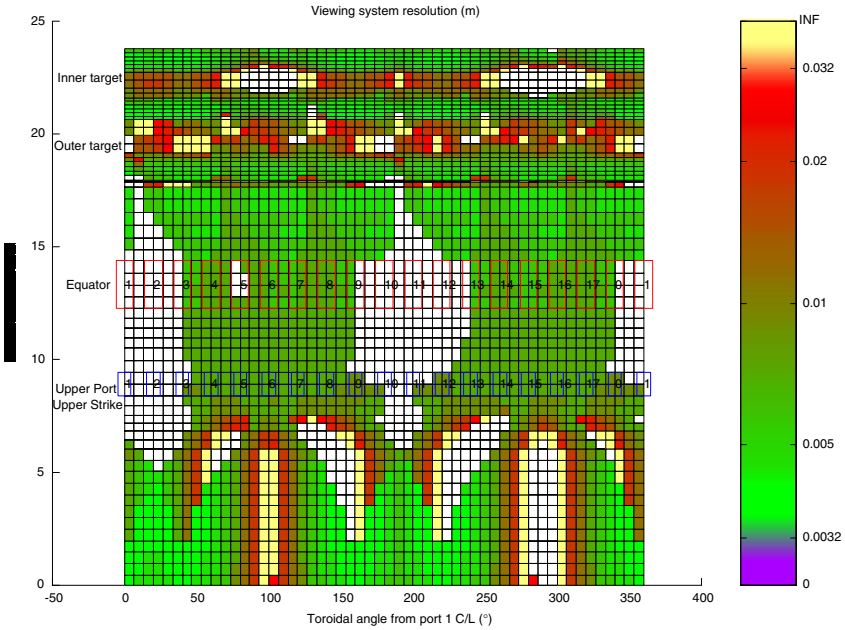

Figure 14. Expected coverage of the ITER first wall by the IR/TV system. The colours correspond to the long-axis dimension of the elliptical viewing spot at the centre of each first wall element in the map, for a system capable of 3 mm resolution at 10 m and normal incidence.

feasibility are not yet sufficiently mature to take a final decision on the most suitable method for ITER.

The measurements of IR thermography can be supplemented in turn by *thermocouples*. These are by necessity slower, but can be used to deduce local power deposition [213]. In ITER these are embedded a few mm behind the divertor targets. Their time response will be rather slow (the characteristic timescale of the divertor target is $\sim$1 s) but they will not be affected by deposition and could be used to steer the discharge away from potentially damaging regimes.

Successful operation of the divertor in a tokamak relies on achieving a 'semi-detached' divertor regime. Several diagnostics can detect whether this is achieved; *Langmuir probes* are one of the most sensitive. For heavily loaded PFCs (10 MW m^{-3}), the design of the Langmuir probe becomes as difficult as that of the target and obviously depends on the details of the target construction.

In ITER, the solution adopted is similar to that employed at JET [214] that is an array of embedded probes made of the target material (CFC) near the target's edge. The probes have heat conduction capabilities that are similar to that of the target plates, and they will erode at a similar rate. This means that the Langmuir probes, as the divertor, will be designed to erode by about 8 mm. If the erosion rate of the Langmuir probe is initially slightly lower, it will tend to become slightly prone of the divertor and the erosion rate will increase. If the erosion rate of the Langmuir probe is initially slightly higher, it will tend to become hidden behind the divertor and thus the erosion rate will decrease. Thus, the process is self-correcting but, as the erosion rate depends on the materials and the temperature, precisely what will happen is hard to predict and will probably vary in time. In practice, this will mean that the effective area of the probe will not be well known and will be time dependent. However, this is not a handicap for the detachment measurement. Probe triplets, separated toroidally, are provided. The probes are cooled by conduction to the water-cooled target support and electrically insulated using radiation-resistant insulators developed for the ITER blanket. In this way the probe is as thermally robust as the target and possibly less stressed mechanically and should have a useful lifetime though it is unlikely that the majority of the probes will survive the full maintenance interval.

There are several other possible techniques that can detect the detachment signature (the sharp ionization front) which is very distinct. For example, multi-sightline CO_2 interferometry can detect the characteristic density pattern. Also, IR thermography will detect a change in the temperature 'footprint' as the conductive heat load drops. Moreover bolometry yields detailed information on the state of detachment of the divertor (see section 3.6). But the Langmuir probes give the most direct indication of detachment, as the temperature drops precipitously to $<\sim$1 eV and the ion saturation current then also drops.

Understanding pumped divertor performance relies on knowledge of a number of parameters, neutral gas pressure and composition both being important. A large variety of gauges and mass spectrometers, many of them commercial or adaptations of commercial systems, are presently in use. For ITER, miniature *pressure gauges* will be placed near the divertor targets. Two suitable designs have been identified, one based on a tetrode ionization gauge ('ASDEX gauge') [215] and the second a miniature Penning gauge using the machine field, similar to the one developed for C-MOD [216]. Either could be placed just behind the ITER target plates. Due to the relatively high electric fields in the sensors, insulation integrity under irradiation has been a concern addressed by R&D [217]. *Residual gas analysers* based on commercial units will be used to monitor cryopump inlet composition, and fast H/D/T ratio monitoring by *'hydrogen monitors'* based on the

spectral analysis of Penning gauge light emission [218] are also planned, although the details of this system are not developed.

In long-pulse machines the divertor becomes, potentially, an expensive consumable item. Divertor material thickness is a compromise between power handling and lifetime; in this calculation the erosion rate is a necessary input. At the same time, excessive erosion, depending on the target material, can lead to unacceptable amounts of co-deposited T. During operation, regimes of high erosion should be identified and avoided before the effects are excessive. One way to do this is by providing for a reliable *erosion monitor*. Possible techniques include speckle interferometry, optical radar systems and, for rather coarse information, doping of the target by spectroscopically unique elements at suitable 'alarm' levels. Speckle interferometry can resolve sub-micron details and by use of a two-colour system can also provide the relevant depth of field [219]. A system is being commissioned for trials in Tore Supra as an erosion monitor of the limiter [220]. Speckle interferometry relies on wide field imaging, so, like an IR camera, would be difficult to implement in the ITER divertor. Optical radar relies on scanning laser beams and can be designed with a more compact front end. It forms the basis of many commercial metrology systems, as well as the inspection system planned for deployment for ITER first wall inspection [221]. In laboratory conditions, optical laser systems have achieved a resolution of $< 2\,\mu$m at distances of 240 m [222] and on NSTX $< 50\,\mu$m at 22 m [223]. Additional information on erosion and deposition may be found by the use of tracers embedded in parts of the divertor target [224] in devices where removal of samples for analysis is possible at suitable intervals.

A dedicated divertor erosion monitor of the optical radar type is, provisionally, planned for ITER and is aimed to meet a resolution of 12 μm/pulse (0.15% of the divertor plate thickness/pulse). Whether a suitable system can be developed for the reactor-like environment of ITER is an open question. In particular, the system may have to distinguish (or use as reference) secondary reflections from the optical train, a common requirement for microwave reflectometry but not normally needed for metrology apparatus.

In a DT-fuelled tokamak, the dust normally generated by various mechanisms becomes a potentially serious safety issue if it reaches significant quantities in mobile form. It is not difficult to generate significant quantities of dust: for a machine the size of ITER, 1 μm removed from the first wall corresponds to several kg of potentially hazardous material. Several techniques are under investigation to provide spot measurements of the amount of dust collected in key areas in the machine (for example below the divertor) in order to estimate the total amount and, potentially, determine the need for preventative cleaning [225]. Such candidate *dust monitors* include modified capacitive pressure gauges [226,227], optical fibre endoscopes inserted between pulses, optical collection trays, electrostatic dust detectors [228] and others.

Most of the systems discussed here are designed for PFC and machine protection and operation. However, they will inevitably also provide a wealth of physics and other information that will be useful in improving our understanding of tokamak physics and the preparation of reactor designs. Taking the systems planned for ITER as an example, the IR camera system is expected to give useful information on recycling (especially toroidal distribution) as well as impurity location. The IR thermography, thermocouples, Langmuir probes and pressure gauges are expected to contribute significantly to our understanding of divertor and ELM physics. Finally the erosion monitor is also a deposition monitor and will help elucidate the flow of material within the divertor.

4. R&D needed for diagnostics

Many of the diagnostics foreseen for ITER are based on systems that are used in present devices. However, not all the presently used techniques and/or components are suited for application in ITER. Moreover, some measurements are unique to ITER, and are therefore not applied in present devices. This calls for specific R&D to develop novel diagnostic components as well as completely new diagnostic techniques. An overview of recent developments in this field is presented in section 4.1. Most of the diagnostic systems to be applied in ITER have components that are positioned close to the plasma in a very hostile environment with large neutron and gamma fluxes (and fluences) leading to a variation of radiation induced effects. Since these issues are generic for many diagnostics much attention is devoted to R&D on irradiation effects on ceramics, conductors, refractive components, etc. An update of the work in this field, since the publication of the ITER Physics Basis, is given in section 4.2. Many diagnostics view the plasma via a mirror positioned behind the first wall or beneath the divertor structure. These mirrors can be amongst others subject to erosion and deposition, the rate of which will depend on the mirror location. The R&D programme on first mirrors (largely devoted to erosion and deposition studies) is described in section 4.3.

4.1. Development of diagnostic components and new concept diagnostic techniques

Although a large fraction of the plasma parameters listed in table 2 can be measured by means of conventional and proven diagnostic techniques, there are several plasma parameters for which completely new approaches should be developed to be able to fulfil their requirements. In this section a number of novel techniques that have recently been proposed and/or tested will be described. This section is certainly not meant to be an exhaustive overview of all new diagnostic techniques proposed, but instead a number of them are given as illustrative examples.

Alpha knock-on neutron tail measurements (see section 3.2) can potentially yield information on the confined alpha particles. The method has been successfully tested at JET using a magnetic proton recoil spectrometer [43]. At ITER the application of such a very large spectrometer is not at all straightforward because of the direct coupling and the large-aperture collimator that are required. Apart from the spatial restrictions this could lead to nuclear activation of components relatively far from the tokamak. For that reason other methods for measuring the alpha knock-on neutron tail are being proposed and tested. One of these is based on a *nuclear emulsion track detector* [46] to be mounted in the radial neutron camera. By using a stack of emulsion foils with one edge facing the

plasma, a small fraction of the recoil protons will remain in the emulsion and provide useful information on the incident neutron energy. The direction of the incident unscattered neutrons in the collimated channels of the ITER radial neutron camera is known to within a few degrees; hence the measured range and direction of the longest recoil proton tracks in the emulsion can be used to calculate the neutron energy. The range of a 14 MeV recoil proton in the nuclear emulsions is $\sim$1000 μm and increases by $\mathrm{d}R/\mathrm{d}E \sim 140\,\mu\mathrm{m\,MeV}^{-1}$ in the 14–20 MeV range of interest. The need to look above 16.8 MeV to avoid the 1 MeV beam-target neutrons in ITER could be avoided if the detectors/emulsions were installed with a more-or-less 'tangential' view. Viewing the neutrons emitted in the opposite direction from the beam injection would allow measurements of neutrons $>$ 15.5 MeV and avoid the factor of $\sim$20 loss in the effective knock-on signal level. The approach has very limited time resolution ($\sim$ few seconds) but features an efficiency that is one to two orders higher than that of the JET magnetic proton recoil spectrometer and gel bubble detectors. Moreover, the emulsions in the compact detector are relatively insensitive to gammas and x-rays.

Traditional methods to diagnose the escaping alpha particles are based on scintillators or Faraday cups, mounted in the vicinity of the first wall where the main losses of alpha particles are expected. However, because of the very high neutron and gamma fluences near the first wall in ITER, it is questionable whether scintillators and Faraday cups can be applied. For this reason alternative methods are being developed. One proposal is based on on-line monitoring of the gamma emission from a *nuclear activation foil* mounted near the first wall. This method has been partly tested on JET [229]. Different types of activation foils were mounted on a removable manipulator. The new activation diagnostic has been used in recent JET alpha particle simulation experiments in which ^{4}He particles were accelerated by ion cyclotron radio frequency (ICRF) heating. An intense population of ICRF accelerated ions (source 10^4–10^5 more intense than fusion ions) has been observed with real-time observation of gamma rays, produced from the reactions ^{9}Be (α, nγ) ^{12}C and ^{12}C (d, pγ) ^{13}C. Significant losses of ICRF accelerated ions (10^{14} ions cm^{-2}) have been observed at the probe location, accumulated over 38 discharges. The deuteron losses dominate; their local pitch angle distribution is highly anisotropic. The alpha particles seem to be better confined, as their losses are not so strong.

A new concept diagnostic that has been already mentioned in section 3.2 is the time-resolved *neutron activation system based on flowing water* [29]. This system has been successfully tested in the laboratory with an activation source and is now ready for demonstration on a tokamak.

A new technique for measuring the radial electric field profile is *Doppler reflectometry*, which is a hybrid diagnostic combining the wave-number selectivity of classical collective scattering with the radial localization of reflectometry. By deliberately tilting the microwave antennas a Doppler frequency shift is induced in the reflected signal spectrum which is directly proportional to the velocity of the turbulence moving in the plasma $E \times B$ rotation frame: $v_{E\times B} + v_{\mathrm{phase}}$. With moderate tilt angles of less than 20° the diagnostic can probe turbulence wavenumbers of several cm^{-1}. At high wavenumbers the phase velocity of the drift-wave turbulence in the plasma edge becomes small which then allows a simple extraction of the E_r. The technique has been extensively tested on ASDEX Upgrade [230], W7-AS [231], Tore Supra [232] and Tuman-3M [233]. Results indicate that not only E_r and E_r shear but also E_r fluctuation measurements are possible [234]. For ITER two Doppler antennas have been proposed for the low field side. The access is the same as for the reflectometer profile systems (section 3.3), which will also provide the cutoff layer position information, giving E_r profiles across the pedestal region using O-mode and the right-hand X-mode cutoffs, while from the high field side the core may be accessible using left-hand X-mode cutoff.

A *fast-wave reflectometer* has been installed and tested on DIII-D for the measurement of the isotope ratio [235, 236]. The system utilizes the ion–ion hybrid cut-off at 18–22 MHz. The ion–ion hybrid cut-off frequency is uniquely determined by the cyclotron frequencies and concentrations of the different species. Very promising first results on the hydrogen concentration (3–67%) have been obtained, which are in good agreement with spectroscopic measurements. The system that is installed at the low field side of DIII-D is a truly independent diagnostic that does not need information from other diagnostics. The maximum penetration depth of the waves in DIII-D is 60 cm. In the near future it is planned to use a swept frequency and to perform a three species measurement, which is directly relevant for ITER. The penetration depth depends on the H/D concentration in DIII-D and the D/T concentration in ITER, but for similar assumptions in both, 60 cm in DIII-D corresponds to about 150 cm in ITER [237].

A new active diagnostic method for runaway electrons has been proposed based on the *laser inverse Compton scattering* (LCS) [238]. When an incident laser photon interacts with a relativistic runaway electron, the energy of the scattered photon is significantly multiplied by the LCS process. The energy multiplication factor is at maximum $4\gamma^2$ in the case of a head-on collision and forward scattering along the motional direction of the electron, where γ is the Lorentz factor. For example, the maximum energy of a photon from a YAG laser ($\lambda = 1.06\,\mu$m, $E_{\mathrm{YAG}} = 1.17$ eV) scattered by the interaction with an electron having an energy of 30 MeV ($\gamma = 60$) is $\sim$16 keV, which is in the x-ray region. Another feature of the LCS process is that most of the photons are scattered along the electron motional direction within a very small angle of $1/\gamma$, i.e. $\sim 1^\circ$ for $\gamma = 60$. Hence, tangential detection is needed. The changes in the spectra of scattered photons have been calculated for different energy distributions of the runaway electrons and been found to be significant. They indicate that the energy distribution of the runaway electrons can be deduced by this method [239, 240]. The method still needs to be demonstrated in existing tokamaks.

In Thomson scattering, usually a grating spectrometer or a filter polychromator are used as the dispersing element. Though these are established methods, there are some disadvantages such as low throughput (especially, in the case of the grating spectrometer) or the necessity of a relative calibration between wavelength channels. Recently, a polarization interferometer based on Fourier transform spectroscopy has been proposed for Thomson scattering [241]. This system can alleviate some of the disadvantages mentioned above. Furthermore, it is a simple and compact system.

For thermal electrons, the optical coherence of the Thomson scattered light at an appropriately chosen optical path delay is a unique function of T_e and n_e. The detection system utilizes a single bandpass filter combined with imaging optics and dual detectors to observe simultaneously both dark and bright interference fringes. The normalized intensity difference between the bright and dark interference fringes will give a direct measure of T_e, even for strongly blue shifted high temperature spectra.

In the field of beam-aided spectroscopy an interesting development is that of an *intense pulsed positive diagnostic neutral beam* [242]. Such a pulsed neutral beam could yield a S/N ratio in CXRS measurements that is approximately 30 times higher than if a CW diagnostic neutral beam (DNB) were used. Therefore, measurements in the plasma core would be feasible with an even higher accuracy or with the same accuracy but for lower carbon contents. An additional benefit would be a much lower power requirement. However, considerable development is still needed to achieve the required performance. In particular a low beam divergence would be needed and this is likely to need significant development. Currently there is no development work in progress.

A *fast-ion charge exchange recombination spectroscopy (CXRS) diagnostic based on* the observation of *re-neutralized beam ions* has been proposed for the measurement of the beam distribution function [243]. A favourable viewing geometry should be chosen to avoid bright interfering lines. Observation of mono-energetic neutrals from a top port results in both a strong red and blue shift, causing a broadening of the spectrum and the appearance of strong intensity at both edges of the spectrum. The enhancement will not show up in actual measurements because the full slowing down spectrum is involved. A proof of principle experiment was done at DIII-D. The time evolution of the re-neutralization effect is about 1 ms. The S/N ratio goes with approximately n_e^{-4}. The measurement is easiest at low densities ($n_e < 5 \times 10^{19}\,\mathrm{m}^{-3}$) because of the visible bremsstrahlung. At high density, the bremsstrahlung is also high, which gives rise to a need for more careful techniques for background subtraction. Recent work at DIII-D has shown that the background can be corrected by installing a second sightline with a nearly identical poloidal view but displaced toroidally to miss the injected neutrals that cause the recombination [237]. Modulation of the beam would be helpful or alternatively beam turn-on/turn-off will provide the data needed to validate the displaced background sightline. The method is sensitive to the portion of the distribution function that matches the velocity of the neutrals. In ITER one can use both the heating and the diagnostic beam to obtain two velocity points in the beam population f_B. A source of interference for the measurement is light emitted by the cloud of thermal neutrals that surrounds the beam (called the 'halo' neutrals). A higher T_i results in a broader halo feature. With the heating beam one obtains a larger Doppler shift and therefore it is possible to select viewing geometries that prevent the desired events from being obscured by the halo feature. It is difficult to avoid the halo feature for the DNB.

Diamond has been tested for its suitability as window material for a wide range of wavelengths from the visible to the microwave region, apart from absorption bands existing around $\lambda \sim 5\,\mu$m. It has excellent properties, such as high mechanical hardness, high heat conductivity and low thermal expansion [75]. In addition, the Verdet constant of diamond is very low which is attractive for infrared polarimetry. The feasibility of chemical vapour deposited (CVD) diamond as a window material for optical diagnostics has been successfully demonstrated in the tangential CO_2 laser interferometer/polarimeter in JT-60U [244]. The Faraday rotation caused by birefringence in the window was negligibly small.

Many of the techniques to monitor the plasma facing surfaces (e.g. wavelength multiplexing thermography, erosion measurements and dust measurements) are also based on novel diagnostic techniques and concepts. As they have been already described in section 3.8, this will not be repeated here.

4.2. R&D programme on radiation effects on materials

A burning plasma experiment, and especially ITER, will present operational and experimental problems not met in present day machines. These problems are related to the expected radiation damage effects as a result of the intense radiation field from the 'burning' plasma. The hot plasma will give rise to high energy neutron and gamma fluxes, penetrating well beyond the first wall, implying the need to use (if need be, develop) materials whose properties are resistant to radiation damage. In the initial phase of operation of ITER it is the radiation flux that will be of concern, whereas in the later technology phase both flux and fluence will play important roles as fluence (dose) dependent radiation damage builds up in the materials. For structural metallic materials the problem of radiation damage is expected to be severe, although tolerable, only near the first wall. However the problem facing the numerous insulating components is far more serious due to the necessity of maintaining intact not only the mechanical but also the extremely sensitive physical properties. An additional concern arises from the need to carry out inspection, maintenance and repair remotely due to the neutron induced activation of the machine. This *remote handling* activity will employ machinery that also requires insulating materials ranging from simple insulation for wires, connectors and motors to optical components such as windows, lenses and fibres, as well as electronic devices such as cameras and various sophisticated sensors.

It is clear therefore that insulating materials will be required to operate under a radiation field in a number of key systems, from heating and current drive to diagnostics and remote handling maintenance systems. All these systems directly affect not only the operation and control but also the long-term reliability of the machine. Furthermore one must remember that ITER is only an intermediate 'technology' machine to bridge the gap between the present day large 'physics' machines and a pre-commercial power reactor. Such power reactors will face radiation flux problems similar to those anticipated in ITER, but the fluence problems will be far more severe. It is also important to note that the radiation flux and fluence levels will be different from one type of device to another depending on the design (for example in ITER and FIRE) and also on location. Due to the general uncertainty in defining radiation levels, most studies of radiation effects have

taken this into account by providing, where possible, data as a function of dose rate (flux), dose (fluence) and irradiation temperature. Although the task ahead is difficult, important advances are being made, not only in the identification of potential problems and operational limitations but also in the understanding of radiation effects, in materials selection and in design accommodation to enable the material limitations to be tolerated.

In recent years, due to the acute lack of data for insulators and the recognition of their high sensitivity to radiation, most work has concentrated on the immediate needs for ITER. Despite the lack of an official framework in which to develop and assign common tasks following the end of the ITER-EDA extension, collaborative work has continued among the European, Japanese and Russian ITER Participant Teams on both basic and applied aspects of radiation damage in insulator materials. This has resulted in considerable progress in the understanding of the pertinent effects of radiation on in-vessel components and materials, in particular for diagnostic applications. Problems that have been addressed and irradiation testing performed include a comparison of absorption and luminescence for different optical fibres and window materials, radiation induced electro-motive force (RIEMF) and related effects for MI cables and coils (see section 3.1), alternative bolometers to the reference JET-type gold-on-mica (see section 3.6), hot filament pressure gauges and electric field effects in aluminas. Recent overviews, together with accumulated references on the general problems can be found in [245–247], while comprehensive details and additional references for all the work discussed below are to be found in several reports [157, 248–251].

Optical fibres. The flexibility and simplification in diagnostic design that the use of optical fibres would allow has prompted an extensive collaborative research programme to find the most suitable type of radiation-resistant fibre. Several different optical fibres have been examined to assess radiation induced absorption and light emission, the viability of high temperature operation and annealing, jacketing material and the influence of hydrogen loading. In addition, parallel work is being carried out on the possibility of photo-bleaching using high intensity lasers to recover transmission, 'holey' fibres for improved transmission and radiation resistance and fibres with extended blue-UV transmission [252–259].

The fibres that have been examined were provided by the EU (STU and SSU polymer jacketed from Heraeus), Japan (MF and FF polymer jacketed, fluorine doped from Mitsubishi and Fujikura) and the Russian Federation (KU1 and KS-4V aluminium jacketed and hydrogen loaded from FORC/IOFAN). Irradiations have been carried out up to total doses in excess of 10 MGy and 10^{22} n m^{-2} and for temperatures from about 30 to 300 °C. Under these conditions the most promising fibres are the hydrogen loaded KU1 and KS-4V. Above 400 nm these fibres show the lowest *radiation induced absorption.* Although the KU1 is the slightly better material up to about 700 nm, the intrinsic oxygenhydride (OH) band and its harmonics notably affect transmission above 800 nm. So for a fibre required transmitting in the visible and infrared regions, the hydrogen loaded KS-4V may be a better choice. There is no doubt that hydrogen loading for any of the other materials would also show marked improvements in their radiation tolerance. It must be noted, however, that above about 5 MGy the beneficial effect of hydrogen loading in suppressing absorption is lost as the conversion to OH centres saturates. Up to 10 MGy the main mechanisms in the radiation damage process are electronic, involving electron and hole trapping. Hence the wide differences observed in induced absorption of the fibres tested due to variations in intrinsic trapping centres (defects and impurities). These trapping centres are thermally unstable, which explains the observation of effective thermal annealing for irradiation at higher temperature or post-irradiation thermal annealing. Above this dose, displacement damage leading to extensive structural damage begins to dominate. As these levels are reached, all the fibres show similar degradation of the optical properties. However by this time the fibres are of little use for diagnostic applications. Furthermore as the extended defects are highly stable, thermal annealing is no longer possible.

All the fibres show intense *radiation induced light emission* (or *radioluminescence*). The light emission comes from two sources: Cherenkov emission due to the passage of relativistic electrons through the material and ionization induced excitation of electronic levels of defects and impurities. The former is common to all the different fibre materials, while the latter is material specific, as is the radiation induced absorption. The Cherenkov emission is essentially temperature independent, but the defect related emission in general shows strong thermal quenching and for irradiation temperatures above about 100 °C may be significantly reduced in intensity. For small samples, windows for example, the different components of the radioluminescence, together with the absorption, can be readily observed. However in the case of fibres this is not so: the observed light emission at the end of the fibre is dominated by the self-absorption and non-uniform irradiation conditions. A broad emission band is generally observed for the fibres peaking at about 500 nm. Below 400 nm self absorption reduces the emission to zero. Furthermore, the better hydrogen loaded fibres exhibit more intense radioluminescence simply due to their lower radiation induced absorption.

The successful application of metal (aluminium) jacketing to the KU1 and KS-4V fibres (plans to similarly coat SSU and STU) is a necessary step towards reliable operation in the harsh radiation environment and at elevated temperatures. The commonly used polymer coating (Acrylate) degrades rapidly at high temperatures, but more so in an ionizing radiation field. As mentioned above, irradiation at high temperature (>150 °C) generally reduces the radiation induced absorption as well as quenches the radioluminescence. Hence metal jacketed fibres will allow operation at higher temperatures, as well as the possibility of post-annealing the radiation induced absorption.

Limited work is now underway to examine the possibility of *in situ* photo-bleaching of the radiation induced damage using high intensity UV lasers, *in situ* hydrogen loading, the potential of so-called 'holey' fibres (fibres containing an array of vacuum, air or liquid filled holes) to improve radiation resistance, as well as fibres to extend transmission into the blue-UV region.

Window materials. Work has concentrated on the KU1 and KS-4V, materials considered suitable for general window

applications and lenses. Results from Europe, Japan and Russia on the gamma radiation induced absorption for bulk KU1 and KS-4V are in general agreement for irradiations up to 100 MGy and temperatures up to 300°C. Under these conditions the induced absorption bands are below 350 nm. In the case of KU1 these bands markedly reduce with increasing temperature, allowing usable transmission down to 250 nm. KS-4V on the other hand is anomalous, the absorption increasing with temperature up to a maximum at about 100 °C. However, it may be safely used above 350 nm [260, 261]. Due to the difficulty of irradiating optical fibres at different controlled temperatures such behaviour has not been reported, but should equally occur for fibres made from KS-4V. CVD diamond windows were irradiated by neutrons at the Japan Materials Test Reactor (JMTR). The degradation of the transmission was small at 10.6 μm in a fluence range smaller than 10^{21} m^2 [157].

Recently completed work on *laser-induced damage* in KU1 and KS-4V has confirmed the limited influence of radiation induced absorption and electrical conductivity on the damage threshold for high power laser transmission. This is not expected to be a problem. On the other hand, metallic deposition due to sputtering or evaporation can seriously reduce the damage threshold even for deposited layers only a few nm thick. The effect is strongly material dependent and requires further examination. Furthermore, self-cleaning with subthreshold laser pulses is not effective for all deposited materials [262–264]. Even more recently severe degradation of the optical and electrical properties of KS-4V due to surface bombardment by hydrogen ions has been reported [265]. This potential problem is being further examined to quantify the risk.

MI cables and coils. It has become evident that the use of mineral insulated (MI) coaxial cables in the expected ITER radiation field must accommodate radiation induced currents and voltages generated between the central conductor and outer sheath, which causes additional noise in the cables. Furthermore, in recent experiments (EU, JA, RF) oriented towards ITER diagnostic needs, evidence has been found that a small voltage along the central conductor itself can be generated due to radiation induced electro-motive force (RIEMF), temperature induced electro-motive force (TIEMF) and radiation induced thermo-electric sensitivity (RITES) effects. This is of serious concern, particularly for the sensitive magnetic coil diagnostics, a prime candidate for plasma current and position control (see section 3.1). Although considerable clarification of the effects and mechanisms involved in RIEMF has been achieved, the number of factors identified which affect both the voltages and currents generated between the central conductor and outer sheath, and along the central conductor itself, has markedly complicated the issue [16, 266–275].

The existence of RIEMF between the central conductor and outer sheath, which can generate potentials of the order of volts together with microamps of current, has been known and used for many years. The work performed for ITER has examined the influence of the materials employed, cable size and surrounding material environment on RIEMF. The following conclusions were drawn: at the onset of irradiation (operation of ITER) gamma induced RIEMF dominates. With irradiation time nuclear reaction effects, in particular beta emission, can also become important giving rise to a time varying RIEMF. These latter effects can be minimized by choosing materials with low neutron capture cross sections. From this point of view, steels or Inconel are preferable to copper for the central conductor. Suitable modelling can now predict the nuclear induced currents both qualitatively and quantitatively. The gamma component can, however, only be predicted qualitatively due to its high sensitivity to the gamma spectrum and surrounding materials. The importance of the insulation, alumina or magnesia, has not been ascertained due to the lack of available MI cables identical in all but the insulation material. However, its role appears to be minor, with no clear differences being reported. Dependence on MI cable size (inner conductor diameter, insulation thickness, outer sheath diameter and thickness) can now be modelled, but again has not been experimentally validated due to the lack of availability of suitable cables. One further aspect that would undoubtedly influence the RIEMF, and may account for odd results and difficulties in model predictions, is coaxial symmetry of the manufactured MI cables. So far this has hardly been addressed, but methods and procedures to control the quality should be high on the list of necessary future actions.

Three recent experiments have confirmed that a voltage can be induced along the central conductor by thermal gradients. Two of these, carried out without radiation at controlled temperatures, show that voltages in the microvolt range can be generated by TIEMF in certain cables for temperature differentials of less than 100 °C [272, 274, 275]. Furthermore the MI cables examined were found to have well localized sensitive regions, but unrelated to coaxial asymmetries. Further work is underway to assess the material composition. The third experimental result [16, 273] obtained in-reactor also points to thermoelectric generation in the microvolt range. In this case nuclear transmutation and/or lattice damage in the central conductor material is believed to modify the initial thermal gradient sensitivity (i.e. RITES). In this experiment the thermal gradients were produced by nuclear heating and in addition by passing an ac current along the central conductor. Available evidence now suggests that voltages along the central conductor of MI cables due to TIEMF and RITES exceed that possibly induced by any asymmetric RIEMF current appearing along the conductor. The present state of knowledge on radiation and temperature effects has recently been reviewed [272]. It is clear that reducing RIEMF and thermal effects while at the same time meeting the more conventional requirements for the affected sensors will be a difficult R&D challenge (see, e.g. section 3.1).

Pressure gauges. An ASDEX pressure gauge mock-up has been irradiated to investigate the impact of neutron and gamma irradiation on the electrical feedthroughs (most critical component of the pressure gauge) [267]. A pressure gauge equipped with instrumentation to monitor on-line the insulation resistances of the feedthroughs was irradiated in a vacuum capsule at the required operating temperature. It was found that the insulation resistance of the feedthroughs remained sufficiently high, $> 2\,\mathrm{M}\Omega$ compared with the required 100 kΩ, to guarantee correct operation of an operational hot filament pressure gauge, even after receiving a

thermal neutron dose of 7.5×10^{23} n m^{-2} [276]. A final test with heated filament is under consideration.

In recent years considerable progress has been made on the identification of potential radiation problems, selection of the most suitable materials and testing of essential components for burning plasma experiments. Due to the urgency of the task, most effort has been focused on the immediate needs for ITER. For future fusion power devices similar radiation effects will be present, with those dependent on radiation flux dominating at the beginning of operation. However, unlike ITER, fluence effects will be of paramount importance. In the near future these must be addressed, if they are not to cause a severe limitation on the lifetime of the device.

4.3. R&D programme on mirrors

Almost 50% of all diagnostics presently foreseen for ITER have an in-vessel mirror as front-end component [277]. Mirrors are used in a very wide wavelength range from ~1 nm up to a few mm. The tolerances in the surface quality of the plasma viewing first mirrors (FM) are strongly related to the wavelength range in which the mirror is used and to the characteristics of the observed radiation that are important (e.g. absolute intensities and polarization characteristics). The longer the wavelength, the less sensitive a specific application is to tolerance in the surface quality of the plasma facing mirrors. The FMs are subject to all kinds of radiation and particles emanating from the hot plasma, which can lead to a deterioration of the mirror characteristics. For metallic FMs the most important factors that result in gradual degradation of their optical properties are erosion due to bombardment by charge-exchange atoms (CXA) and deposition of contaminants. Which of these two effects is dominant depends strongly on the location of the FM [278].

The modification of the optical properties of FMs by erosion and deposition is investigated in simulation experiments. Significant progress has been achieved in understanding the effects of long-term bombardment of mirrors by CX atoms. [279]. These findings were confirmed in a dedicated experiment in TEXTOR, where single crystal and polycrystalline Mo mirrors were exposed together with single crystal W mirrors under identical erosion dominated conditions in the SOL plasma. The energy of impinging D ions corresponded to the expected energy of CXA in ITER. The ion fluence accumulated during the exposure correlated with the CXA fluence onto the first mirror surface during several hundreds of ITER discharges. After the exposure a significant degradation of the specular reflectivity was measured on the polycrystalline mirrors but not on the single crystal ones. Erosion caused a negligible effect on the polarization characteristics of the mirrors [280].

Simulation experiments on single crystal W and Mo mirrors have shown that mechanical treatment of mirrors (e.g. during polishing) can destroy the crystal structure at the surface of the mirror. Therefore, removal of this surface layer by sputtering is recommended as the final procedure in the manufacturing process of the mirrors, before their installation in the tokamak [279].

Long-term exposure of various single crystal and polycrystalline mirrors has been made in Tore Supra. The surfaces of the mirrors suffered from erosion mainly due to glow conditioning discharges and this was confirmed by subsequent measurements in the laboratory and by modelling. This outlines the importance of protecting the FM during conditioning procedures in ITER [281].

The effects of deposition on properties of mirrors are being investigated both in tokamaks and in laboratory experiments. In one experiment, a periscope-like mirror system was exposed in the scrape-off-layer of TEXTOR for more than 120 plasma discharges in deposition-dominated conditions [282]. Despite the fact that deposits with a thickness of up to 300 nm were found on the FM, no deposition of impurities was detected on the mirrors located further in the periscope.

The first dedicated tests of diagnostic mirrors in a tokamak divertor plasma were made in DIII-D [283, 284]. The mirrors were exposed during a series of ELMy H-mode discharges with partially detached divertor plasmas. Such a regime of operation is proposed as a working regime for the ITER divertor. Two dedicated exposures were made: with mirrors at room temperature and with heated mirrors, where the mirror holder was kept at 80–140 °C. A significant deposition of carbon of up to 100 nm was detected on the mirror surface of the room temperature mirrors, whereas for the heated mirrors the carbon deposition was fully suppressed and degradation of the mirror optical properties substantially reduced. This illustrates the necessity of developing techniques for both an active/passive prevention of deposition and for mitigation of the consequences.

An extensive investigation programme is presently running in JET [285]. Sets of polycrystalline molybdenum and stainless steel mirrors are being exposed in the divertor region and in the main chamber. Some mirrors are protected with shutters against the conditioning discharges.

Presently it is believed that the substrate material largely influences the amount of deposition that occurs in a given situation. Specifically, the deposition of impurities is expected to be more enhanced on a carbon or carbonized metal substrate rather than on pure metallic surfaces. A dedicated research programme is underway on the TEXTOR [286, 287] and TCV tokamaks [288] and in the University of Basel to investigate these effects.

Cleaning of the deposits on the mirrors is another way to reduce the contaminants on their surfaces. The effectiveness of H-glow discharge cleaning as a mirror preparation technique was clearly demonstrated in a recent experiment done at the University of Basel [280]. Two cleaning procedures of 15 min each were found to be sufficient to restore the reflectivity of Mo mirrors caused by oxidation during their storage in air before exposure in TEXTOR. The development of methods for *in situ* cleaning of deposited films from FMs is an important mitigating technique. Several cleaning methods are being investigated: chemical erosion of the deposited layers by ions from a low-temperature deuterium plasma [279], CH_4–Ar and H_2–Ar mixture plasmas [289] and removal of the layers by laser ablation [290]. Cleaning of mirrors by laser ablation demonstrated that the mirrors could be completely cleaned by 30–50 laser pulses with > 0.12 J cm^{-2} [291]. In an ECR discharge the cleaning rate of a C–H film from glass was found to depend on the orientation of the sample surface relative to the magnetic field: it varied from 2.5 nm min^{-1} for the

perpendicular direction up to 0.5 nm min^{-1} for the parallel direction [292]. A laser cleaning scheme to counteract the buildup of deposits on the window of a LIDAR Thomson scattering diagnostic was successfully implemented on JET [293] and JT-60U [294].

Recently, results were published of calculations of the flux and mean energy values of CX atoms to the first wall as a function of the poloidal azimuth in the ITER vacuum vessel (VV). At the outer first wall, within ±1.5 m from the midplane, the predicted values are $\sim 2 \times 10^{15}$ cm^{-2} s^{-1} and ~350 eV, respectively [295], however, higher estimates exist [296]. Since the FMs are usually indented with respect to the first wall, the CXA flux to their surfaces will be less. In the worst case the reduction of the CXA flux is only a factor of 2, when the FM is rather close to the plasma and when not viewing the plasma through a small entrance pupil. The reduction of the CXA flux with respect to that at the first wall can be orders of magnitude if the FM views the plasma through a small entrance pupil (like the FM of the H_α diagnostic) or when it is placed in a deep duct (e.g. the FM of the LIDAR system).

For ITER a choice has been made to use beryllium as the material for the first wall. Therefore, it can be expected that beryllium will be the main component in the deposited layers and that shortly after the start of ITER operation, in-vessel metal mirrors in locations, where deposition is dominating sputtering, will have optical properties close to those of the bulk Be mirrors. For this reason, investigations on the behaviour of Be mirrors in conditions relevant to ITER environment were studied at Kharkov [297]. It was found that bombardment by keV-range D^+ ions, in a vacuum containing oxygen as a trace element, produced a fast drop in the reflectance of Be mirrors. This is probably due to a partial transformation of an intrinsic BeO film into a $Be(OD)_2$ film. The backward reflectance could be restored by a combination of annealing in vacuum (up to 200–300 °C) and bombardment by low-energy D^+ ions (20–60 eV). These results give some hope that in a fusion reactor, with a similar temperature of the first wall and plasma facing components and with the low energy portion of the CXA flux considerably exceeding the high energy portion [296], a similar effect would counteract the degradation of reflectance of Be mirrors due to the influence of higher energy tail in CXA energy distribution.

Radiation damage by low energy He-ions can be significant and more serious than that of hydrogen isotopes. Therefore, the effects of He-irradiation and the underlying physics are being investigated in laboratory experiments for Mo, Fe-9Cr and W. Mirrors that were irradiated by He-ions from a source were found to have a significantly reduced reflectivity due to the formation of bubbles, blisters and holes [298–300]. It is not yet clear whether there are implications for the FMs in ITER and this is under investigation.

For the mirrors to be used for Thomson scattering, the cumulative laser damage is an additional factor which leads to an increased degradation rate of the optical properties, depending on the total number of laser pulses. Significant progress has been achieved in investigation of the effects of frequently repeated laser pulses on mirror degradation in a simulation experiment in which the total number of laser pulses exceeded 2×10^5 [301]. The data from the experiment can be described by a simple model for mirror degradation due to a repeated heating of the laser spot, which is reminiscent of a mechanical fatigue phenomenon: $F_N = F_1 N^{s-1}$, where F_1 is the laser-induced damage threshold in a single test, F_N the same as in an N-pulse test and s is a numerical factor (0.89 for Mo and 0.82 for W).

Experiments to understand the environmental impact on the optical properties of FMs have been included in the experimental programmes of various fusion devices. The main conclusions from these experiments are summarized briefly in table 5.

5. Integration in the tokamak

Individual diagnostic systems have to be installed on the tokamak in a manner that makes the best possible use of limited space. The number of ports in ITER that is available for diagnostics is rather limited, especially if compared with present devices, where each diagnostic has its own specific port. To implement all the diagnostics which are required to measure the multitude of plasma parameters on the ITER tokamak, it is necessary to integrate multiple diagnostic systems into specific ports. ITER is prototypical in the sense that a very thorough integration analysis is required to find the optimum distribution of diagnostics over the available ports. Several factors have to be taken into account in this analysis: measurement requirements, shielding, activation and tritium containment requirements, total system path length and complexity and maintenance requirements. Unavoidably, priorities have to be set and within diagnostics this is done according to the expected role of the associated measurements. Systems which provide measurements for machine protection and basic plasma control are given the highest priority, followed by those which provide measurements for control of high performance modes and physics studies. It should be realized that all diagnostics in ITER, including those that are listed under machine protection, basic control and advanced control, are expected to give valuable input to physics studies. Even stronger stated, the use of diagnostics for physics measurements will be crucial for the success of ITER. This is also evident from the right column in table 1.

Diagnostic components are installed in four locations—within the vacuum vessel, in equatorial ports, in upper ports and in divertor cassettes and ports. A cut-out view of ITER with some typical diagnostics upper and equatorial ports, as well as instrumented diagnostic cassettes, is given in figure 15. The diagnostic control and data acquisition area is to the west of the tokamak.

Ex-vessel transmission lines take diagnostic signals back to the diagnostic area. These include laser and collected light beams and waveguides (Thomson scattering, reflectometry, electron cyclotron emission and absorption, polarimetry and collective Thomson scattering). The guidelines for routing these have been drawn up and include such aspects as avoiding building structural elements, minimizing the number of penetrations through the building barriers (though not necessarily crossing barriers orthogonally), sealing lines (to the building and internally), keeping microwave and quasi-optical waveguide systems straight and well supported, changing direction with a minimum number of well separated mitre

Table 5. Overview of mirror work ongoing on various devices.

Facility/Institution	Overview of the investigations on first mirrors	Main results
Tore-Supra [28]	• Long-term exposure of single crystal and polycrystalline Mo, Cu and SS mirrors in the main chamber. Modelling of the deposition patterns on mirrors.	• The smallest degradation of optical performance on Mo mirrors, the largest on Cu mirror samples. • Modelling and dedicated lab experiment have confirmed that the largest part of erosion was due to conditioning glow discharges exposing the un-protected mirrors. • Large differences were found in the erosion rate of Mo, Cu and SS, not corresponding to the published data for sputtering yields: SS seemed like 'protected' from erosion in an environment polluted with carbon.
T-10 [291]	• Exposures of SS and Mo mirrors installed at different distances from plasma and heated up to different temperatures (in progress).	• Mirror samples were exposed under deposition-dominated conditions. • The deposition efficiency on the mirrors un-protected from conditioning discharges was significantly higher than that on protected mirrors. • Mirror samples in plasma shadow have preserved their initial reflectivity. • Laser ablation was successfully applied to clean the deposited films.
TEXTOR [280, 282]	• Comparative studies of single crystal and polycrystalline W, Mo, Rh coated mirrors under erosion and deposition conditions. • Experiments with periscope mirror system—impurity transport in the diagnostic ducts, deposition mitigation. • Surface finishing test—the effect of the mirror finishing on their performance under erosion conditions.	• Single crystal mirrors have preserved their optical properties after exposure in erosion conditions, unlike polycrystalline mirrors. • Negligible effect of erosion on polarization characteristics in a wavelength range 300–800 nm for both polycrystalline and single crystal mirrors. • First attempt to imitate the diagnostic duct in a tokamak with a periscope mirror system: no carbon transport, no deposition is detected beyond the first FM.
TCV [288]	• Exposure of mirrors from different materials (Mo, W, Si) into the divertor floor region. The samples are recessed behind the front surfaces of the divertor tiles to avoid direct plasma impact.	• Under similar exposure conditions, the mirror substrate has been found to strongly influence the thickness of layers deposited on the mirror.
DIII-D [279, 280]	• Investigations of single crystal and polycrystalline Mo mirrors in the divertor region under ITER-relevant plasma conditions. • An attempt at the active mitigation of the deposition by heating the mirrors.	• Carbon deposition was fully suppressed by heating the mirrors up to the moderate temperatures of 80–140 °C. • The degradation of the optical reflectivity of the heated mirrors is minimized.
JET [285, 288]	• SS and Mo polycrystalline mirrors placed in the main chamber and divertor of JET.	• Results will be available after the removal of mirrors.
LHD [302]	• SS un-protected mirrors were located in LHD divertor and diagnostic pumped duct for a long-term exposure subjected to the cleaning discharges and periodical boronization procedures (in the second experiment).	• Closest to plasma, mirror became cleaner than it was initially and was a little eroded (∼150 nm); mirrors in divertor area and in the duct became coated with C–Fe (∼30 nm thick) and C–H films (∼60 nm thick), correspondingly.
NSTX [303]	• Time-resolved measurements with quartz crystal microbalances (QMB) in a first-mirror-like geometry.	• Deposition of carbon, oxygen and deuterium. • A slow rise in deposition in the inter-pulse period was also observed and this may be related to the condensation of polymer-like films after each discharge. • Modelling indicated that the deposition was not due to quiescent processes in the discharge, suggesting that transients such as ELMS and disruptions and also evaporation and condensation of polymer-like films should be considered in predicting the spatial distribution of co-deposited tritium in ITER.

Table 5. Continued.

		• Deposition on a rear facing QMB suggests that the cleaning may be needed even for mirrors that do not face the plasma directly.
HL-2A	• Exposure of polycrystalline Mo and Cu mirrors in main chamber for long time. • Investigation of shield cap (cone and column shield) for metal mirror in main chamber.	• C, O, Si and Cr deposition matter have been found on the mirror surface. The reflectivity of copper mirror decreases more rapidly than that of Mo, especially at short wavelengths. • The mirror is polluted easily during glow discharges and wall processing than during Ohmic discharge. • The protective effect of a cone shield is better than a columnar one.
University of Basel	• Comparative tests of a variety of ITER-relevant materials (Cu, stainless steel and Mo) exposed to low temperature deuterium plasma with controlled partial pressures of methane in the gas mixture.	• Under similar conditions, markedly different erosion/deposition patterns are observed on the different materials.
IPP Kharkov [279, 297, 304]	• Simulation experiments using ECR-heated steady-state discharge in deuterium to investigate long-term sputtering effects on polycrystal (pc), single crystal (sc), metal film on metal substrate (fm) from different metals and bulk amorphous mirrors. • Study of the effect of mirror contamination by C-based film. • Development of a method for *in situ* distinction between the reasons of mirror degradation (CXA sputtering or contamination).	• The degradation rate of sc mirrors is significantly lower than of pc mirrors from the same metals (SS, Mo and W); the degradation rate of best Rh and Mo fm mirrors can guarantee their serviceability if the CXA flux to them will be weakened more than one order of magnitude in comparison with the first wall flux. • A comparative analysis was done of the characteristics of contaminating films from several fusion devices. The preliminary results demonstrate that the mirror surface quality can be controlled *in situ* by analysing the image of the test object with sharp luminous edges.

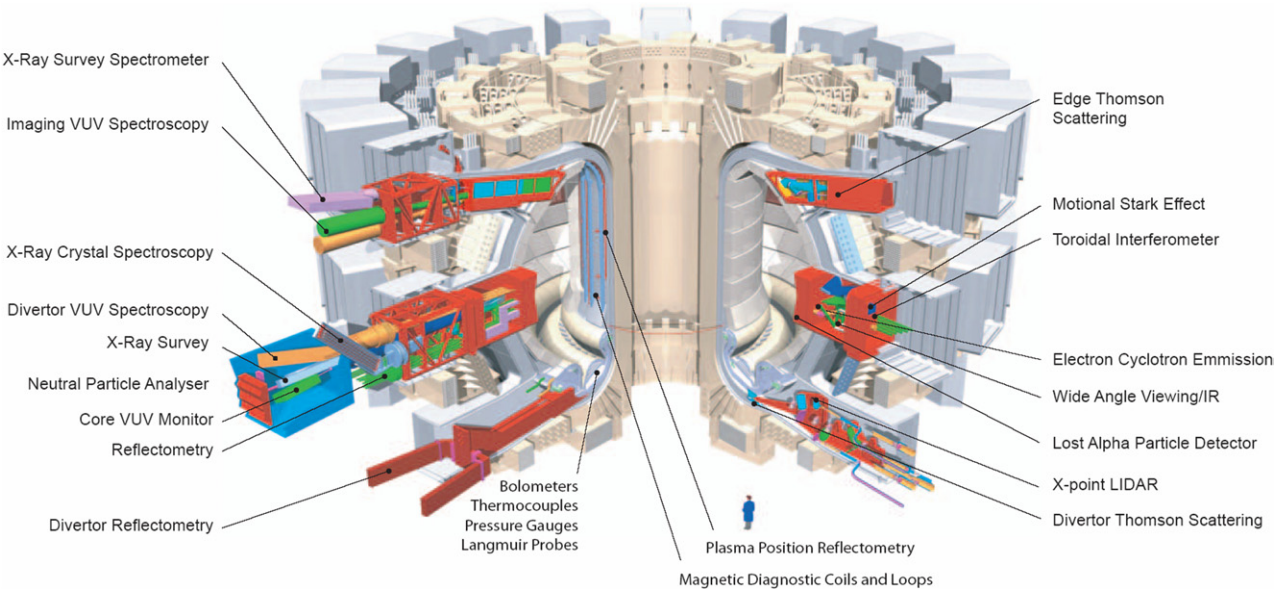

Figure 15. Cut-out view of ITER to visualize some typical diagnostics in upper and equatorial ports, as well as in the diagnostic divertor cassettes.

bends, as near to 90° as possible, minimizing the total waveguide length and leaving space for manual access to bends and joints.

In-vessel installations. The principal diagnostic components mounted in the vacuum vessel are sensors for the magnetic diagnostics, bolometers, soft x-ray and UV detectors and waveguides for reflectometry. A number of them will provide measurements essential for basic tokamak operation. Diagnostic systems are present in all sectors of the vacuum vessel and the number and location of systems is driven by measurement considerations. Particularly on the inboard side of the VV, the limited space for cabling makes particular

Diagnostic - unit	1	2	3	4	5	6	7	8	9	10	11	12	13	14	15	16	17	18
Outer flux loops - loop feed point				3												3		
Outer vessel sensors - 2-axis coil pair				40		40		40					40		40		40	
Outer vessel sensors (steady state) - 2-axis Hall probe			40		40		40					40		40		40		
Continuous flux loop - loop feed point				2						2						2		
HF coil poloidal array - coil			20			20			20			20			20			20
MHD - dedicated saddle loop	8		8		8		8		8		8		8		8		8	
Partial loops			18			18			18			18			18			18
Resistive wall mode sensors - coil		1			1			1			1			1			1	
Tangential, normal and toroidal coils, hardwired coil		34						34						34				
Tangential, normal and toroidal coils, replaceable coil				34						34						34		
Diamagnetic loop			1						1						1			
Diamagnetic loop compensation coil			1						1						1			
Diamagnetic loop compensation saddle loop			2						2						2			
Halo Rogowski poloidal array - coil	14			14			14			14			14			14		
Halo Rogowski toroidal array - coil	4	4	4	4	4	4	4	4	4	4	4	4	4	4	4	4	4	4
Vertical neutron camera (VV divertor level) - collimator						2												
Microfission chambers - detector			6									6						
Neutron activation (^{16}N fluid) - irradiation station							1											
Neutron activation (foil capsule) - irradiation station						4	1				3	1						1
Lost alpha detector	2																	
Collective Thomson scattering - waveguide												8						
Bolometer array - miniature camera with 5 lines of sight	4					4	5	1							2	4	3	
Soft x-ray array - detector with 2 or 3 lines of sight	13	6	6	4	6						14		16	4				
Position reflectometry - waveguide and antenna		2												2				
Fast-wave reflectometry - coil (quantity and location unknown)																		
Main reflectometry (high field side) - waveguide and antenna								4									4	
Refractometry - waveguide and antenna									4									
Thermocouples - inboard thermocouple element	4	4	4		4			4	4		4			4			4	
Thermocouples - outboard thermocouple element	3			6						6						6		
Dust monitor - location (type and location unknown)																		
Cryostat cabling - 100 core loom			5		5		5					5		5		5		
Divertor port cabling - 80-way feedthrough		8		3		1		8		4		1		6		7		1
Upper port cabling - 48-way feedthrough	4	3	5	3	3	5	5	3	3	5	4	2	5	3	4	6	2	4
VV wall poloidal cable conduits - 36-core loom	3	2	4	2	2	4	3	2	2	3	2	2	3	2	2	4	2	2

ITER_D_22239V

Figure 16. Distribution of diagnostics mounted on the vacuum vessel. The bold numbers in the top row of the figure refer to the toroidal location (sector) on the vacuum vessel. The numbers in the table indicate the total number of diagnostic units of each type.

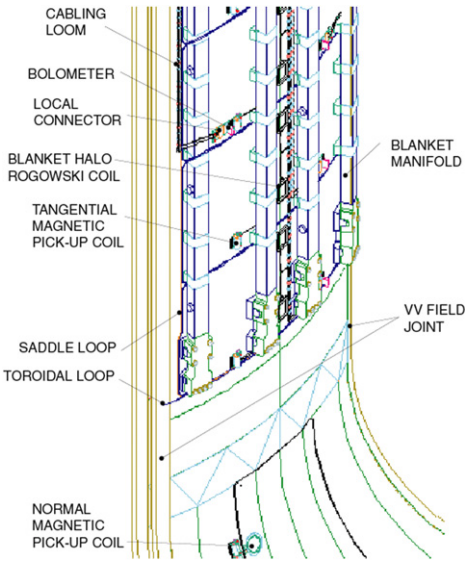

Figure 17. Part of the inboard vacuum vessel with blanket and divertor removed, showing diagnostic sensors (magnetic pick-up coils and bolometers) positioned near blanket gaps and cabling looms running alongside the blanket cooling manifolds.

demands on the allocation of systems. The locations of the in-vessel diagnostics are summarized in figure 16.

The integration of the diagnostic components (shown in figure 17) has to follow certain guiding principles. For example, the magnetic pick-up coils require a particular distribution with respect to each other, and microfission chambers are located at two toroidal positions. Sensors are mounted at sites where the maximum protection possible is sought from the blanket modules, with standard cut-outs provided if extra space is required. Where necessary the plasma is viewed through the gaps between blanket modules, which may have to be locally widened. Sensors and cabling are cooled by conduction to the vacuum vessel and thermal radiation to the blanket, yet must still operate at elevated temperatures. Systems essential for tokamak operation require either redundancy or reparability. Attention also has to be paid to the installation of the cabling and the sensors and this has to be integrated into the assembly plan of the vacuum vessel.

Equatorial port diagnostic installations. Of the 18 equatorial ports on ITER, three regular ports are dedicated to diagnostics, with two more that are allocated to remote handling outside the tokamak operation having diagnostics that can be removed rapidly. The number of diagnostic systems, or their capacity (number of channels, etc), that can be accommodated on ITER depends on this quantity, their location with respect to the heating beams, uniformity of distribution, etc.

Many factors are taken into account in optimizing the distribution of diagnostics within the ports available and some guiding principles have been developed. Because

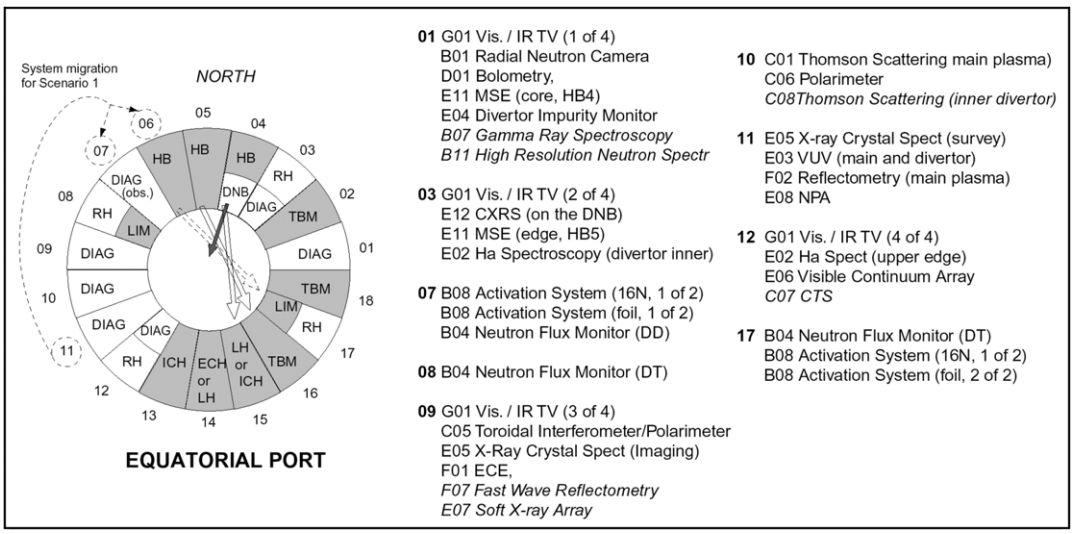

Figure 18. Allocation of diagnostics to equatorial ports (showing relocation of systems on port 11 which will be necessary if heating upgrade scenario 1 (additional RF systems) is selected).

of neutron streaming considerations, typically no more than two systems with large labyrinths can be installed in one port, with large-aperture systems placed near the port centres; distributed systems are uniformly located toroidally, sometimes coordinated with the location of corresponding systems in the upper ports. Active spectroscopy systems have to view the diagnostic or heating neutral beams. (Charge-exchange recombination spectroscopy has to view the diagnostic neutral beam and motional Stark effect spectroscopy a heating neutral beam.) The directly coupled systems (neutral particle analyser, vacuum ultraviolet spectrometer and x-ray crystal spectrometer) will be in secondary containment and so can be allocated to any port. Systems sensitive to gas and pellet injection must be positioned away from these systems. The reference port allocation that takes into account these requirements is shown in figure 18.

In-vessel diagnostic equipment in each equatorial port is mounted in a port plug assembly as shown in figure 19. This provides the primary vacuum boundary at that port, as well as the feed-out for diagnostic signals (windows and feedthroughs) and feed-in for control signals. Within the primary vacuum it provides the support for the diagnostic equipment, the shielding (equivalent to that lost accommodating the diagnostic channels) and the support for the blanket shield module with its first wall protection and shielding. First wall apertures are minimized by generally making use of common apertures. The most severe design conditions are seen where diagnostics must obtain a tangential view of the plasma and then necessarily extend far forward into apertures in the blanket.

The front portion of each diagnostic port plug is a blanket shield module, which performs the first wall function and provides shielding equivalent to blanket modules and vacuum vessel at this location.

Accommodating diagnostic channels within labyrinths in the port plug brings about the most significant limitations to the diagnostics. The primary concern is to provide sufficient shielding, equivalent to that lost accommodating the diagnostic channels, to limit the nuclear heating of the cryogenic coils of the magnet system, and this brings competition for space

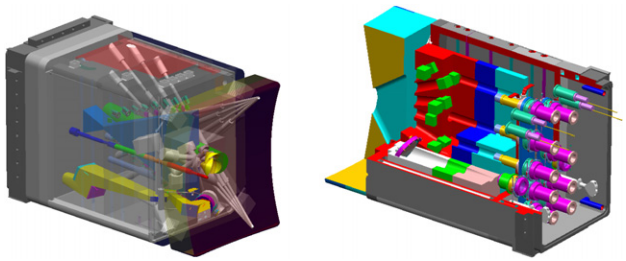

Figure 19. Equatorial port plugs. Left: (port plug #01) showing first wall apertures minimized and the internal complexity mainly of apertures and right: (port plug #10) showing the physical congestion experienced at the flange face.

between the diagnostics. The shielding is also required to avoid activation of the reweldable flange components of the port duct. Modular subassemblies are used within the port plugs. Services and cooling connections, mechanical attachments, positioning and alignment are simplified to standardized arrangements using standard tooling. Before and after maintenance of the port, the plugs are tested in a dummy port test stand. The port plug modularity allows a single concept for remote maintenance of all the port plugs and a standardized approach for hot cell maintenance.

The safety rules for the primary vacuum boundary require a double barrier for fragile or complex elements such as windows. In some ports there are a relatively simple connection between the port plugs and the port cell equipment while in others there are substantial connections of transmission lines or vacuum extensions. The latter, for the vacuum ultraviolet, x-ray crystal spectrometry and the neutral particle analysis systems, requires the use of welded vacuum extension(s) and these are contained in dedicated shielded containment enclosures.

Diagnostic equipment beyond the port plug is generally attached to the port plug flange but is sometimes incorporated in the building or biological shield plug depending on alignment needs, weight, etc. This must all be removed to access the port plug.

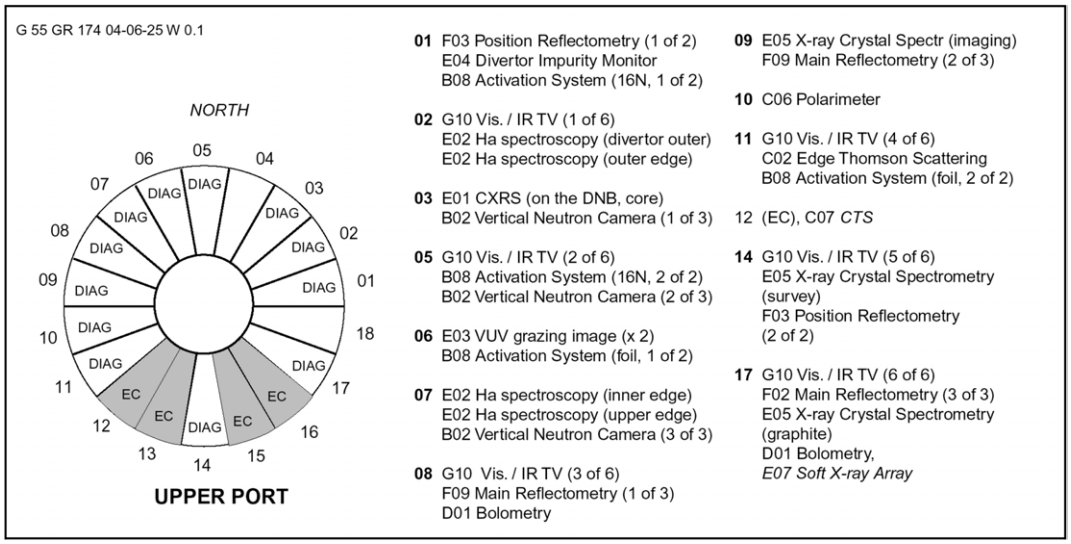

Figure 20. Allocation of upper port plug diagnostics.

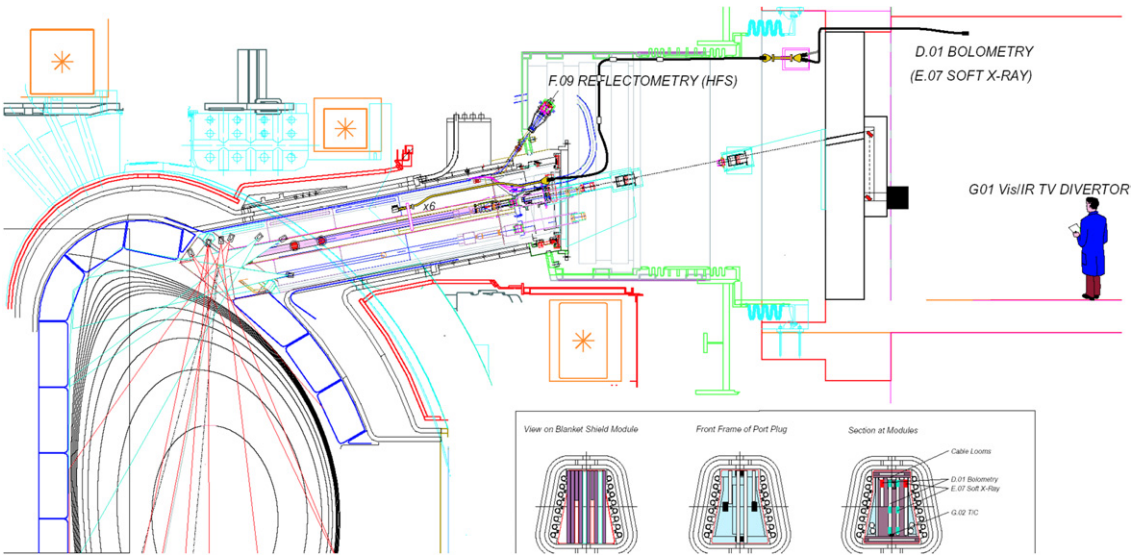

Figure 21. Upper port #08 with the port plug installed. The reflectometry waveguides and vv diagnostic cabling (not shown) are fixed in the port. The bolometer cameras are mounted in the first module of the port plug and the visible/infrared TV periscope is located in the long-central tube.

Upper port diagnostic installations. Diagnostic equipment is installed in port plugs in the upper ports using the same concepts and approaches as those developed for the equatorial ports. Again a similar set of optimization guidelines has been used in the allocation of specific diagnostic systems, as shown in figure 20. Here not more than one high neutron throughput (large viewing aperture) system per port is allowed. The port plugs are, however, significantly longer than those at the equatorial plugs and generally less heavily electromechanically loaded. One frequent general variant of the port plug design is the presence of a central tube extending to the full length, as shown in figure 21, used in some cases to improve the maintenance access to components at the front of the port plug. Generally a steep view into the plasma core or divertor legs is required, necessitating some exposed sites for mirrors, etc. Nevertheless the diagnostic system is the primary system at this level and makes as much use of these ports as possible. Thus 12 of the 18 upper ports have diagnostic equipment installed in diagnostic port plugs and the ports are also the main conduit route for VV diagnostic cabling.

Divertor diagnostic installations. In the divertor, diagnostic components are concentrated in the cassettes that can be accessed by the three remote handling ports and two diagnostic ports. Divertor ports must also accommodate cryopumps, gas and pellet injection systems, glow discharge cleaning probes, in-vessel remote viewing equipment, maintenance detritiation systems, cassette remote handling (RH) features and neutron shielding. Guiding principles have also been developed for allocation of diagnostics to ports at this level. RH systems have to be installed with toroidal symmetry (divertor port #2, 8 and

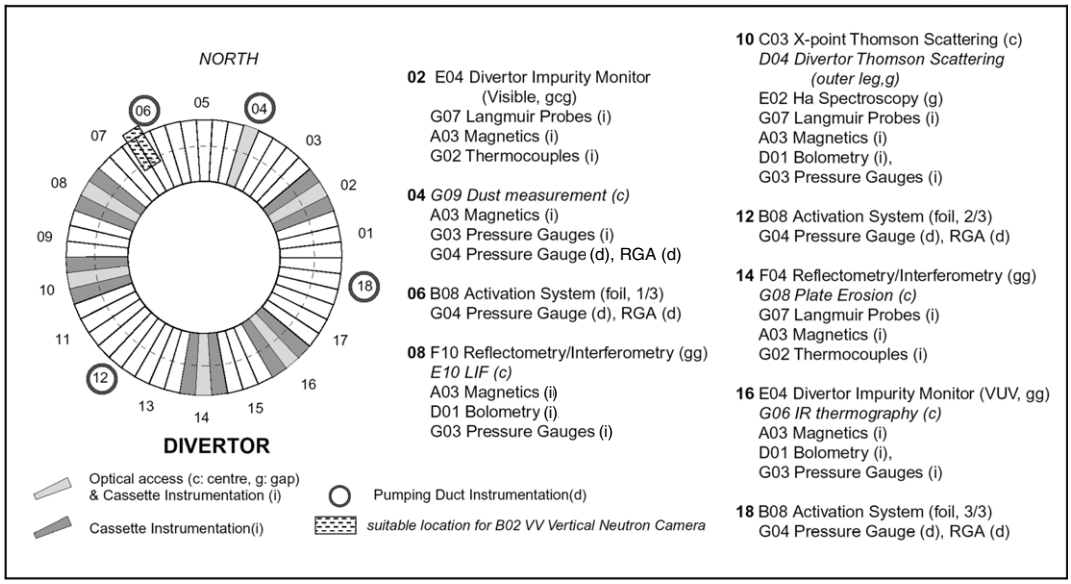

Figure 22. Allocation of diagnostics and other systems at the divertor.

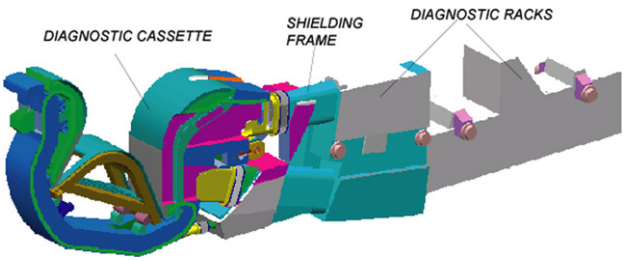

Figure 23. Arrangement of divertor diagnostic cassette and diagnostic racks, shown as assembled in the torus and port.

14); diagnostic ports have a large part obscured by the toroidal rails bearing the cassettes; systems requiring heavy wiring are distributed toroidally as evenly as possible; diagnostics with substantial equipment on a divertor cassette, or with equipment in the port, are located on central cassettes at the three RH ports, #2, #8 and #14; and the magnetic pick-up coils require uniform distribution over six toroidal positions. The distribution of diagnostics at this level is shown in figure 22.

Optical diagnostics make use of the central aperture of the cassette and the gaps between the cassettes, which are widened in special cases. At the centre of each location available to diagnostics there is a diagnostic cassette. This is a standard divertor cassette modified to incorporate optical and microwave diagnostics while allowing remote maintenance in the same way as for standard cassettes. On either side of this are two instrumented cassettes. special modular assemblies incorporating sensors, such as Langmuir probes, bolometers, pressure gauges, halo current Rogowski coils and wiring, are mounted on the cassette sides.

In the divertor (RH- or diagnostic-) ports, diagnostic equipment is installed in diagnostic 'racks' which make use of the rails in the port provided for the cassette removal tools (see figure 23). Permanent cabling for instrumented and diagnostic cassettes is routed along the port.

6. Summary of progress in key issues identified in the ITER Physics Basis

Since the publication of the ITER Physics Basis (IPB) in 1999 [7], much progress has been made in the development of diagnostics for burning plasmas and especially ITER. Many of the developments have been stimulated and guided by the ITPA Topical Group on Diagnostics. The Topical Group has highlighted the most important and urgent topics as high priority issues and this has drawn the attention of the international diagnostics community to the problems and stimulated work on them. The high priority issues are reviewed on an annual basis. The progress in the resolution of the main issues since the publication of the IPB is described in this section. Table 6 gives a comprehensive brief summary of the progress in all the issues identified in the IPB.

The established technique to measure the fuel ratio n_D/n_T in the plasma core is based on neutral particle analysis (NPA). It is questionable whether the NPA can be used to measure the fuel ratio in the core ($\rho < 0.3$) of ITER. Therefore, it is important to develop alternative techniques. One potential alternative is the fast-wave reflectometer/interferometer. Such a system has been successfully demonstrated on DIII-D in H/D plasmas [236]. A fast-wave reflectometer is presently being designed for JET. Another method that has been suggested is to measure the fuel ratio by means of a fast-ion collective Thomson scattering in the microwave region [35]. This can be done in conjunction with the system that is required for studies of confined alpha particles and fast ions, albeit an additional array of receiver horns is required.

Techniques are required which are capable of measuring erosion of the target plates in real time: various systems have been studied including Speckle interferometry [220] and optical radar. The latter system has been used on TFTR [305] and a dedicated system has been proposed and designed for ITER [306]. This system in principle meets the ITER target requirements for measuring the erosion and now needs to be

Table 6. Progress in the field of diagnostics.

Requirement	Progress since the ITER Physics Basis
Open issues at the time of the ITER Physics Basis	
Development of alternative methods for measuring core n_D/n_T ratio.	The measurement of the isotope ratio by a fast-wave reflectometer has been demonstrated on DIII-D. Feasibility studies have demonstrated that the ratio can be also measured by fast-ion collective Thomson scattering.
Development of methods for measuring divertor tile erosion in real time.	An optical radar system has been designed that in principle can measure the erosion within the requirements. The method still needs to be demonstrated in a present device.
Determination of lifetime of plasma facing mirrors used in optical systems and determination of lifetime of optical elements in the divertor.	Much work has been done in this field. Erosion of mirrors is no longer thought to be a problem because the effects on the reflectivity and the polarization of the reflected light are small. Present research concentrates on quantifying deposition and developing models for understanding deposition, as well as on developing protection and mitigation methods.
Development of methods of measuring the energy and density distribution of confined alpha particles.	It was demonstrated that fast-ion collective Thomson scattering can diagnose the confined alpha particle populations over the full radial profile and within the measurement requirements. Other methods based on charge exchange recombination spectroscopy, neutral particle analysis and neutron emission spectroscopy are also under investigation.
Development of methods of measuring the number and energy of escaping alpha particles.	This is still a field of high concern. It is not clear whether standard methods to diagnose escaping alpha particles (scintillators and Faraday cups) can withstand the vulnerable environment. Methods based on real-time activation and imaging bolometers are being tested but their application to ITER is not clear.
Devise new concepts for measuring light in core impurities (e.g. He ash) that do not rely on the diagnostic neutral beam.	In case the diagnostic neutral beam could be avoided, this would be a large cost-saver. No new concepts have been developed since the IPB. But the DNB has been incorporated in the measurement of more parameters and now therefore has a wider support.
Devise new concepts for measuring $j(r)$ that can be applied to ITER with sufficient spatial resolution.	Since the potential show-stoppers for polarimetry (lifetime of retro-reflectors) and MSE (lifetime and neutron throughput of optical viewing system) have been resolved, this point has been taken off the list.
Determination of impurities in divertor using only visible and UV spectroscopy.	Much progress was reported in this field. Although the developments are promising, it still needs to be assessed whether all necessary measurements can be made using only visible and UV spectroscopy.
Development of new methods to measure steady-state magnetic fields accurately in a nuclear environment.	Radiation-hard Hall probes have been developed that are claimed to be able to measure steady-state magnetic fields outside the ITER vacuum vessel. Integrators that are compatible with 1000 s operation have been developed. Main problems in the field of magnetic measurements are the effects of the radiation and thermal induced electromotive forces and the radiation induced thermo-electric sensitivity.
Demonstration of direct measurement of local electric field.	This measurement is relatively low on the priority list and therefore not much progress has been reported, albeit a HIBP system for ITER has been proposed.
Measurement of runaway electrons.	A feasibility study for measuring runaway electrons by observing their synchrotron emission has demonstrated its applicability to ITER.
Measurement of core density profile and MHD activity.	This is no longer thought a point of major concern. The core density profile can be measured by various methods, as well as the MHD activity.
Measurement of density profile across divertor leg.	Various methods have been proposed (divertor Thomson scattering, spectroscopy and LIF) and good progress has been made, albeit no method proposed thus far can match the measurement requirements.
New issues	
Review requirements for measurements of neutron/alpha source profile and the assessment of possible methods of measurement.	A combination of radial and vertical neutron camera is proposed to measure the 2D neutron/alpha source profile. It still needs to be demonstrated by simulations that a full 2D measurement is required and that the proposed system can resolve the expected asymmetries.
Development of measurement requirements for dust and assessment of techniques for measurement of dust.	This new issue is combined with the one on erosion mentioned above. A strategy for handling dust still needs to be developed as well as requirements for the measurement of dust.
Determination of the outgassing rates of mineral insulated cables and developing methods to reduce the outgassing rates.	ITER will have several tens of km of mineral insulated (MI) cable in the vessel. The outgassing rate of the cables can have a large effect on the pump-down rate of the vessel. Present studies are focused on studying the outgassing rates of various types of cables with and without artificially made perforations.
Measurement of core density fluctuations.	This measurement is relatively low on the priority list and therefore not much progress has been reported. It is envisaged that core density fluctuations are obtained parasitically by the various reflectometer systems.

tested in a present device (preferably one with relevant erosion rates).

The development of plasma viewing mirrors that can fulfil their specific functions under the specific environmental conditions in ITER is a very important subject that has been a high priority issue for many years. Considerable progress has been reported since the publication of the IPB and has been summarized in section 4.3.

Much progress has been made in the development of diagnostics that can measure the confined alpha particles. Fast-ion collective Thomson scattering in the microwave region can diagnose the confined alpha particle population over the full radial profile and largely meets the measurement requirements [35]. Other methods including charge-exchange recombination spectroscopy, neutral particle analysis and neutron emission spectroscopy can be also applied to study the alpha particles in specific energy ranges. The measurement of the escaping alpha particles is very difficult. Potential techniques under investigation in present devices such as scintillators and Faraday cups may not be able to cope with the vulnerable environmental conditions. New methods based on real-time activation [229], imaging foils [177] and ceramic scintillators [52] have been proposed, and some of them are being tested. However, their potential for application in ITER is still unclear.

The main motivation for the diagnostics neutral beam (DNB) is to provide the measurement of the spatial distributions of light impurities in the plasma core, and especially the He ash, through charge-exchange recombination spectroscopy (CXRS). If the measurement could be made without a DNB there would be a significant cost saving, but no new concepts that could provide this measurement have been found. The presence of the DNB is being fully exploited and it is now also expected to provide information on the q-profile through the motional Stark effect (MSE).

At the time of the IPB, very difficult implementation problems had been identified for both the polarimeter (the lifetime of the corner cube reflectors) and the motional Stark effect (MSE) system (lifetime of the mirrors and neutron throughput through the optical viewing system). Hence new concept techniques for measuring the current density profile were being sought but unfortunately none were found. However, it appears that the implementation problems can be solved and a successful application of both these techniques is expected.

In the area of magnetic field measurements, integrators have been developed that are compatible with 1000 s operation of ITER. Radiation-hard Hall probes have been developed that are claimed to be able to measure steady-state magnetic fields at locations immediately outside the ITER vacuum vessel [307]. Inside the vacuum vessel one still has to rely on magnetic coils and many irradiation experiments have been devoted to understand the effects of the radiation induced electro-motive force (RIEMF), temperature induced electro-motive force (TIEMF) and radiation induced thermo-electric sensitivity (RITES). In general it is thought that coils can be manufactured that can withstand the specific conditions in ITER, but much further work is needed to find the optimum material and geometry choices for the coils.

Various methods have been proposed for the measurement of the local electric field in the ITER plasma core. For example, a heavy-ion beam probe system has been proposed for ITER [308] and could potentially measure the electric field for $\rho > 0.7$. More recently, considerable progress has been reported in the field of Doppler reflectometry (see section 4.1). Results indicate that it should be possible to measure E_r and the E_r shear and also fluctuations in E_r [234].

Existing techniques for the measurement of runaway electrons, e.g. the measurement of the x-ray emission, will be difficult or even impossible because of the intense gamma background. Much work has been devoted to developing a diagnostic based on the observation of the synchrotron emission from the runaway electrons [205]. Such a system is thought to be able to measure simultaneously the runaway current, energy and pitch angle distribution. A feasibility study has demonstrated that such a system could be implemented on ITER [205].

At the time of the IPB, the measurement of the core density profile and also of the MHD activity were thought to be points of major concern. Since the core density profile as well as the MHD activity can be measured by various methods, this is no longer thought to be an issue.

The final issue that was mentioned in the IPB was the measurement of the density profile across the divertor leg. There have been developments in diagnostics that can provide density information on the divertor including divertor Thomson scattering, spectroscopy and laser-induced fluorescence. However, none of these methods can meet the measurement requirements which are very demanding (spatial resolution of 3 mm across the leg). In principle, this measurement can be made by reflectometry and a system is tentatively planned for ITER, but there has not been a successful demonstration of the technique in the divertor region.

Since the publication of the IPB a number of new issues have been defined. One of them concerns the measurement (and the requirements) of the two-dimensional neutron/alpha source profile. Although it is generally assumed that both a vertical and radial neutron camera (VNC and RNC) are required to measure the 2D source profile, to be able to diagnose potential asymmetries in this profile, it is thought to be necessary to have this assumption supported by modelling calculations. The design of the RNC for ITER is well advanced. A design for a VNC viewing up from the divertor port is under development.

The potential of dust being a safety hazard was only just beginning to be realized about the time of the IPB and so the measurement of dust was not required at that time. Measurements of dust can only be made in specific locations but the safety inventory limits are set on the total amount of dust on the hot and cold surfaces. The requirements for the measurement of dust are still being developed. Only after these have been determined will it be possible to select and design specific diagnostic systems. On the other hand, progress with techniques which can measure dust—for example, Mie scattering [309], electrostatic grids [228] and capacitive microbalances [226]—has been reported, but much more progress is needed in this specific field.

ITER will have several tens of km of mineral insulated cables in the vessel. The outgassing rate of these cables can have a large effect on the pump-down rate of the vessel. Present

studies are focused on studying the outgassing rates of various types of cables with and without artificially made perforations.

Finally, the measurement of core density fluctuations has been identified as a potential issue. This measurement is difficult to make because of accessibility problems. However, it is expected that there will be some capability using reflectometry, although the application will require special antennas viewing from the (difficult) high field side and the use of the lower x-mode cut-off.

In conclusion it can be stated that much progress has been made in the field of diagnostics since the ITER Physics Basis. A number of issues have been resolved and a few new issues have been formulated.

7. Assessment of measurement capability for ITER

The development of diagnostics for ITER is still in progress and more design and R&D is needed before the diagnostics are ready for implementation. However, it is useful to try and assess where the development stands at this stage relative to the defined measurement requirements as a guide to where future work should be focused. The ability of the diagnostic systems to meet their individual measurement requirements depends on factors that are in general different for each generic group of diagnostics, and so these are assessed separately. As usual the discussion is based on the ITER systems.

For the magnetic diagnostics, it is expected that it will be possible to install a configuration of sensors that will meet the measurement requirements and so it should be possible to measure the appropriate plasma parameters to the desired level of resolution and accuracy. A particularly difficult area is the repair and maintenance of the in-vessel diagnostic components and so a key issue is the lifetime of the in-vessel coils and loops. Although it is believed that necessary lifetimes (no change during the machine life) can be achieved using materials examined in the supporting radiation effects R&D programme, at least one backup system should be included for key control measurements. The most vulnerable sensors are in the divertor cassette and have been designed for quick replacement.

In situ irradiation tests of magnetic coils have shown that multiple effects, in particular, RIEMF and RITES, can occur simultaneously and, in application on ITER, could lead to spurious voltages which would compete with the signal voltages. Extensive tests have been carried out. Although there are still aspects of the results not fully understood, it is probable that coils can be developed for ITER in which the combined action of RIEMF, RITES and other related effects is tolerable, and it may be possible to use the coils for measurements on long-(>1000 s) pulses. The development of steady-state sensors and long-pulse integrators also shows progress and it is likely that Hall sensors can be developed for applications outside the ITER vacuum vessel.

No insurmountable difficulties are expected for the implementation of the neutron flux monitors and activation systems. However, the ability of the neutron cameras to provide the measurements for which they are intended, for example the total fusion power and the neutron source profile, is directly linked to the available access. A wide angle of view is necessary in the radial or vertical directions and preferably in both, in case there are significant asymmetries in the profile of the neutron emission. It is believed that this can be achieved in the radial direction and so it should be possible to obtain the total fusion power with the radial camera. If the neutron emission can be relied on to be constant on a flux surface, then the radial measurements combined with the magnetic measurements should be enough to deduce the neutron source profile. Under some conditions, for example at high levels of ICRH with low Q value when asymmetric distributions of fast ions are created, the neutron emission may not be a constant on a flux surface and two views will be needed. A concept for a vertical viewing camera at the lower level is under development but several difficult interface issues need to be worked through.

Compact neutron spectrometers exist and it is feasible to install them in the radial neutron camera. However, high resolution spectrometers are needed for some measurements and these tend to be large and/or require a close coupling to the plasma, and implementation on ITER is problematic. The most suitable would appear to be a high resolution time-of-flight spectrometer but the performance of currently available instruments is not adequate and some R&D is needed. The calibration of the neutron diagnostics is another difficult area and requires development for ITER conditions.

All optical/IR, spectroscopic and microwave systems view the plasma with a mirror and a critical issue is the lifetime of this component. It is believed that solutions for the first mirrors exist where they operate in situations where the dominant potentially damaging mechanism is erosion due to the bombardment of high energy neutral particles. This may be the case for most systems installed in the equatorial and upper ports. However, it is possible that deposition of eroded first wall material or viewing duct material will also occur, leading to a degradation of optical performance. Mitigating methods in this case would be baffles in the duct, cleaning techniques and/or shutters in front of the mirror. Shutters are highly desirable and will be incorporated, but their duty specification is not yet established. Their engineering design still requires detailed study.

For diagnostic components in the divertor, it is probable that deposition of eroded material will be the dominant potentially damaging mechanism. At this stage, only limited information is available on this process. More investigations and developments are required before the extent of the problem is really known and the most effective countermeasures can be selected. Alternative views from the equatorial and upper ports are provided where possible.

A bolometer that is believed to be sufficiently radiation hard for use during the initial DT operation exists, but a device with enhanced radiation hardness may be required for the anticipated end-of-life fluence level of the machine. Potentially suitable devices are being investigated in a supporting R&D programme. Dedicated development is likely to be necessary.

A design for the implementation of the spectroscopic systems which require direct coupling to the vacuum vessel (x-ray crystal, VUV spectrometers and NPA systems) has been developed for the measurements on the main plasma and it is believed that good performance will be achieved. In the divertor the VUV measurements are more difficult, and the visible and near UV capability needs to be exploited.

Table 7. Assessed measurement capability relative to requirements.

GROUP 1a Measurements for machine protection and basic control	GROUP 1b Additional measurements for control in specific scenarios	GROUP 1c Additional measurements for performance evaluating and physics
Plasma shape and position, separatrix–wall gaps, gap between separatrixes	Neutron and α-source profile	Confined α-particles
Plasma current, $q(a)$, $q(15\%)$	Helium density profile (core)	TAE modes, fishbones
Loop voltage	Plasma rotation (toridal and poloidal)	T_e profile (edge)
Fusion power	Current density profile (q-profile)	n_e, T_e profiles (X-point)
$\beta_N = \beta_{tor}(aB/I)$	Electron temperature profile (core)	T_i in divertor
Line-average electron density	Electron density profile (core and edge)	Plasma flow (divertor)
Impurity and D,T influx (divertor and main plasma)	Ion temperature profile (core)	$n_T/n_D/n_H$ (edge)
Surface temp. (divertor and upper plates)	Radiation power profile (core, X-point and divertor)	$n_T/n_D/n_H$ (divertor)
Surface temperature (first wall)	Z_{eff} profile	T_e fluctuations
Runaway electrons	Helium density (divertor)	n_e fluctuations
'Halo' currents	Heat deposition profile (divertor)	Radial electric field and field fluctuations
Radiated power (main plasma, X-point and divertor)	Ionization front position in divertor	Edge turbulence
Divertor detachment indicator (J_{sat}, n_e, T_e at divertor plate)	Impurity density profiles	MHD activity in plasma core
Disruption precursors (locked modes, $m = 2$)	Neutral density between plasma and first wall	
H/L mode indicator	n_e of divertor plasma	
Z_{eff} (line-averaged)	T_e of divertor plasma	
n_T/n_D in plasma core	Alpha-particle loss	
ELMs	Low m/n MHD activity	
Gas pressure (devertor and duct)	Sawteeth	
Gas composition (divertor and duct)	Net erosion (divertor plate)	
Dust	Neutron fluence	

Note: Expect to meet measurement requirements; performance not yet known; expect not to meet measurement requirements.

For the microwave measurements (electron cyclotron emission and reflectometry) which are made from the low-field side, no insurmountable problems are foreseen. A conceptual design exists for the installation of the antennas and waveguides for the reflectometry measurements on the high field side and at various locations on the poloidal cross-section for the plasma position reflectometer. The details of these designs are under development.

The integration of waveguides through the divertor ports and in the divertor cassettes has been studied and appears feasible. However, the R&D on the associated diagnostics, in particular divertor reflectometry, is still at an early stage, and so the optimum design for the diagnostics and the information that can be obtained from these measurements are not certain.

A promising design has been developed for the wide-angle visible/infrared viewing diagnostic and it is expected that it will meet its measurement specifications. A key issue is the extent of surface coverage that is necessary. For the current ITER design, sufficient cameras are envisaged to give coverage of 75% with resolution in the range 3–30 mm. About 56% of the inner divertor target plates and 70% of the outer divertor target plates are covered. Measurement of the surface temperature of the divertor plates is important for operation and conventional imaging systems are difficult to implement in the restricted divertor space. The novel IR multiplexing technique has the potential to provide the required measurements but there is no experience with using such a technique on existing machines.

No insurmountable difficulties are foreseen with the basic operational diagnostics such as pressure gauges and gas analysers.

Substantial progress has been made with the design of the diagnostic neutral beam and its integration onto the tokamak. It is expected that charge-exchange recombination spectroscopy (CXRS) will provide measurements of the He ash in the core as required.

Returning to the parameters that have to be measured (table 1), it is convenient to group them into three basic groups: those required for basic machine protection and basic plasma control (group 1a); those that may be used in more advanced control (usually profile measurements) (group 1b); and additional measurements for performance evaluation and physics studies (group 2). The design and R&D work carried out to date has shown that it should be possible to measure many of them at the specified level. In particular, it is expected that most of those needed for machine protection and basic control will be measured as required. There are difficulties with some of the measurements necessary for advanced control, for example the lost alphas, but it is too early in the design process to determine what consequential effects, if any, there will be on the operation of the tokamak. Some of the measurements that are intended solely for physics purposes also have implementation difficulties. The assessed situation relative to the defined measurement requirements for each parameter is shown in table 7.

Current design and R&D work is focused on the areas where the requirements are not yet met. In one area, the measurement of dust, the measurement requirements are not yet sufficiently developed to enable systems to be designed even at the conceptual level. However, candidate measurement techniques are being developed in the laboratories of the ITER partners and work is ongoing to determine a strategy for dealing with dust. Once this is developed the measurement requirements can be specified.

For the integration of diagnostic components with the main elements of the tokamak, feasible concepts have been developed for the installation and maintenance of diagnostic sensors and components in the vacuum vessel, in upper and equatorial ports and in the divertor region. The interfaces with the vacuum vessel, other machine components, assembly and maintenance facilities have been developed. At the equatorial and upper levels, guidelines for optimizing the distribution of diagnostics into the available ports have been developed and applied. Promising design concepts for the port plugs that will allow the installation of multiple diagnostics into each port have been developed. At the divertor level, the concept of installing diagnostic components on, and in, the divertor cassettes allows for relatively easy installation and maintenance. Engineering development and analysis of these concepts is needed.

8. What can be learnt from operation on ITER

During the later phase of the ITER programme there will be prolonged operation of the tokamak at high levels of fusion power, probably utilizing only one or two plasma operating scenarios. The chosen operating scenarios are likely to be those that will be used in the prototype reactors that will follow ITER. A high number of high performance, essentially identical, pulses are expected. On the approach to this phase, and during the phase itself, extensive information will be obtained which will enable the establishment of the base on which the diagnostics for the reactor grade machines that will follow ITER (next step device (NSD)) can be selected and designed.

The measurements needed to support the selected high performance operation scenarios, and the role of the individual measurements in the control and evaluation of the plasma performance, will be determined. Similarly, the measurements necessary for protecting the plasma facing components, especially the first wall and divertor from damage due to off-normal events for these particular scenarios, will be selected. The specifications of the measurements—parameter ranges, time and space resolutions, accuracies, etc—will also be determined. The requirements of the diagnostic system to support reactor grade operation will thus be established on the basis of experience with ITER.

As pointed out in section 1, several environmental aspects, especially the high levels of neutron flux and fluence, nuclear heating, gamma radiation and plasma irradiation, will give rise to the occurrence of physical phenomena, such as RIEMF, radiation induced conductivity (RIC) and radiation induced absorption, in the materials of the diagnostic components. These will limit the lifetime of components and sensors, and can generate spurious signals. Tests with fission reactors, plasma simulators and current tokamaks can approach the conditions expected in high performance ITER operation but the combination of conditions that will occur in ITER, and devices that follow ITER, cannot be created. Operation at high performance levels in ITER will enable the extrapolation of the database of these effects to the reactor-relevant domain, and in that domain tests and validation of the theories and models of these effects will be performed.

While it is possible to achieve values of plasma parameters in today's tokamaks that are similar to those expected in ITER, such conditions can usually only be produced for short times and not in combination. Nevertheless, they can be achieved for sufficiently long enough to validate the underlying physics of most of the candidate diagnostics and this has been done or is underway. In some cases, however, this is not possible. For example, under some plasma conditions it is expected that the ITER plasma temperature will be very high ($T_e > 40$ keV). At these levels, effects not usually experienced in current applications will be prominent, for example, relativistic effects in Thomson scattering, electron cyclotron emission and reflectometry measurements. Similarly, the fusion burn conditions of ITER will represent a unique opportunity for testing the physics of fusion product diagnostics. Examples include the alpha knock-on effect and the possibility to separate the neutron emission from fuel ions of different energies.

Several diagnostics to be implemented on ITER are specifically focused on the high performance, long-pulse operation, for example, diagnostics for the confined and escaping alpha particles, measurements of steady-state magnetic fields, plasma position reflectometry and diagnostics for the measurement of erosion and dust. Only a limited validation of these can be achieved on existing machines because of insufficient plasma performance. On the other hand, the measurements they provide are expected to be needed for the step beyond ITER. Operation on ITER will provide a unique experience and establish the base of performance necessary for a selection of the next step.

Clearly it would not be practical to install on an NSD all the diagnostics that are currently planned for ITER. The intended routine operation of the device utilizing only one or two operating scenarios should mean that a smaller number of measurements, and hence diagnostic systems, would be needed. The use of predictive and analysis codes, which combine the data from multiple diagnostics in an intelligent way, should also reduce the number of measurements required, and experience with these codes on ITER will enable the selection of the optimum set of measurements to be made. Moreover, the experience gained in operating diagnostics on ITER should enable the systems that are best able to cope with the harsh environment to be selected. Real-time handling and processing of large quantities of data, including real-time data validation, and possibly in-pulse calibration will also be needed and techniques and hardware to perform these functions will be developed. On the basis of experience on ITER, it should therefore be possible to optimize the diagnostic system for an NSD in terms of both the measurements required and the measurement systems.

The long pulses will mean that real-time handling and processing of large quantities of data, including real-time data validation, and possibly in-pulse calibration will also be needed. Techniques and hardware to perform these functions will be developed.

It is unlikely that there will be a diagnostic neutral beam on a NSD and so there is a specific requirement to develop techniques and hardware to obtain the necessary information for the control and analysis of the tokamak without one. It may be possible, for example, to use the measurement of He near the edge by passive means as the control measurement on the He ash. Such possibilities will be explored on ITER.

As explained in section 5, the diagnostic components located in ports will be embedded in shielding plugs and access to these will be very limited. After only a limited fusion operation the plugs will be activated and also, possibly, contaminated and all handling will have to be done using special tools. The infrequent access will also require the integration into the plugs of dedicated calibration and alignment equipment. The use of port plugs is a new concept for the implementation of tokamak diagnostics. It is likely to be the concept employed on a NSD and so valuable experience with this approach will be gained on ITER.

The combination of these factors—requirements, environmental effects, underlying physics and diagnostic performance—will be experienced on ITER for the first time. It is probable that there will still be an extrapolation in plasma performance from ITER to the next step device. The experience gained on ITER will reduce the uncertainties in this extrapolation and provide the basis on which an informed choice of diagnostics can be made and diagnostic systems designed for an NSD.

9. Summary

In order to execute the planned experimental and operational programme of ITER it will be necessary to measure an extensive range of plasma and first wall parameters. The measurements will be used for machine protection, plasma control and physics evaluation. In total about 45 parameters will have to be measured. A careful analysis of the expected operation and performance of the plasma, and the intended use of the measurements, has enabled a detailed determination of the specifications for each parameter to be made. These specifications act as the target for the diagnostic design. The development of these specifications is an ongoing activity and is carried out in collaboration with all the ITPA Topical Groups. The development is expected to continue at least through to the initial operation of the machine.

Relative to previous and existing fusion machines the environment of ITER will be harsh. Depending on their location, diagnostic components will experience levels of radiation (neutron, gamma and electromagnetic), particle bombardment and nuclear heating far higher than on existing machines. The highest level will be experienced by components near the first wall and in the divertor where the typical values for the neutron flux levels will be $3 \times 10^{18}\,\mathrm{n\,m^{-2}}$ and the end-of-life fluence will be $\sim 3 \times 10^{25}\,\mathrm{n\,m^{-2}}$ with a corresponding end-of-life material damage up to $\sim$1 dpa. The neutron heating will be typically $1\,\mathrm{MW\,m^{-3}}$ compared with essentially zero on existing machines. As a consequence many radiation/environmentally induced phenomena have to be taken into account in diagnostic design for the first time, for example radiation induced conductivity (RIC) and radiation induced EMF (RIEMF) in cables and radiation induced absorption and luminescence in optical materials. The key phenomena have been identified and an extensive R&D programme is in progress to characterize and to gain an understanding of the effects. On the basis of the results of this R&D it is possible, through a combination of careful material selection and diagnostic design, to minimize the impact of the environmental effects and especially to try to ensure adequate lifetime of the components. This is the approach that is being adopted in the preparations for ITER diagnostics.

In order to meet the measurement requirements, the diagnostic system will be comprehensive. It will comprise individual measurement systems drawn from all the main generic diagnostic groups—magnetics, neutron systems, optical and microwave systems, spectroscopic, bolometric, probes, pressure gauges and gas analysers. In total there will be about 40 independent diagnostic systems. Most of the needed systems have been selected and are currently under design. Each system has its own particular implementation difficulties and is affected by the environment in different ways. In most cases the difficulties have been identified and work is underway to cope with them. For some systems the state of preparation is such that detailing can begin and construction started as needed. In some cases, more design is needed while in others some R&D is outstanding: in particular further R&D is needed on the radiation effects on the in-vessel magnetic coils, the procedures and equipment for calibrating the neutron systems and the impact of erosion and deposition on the first mirrors and measures to minimize them. In a few areas, for example escaping fast ions and alpha particles, it appears to be very difficult/impossible to install the required sensors and new diagnostic techniques are required.

The diagnostic components will be installed in multiple locations: inside and outside of the vacuum vessel, in upper and equatorial ports, in and below divertor cassettes, in port cells and in the remote diagnostic building. The integration of the diagnostic components with the other tokamak systems is an important and major task. It obviously has to meet the requirements of the diagnostic for plasma access, but it also has to satisfy stringent engineering requirements—for example on neutron shielding, tritium containment and vacuum integrity—which arise because the ITER machine is a nuclear device. Methods for meeting these requirements consistent with maintaining the performance of the diagnostics have been developed. Within the ports, the diagnostic components will be installed in port-plugs and these will contain modules to ease the maintenance and construction. A key parameter is space in the available ports and this is distributed among the diagnostics according to the role of the measurements that the diagnostic provides, with priority given to those systems that provide measurements for machine protection, followed by those needed for basic plasma control. Guidelines for the integration and prioritization have been developed.

Since the publication of the ITER Physics Basis considerable progress has been made in several areas identified at that time as particularly difficult. These include the development of alternative techniques for the measurement of the fuel mix ratio (fast-wave reflectometry); the erosion of the divertor plates in real time (speckle interferometry and optical radar); and the number density and velocity distribution of the fast ions including alpha particles (collective scattering). Progress has been made in understanding and mitigating key environmental effects including the effects of erosion and deposition of first mirrors and the effects of radiation on magnetics coils and cables (RIEMF, RIC, etc). On the other hand, some new issues have been identified. These include the need for, and design of, a vertical viewing neutron camera and measurements of dust. These are being addressed in the current work.

On the basis of the work carried out thus far, it is possible to make an assessment, relative to the specified measurement requirements, of the performance of the diagnostic system planned for ITER. Of course, the assessment is subject to considerable uncertainty because the design and R&D are not yet completed. The assessment shows that the measurements necessary for machine protection and basic plasma control should be made at the required level. However, the measurements necessary for the control of plasma scenarios that rely on real-time feedback control of profiles, for example the q-profile, are subject to greater uncertainty. It is expected that the measurements necessary to support the main needs of the physics programme will be made although clearly the number of diagnostics that can be installed is limited and there will inevitably be limitations in the information that can be obtained.

Finally, looking towards the next step devices that will follow ITER, the implementation and operation of diagnostics on ITER will enable the establishment of a base of information and experience on which diagnostics for these reactor grade machines can be selected and designed. The information and experience that will be obtained includes the optimum set of measurements needed to support the selected high performance operation scenarios; the use of predictive and analysis codes to combine data from multiple diagnostics so as to minimize the number of measurements needed; the performance of diagnostics under environmental and plasma conditions that cannot be reached in current machines, in particular under high levels of fusion heating; the validation of diagnostics especially developed for long-pulse operation; and the validation of techniques and hardware for real-time handling and processing of large quantities of data, including real-time data validation, and possibly in-pulse calibration. Experience with the engineering concepts and procedures that are being developed for the integration and implementation of diagnostics on ITER, the first fusion nuclear device, will also be invaluable for the development of fusion. There will still be an extrapolation from ITER to a reactor scale device but the experience of preparing and operating diagnostics on ITER will reduce the uncertainties in this extrapolation for the plasma and first wall measurement system.

References

[1] Costley A.E. *et al* 2005 *Fusion Eng. Des.* **74** 109
[2] Costley A.E. *et al* 2006 Fusion Energy 2006 *Proc. 21st Int. Conf. on Fusion Energy 2006 (Chengdu, 2006)* (Vienna: IAEA) CD-ROM file (IT/1-5)
[3] Donné A.J.H. *et al* 2006 in Fusion Energy 2006 *Proc. 21st Int. Conf. on Fusion Energy 2006 (Chengdu, 2006)* (Vienna: IAEA) CD-ROM file (IT/P1-24)
[4] Costley A.E. *et al* 2001 *Proc. 28th EPS Conf. on Controlled Fusion and Plasma Physics (Funchal, Portugal)* vol 25A (ECA) paper OR.27. http://epsppd.epfl.ch/Madeira/html/authors/nav/AutC04fr.html
[5] Costley A.E. *et al* 2002 Requirements and issues in diagnostics for next step burning plasma experiments *Advanced Diagnostics for Magnetic and Inertial Fusion* ed P. E. Stott *et al* (New York: Kluwer/Plenum) p 1
[6] Donné A.J.H. and Costley A.E. 2004 *IEEE Transact. on Plasma Sci.* **32** 177
[7] ITER Physics Expert Group on Diagnostics *et al* 1999 *Nucl. Fusion* **39** 2541
[8] Ebisawa K. *et al* 2001 *Rev. Sci. Instrum.* **72** 545
[9] Costley A.E. *et al* 2002 Fusion Energy 2002 *Proc. 19th Int. Conf. on Fusion Energy 2002 (Lyon, 2002)* (Vienna: IAEA) CD-ROM file (CT-5) and http://www.iaea.org/programmes/ripc/physics/fec2002/html/fec2002.htm
[10] Shimomura Y. *et al* in Fusion Energy 2000 *Proc. 18th Int. Conf. on Fusion Energy 2000 (Sorrento, 2000)* (Vienna: IAEA) CD-ROM file (ITER/1) and http://www.iaea.org/programmes/ripc/physics/fec2000/html/node1.htm
[11] Donné A.J.H. *et al Proc. 18th Int. Conf. on Fusion Energy 2000 (Sorrento, 2000)* (Vienna: IAEA) CD-ROM file (ITER P/09) and http://www.iaea.org/programmes/ripc/physics/fec2000/html/node1.htm
[12] Vayakis G., Walker C. and International Team and Participant Teams 2003 *Rev. Sci. Instrum.* **74** 2409
[13] Bolshakova I. *et al* 2003 *Proc. 30th EPS Conf. on Controlled Fusion and Plasma Physics (St Petersburg, Russia)* vol 27A (ECA) P-4.68 http://epsppd.epfl.ch/StPetersburg/PDF/P4_068.PDF
[14] Duran I. *et al* 2004 *Proc. Int. Conf. on Plasma Physics (Nice, France)* http://hal.ccsd.cnrs.fr/view_by_stamp.php?label=ICPP2004&langue=en&action_todo=view&id=ccsd-00001781&version=1
[15] Spuig P. *et al* 2003 *Fusion Eng. Des.* **66–68** 953
[16] Vayakis G. *et al* 2004 *Rev. Sci. Instrum.* **75** 4324
[17] Orsitto F. *et al* 2006 *Proc. 21st Int. Conf. on Fusion Energy 2006 (Chengdu, 2006)* (Vienna: IAEA) CD-ROM file (IT/P1-27).
[18] Sasao M. *et al* 2004 *Plasma Phys. Control. Fusion* **46** S107
[19] Krasilnikov A.V. *et al* 2005 *Nucl. Fusion* **45** 1503
[20] Nishitani T. *et al* 1998 In vessel neutron monitor using micro fission chambers for ITER *Diagnostics for Experimental Thermonuclear Fusion Reactors 2* ed P.E. Stott *et al* (New York: Plenum) p 491
[21] Asai K. *et al* 2004 *Rev. Sci. Instrum.* **75** 3537
[22] Krasilnikov A.V. *et al* 2004 *Instrum. Exp. Tech.* **47** 5
[23] Marcus F.B. *et al* 1998 *Diagnostics for Experimental Thermonuclear Fusion Reactors 2* ed P.E. Stott *et al* (New York: Plenum) p 419
[24] Start D.F.H. *et al* 1999 *Nucl. Fusion* **39** 321
[25] Popovichev S. *et al* 2004 *Proc. 31st EPS Conf. on Controlled Fusion and Plasma Physics (London, UK)* vol 28G (ECA) paper P5-173 http://epsppd.epfl.ch/London/pdf/P5_173.pdf
[26] Gorini G. *et al* 1998, Fuel density measurement in burning plasmas using neutron spectrometry *Diagnostics for Experimental Thermonuclear Fusion Reactors 2* ed P.E. Stott *et al* (New York: Plenum), p 463
[27] Okada K *et al* 2005 *Proc. 32nd EPS Conf. on Controlled Fusion and Plasma Physics (Tarragona, Spain)* vol 29C (ECA) paper P4.096 http://epsppd.epfl.ch/Tarragona/pdf/P4_096.pdf
[28] Barnes C.W., Loughlin M.J. and Nishitani T. 1997 *Rev. Sci. Instrum.* **68** 577
[29] Nishitani T. *et al* 2003 *Rev. Sci. Instrum.* **74** 1735
[30] Kondoh T. *et al* 2003 *Rev. Sci. Instrum.* **74** 1642
[31] Bindslev H. *et al* 2001 *Fusion Eng. Des.* **53** 105
[32] Bindslev H. *et al* 2002 Fast ion dynamics measured by collective thomson scattering *Advanced Diagnostics for Magnetic and Inertial Fusion* ed P.E. Stott *et al* (New York: Plenum) p 311
[33] Bindslev H. *et al* 2006 *Phys. Rev. Lett.* **97** 205005
[34] Bindslev H. *et al* 2004 *Rev. Sci. Instrum.* **75** 3598
[35] Meo F. *et al* 2004 *Rev. Sci. Instrum.* **75** 3585
[36] Egedal J. *et al* 2005 *Nucl. Fusion* **45** 191
[37] Kondoh T. *et al* 2006 *Rev. Sci. Instrum.* **77** 10E505
[38] von Hellermann M. *et al* 2003 *Proc. 30th EPS Conf. on Controlled Fusion and Plasma Physics (St Petersburg, Russia)* (ECA) vol 27A paper O4-2D http://epsppd.epfl.ch/StPetersburg/PDF/O4_002D.PDF
[39] Tugarinov S. *et al* 2003 *Proc. 30th EPS Conf. on Controlled Fusion and Plasma Physics (St Petersburg, Russia)*

vol 27A (ECA) paper P4-057 http://epsppd.epfl.ch/StPetersburg/PDF/P4_057.PDF
[40] Sasao M. *et al* 1996 *Nucl. Fusion* **35** 1619
[41] K. Shinto *et al* 2005 Design of a fast neutral he beam system for feasibility study of charge-exchange alpha-particle diagnostics in a thermonuclear fusion reactor *Proc. 2005 Particle Accelerator Conf. (Knoxville, Tennessee)* p 2630 http://accelconf.web.cern.ch/accelconf/
[42] Sasao M. *et al* 2006 *Rev. Sci. Instrum.* **77** 10F130
[43] Källne J. *et al* 2000 *Phys. Rev. Lett.* **85** 1246
[44] Fisher R.K. *et al* 2001 *Rev. Sci. Instrum.* **72** 796
[45] Trusillo S. and Agureev V. 2001 Knock-on neutron detector based on a bubble chamber with flowing liquid *Progress Meeting on ITER Diagnostics (St Petersburg, Russia, November 2001)*
[46] Fisher R.K. 2004 *Rev. Sci. Instrum.* **75** 3556
[47] Afanasiev V.I. *et al* 2003 *Proc. 30th EPS Conf. on Controlled Fusion and Plasma Physics (St Petersburg, Russia)* vol 27A (ECA) paper O-4.4D http://epsppd.epfl.ch/StPetersburg/ PDF/O4_004D.PDF
[48] Kiptily V. *et al* 2002 Gamma-rays: measurement and analysis at JET *Advanced Diagnostics for Magnetic and Inertial Fusion* ed P.E. Stott *et al* (New York: Plenum) p 141
[49] Kiptily V.G. *et al* 2004 *Phys. Rev. Lett.* **93** 115001
[50] Kiptily V.G., Cecil F.E. and Medley S.S. 2006 *Plasma Phys. Control. Fusion* **48** R59
[51] Konovalov S.V. *et al* 2001 *Proc. 28th EPS Conf. on Controlled Fusion and Plasma Physics (Funchal, Portugal)* vol 25A (ECA) paper 2.034 http://epsppd.epfl.ch/Madeira/html/sessions/nav/Poster19fr.html
[52] Sasao M. *et al* 2005 Integration of lost alpha-particle diagnostic systems on ITER *Proc. 9th IAEA Technical Meeting on Energetic Particles in Magnetic Confinement Systems (Takayama, Japan)* paper OT11 http://htpp.lhd.nifs.ac.jp/IAEATM-EP2005/IAEA_papers_final/OT11__Sasao_paper.pdf
[53] Costley A.E. 2005 Laser-based plasma diagnostics for ITER and beyond *Proc. 12th Int. Symp. on Laser Aided Plasma Diagnostics (Snowbird)* (Davis: University of California)
[54] Gowers C., Beurskens M. and Nielsen P. 2000 *J. Plasma Fusion Res.* **76** 874
[55] Walsh M. *et al* 2006 *Rev. Sci. Instrum.* **77** 10E525
[56] Razdobarin G. *et al* 2006 *Proc. 21st Int. Conf. on Fusion Energy 2006 (Chengdu, 2006)* (Vienna: IAEA) CD-ROM file (IT/P1-25)
[57] Pasqualotto R. and Nielsen P. 2003 *Rev. Sci. Instrum.* **74** 1671
[58] Kempenaars M. *et al* 2004 *Rev. Sci. Instrum.* **75** 3894
[59] Bartlett D.V. 1996 Physics issues of ECE and ECA for ITER *Diagnostics for Experimental Thermonuclear Fusion Reactors* ed P.E. Stott *et al* (New York: Plenum) p 183
[60] Donné A.J.H. and Schokker B.C. 1996 Advantages and limitations of microwave diagnostics in ITER *Diagnostics for Experimental Thermonuclear Fusion Reactors* ed P.E. Stott *et al* (New York: Plenum) p 215
[61] Bartlett D.V. 1997 Physics aspects of the ITER ECE system design *Proc. 10th Workshop on ECE and ECH (Ameland, Netherlands)* (Singapore: World Scientific) p 255
[62] Vayakis G. *et al* 2006 *Nucl. Fusion* **46** S836
[63] Zhuang G. *et al* 2005 *Plasma Phys. Control. Fusion* **47** 1539
[64] de la Luna E. *et al* 2003 *Rev. Sci. Instrum.* **74** 1414
[65] Mukhin E.E. and Razdobarin G.T. 2003 *Proc. 30th EPS Conf. on Controlled Fusion and Plasma Physics (St. Petersburg, Russia)* vol 27A (ECA) paper 0-1.5A http://epsppd.epfl.ch/ StPetersburg/PDF/O1_005A.PDF
[66] Razdobarin G.T. 2004 Report of Thomson scattering specialist working group *6th Meeting of the ITPA Topical Group Meeting on Diagnostics (Naka, Japan)* (refer to Gennadiy.Razdobarin@mail.ioffe.ru)
[67] Kochergin M.M. *et al* 2003 *Plasma Dev. Oper.* **11** 1
[68] Watkins J.G. *et al* 1999 *J. Nucl. Mater.* **266–269** 980
[69] Mukhin E.E. *et al* 2004 *Rev. Sci. Instrum.* **75** 1261
[70] Loarte A. *et al* 2004 *Phys. Plasmas* **11** 2668
[71] Nielsen P. 2001 Thomson scattering in ITER *Proc. 10th Int. Symp. On Laser-Aided Plasma Diagnostics (Fukuoka, Japan)* p 401
[72] Yoshida H. *et al* 2004 *Japan. J. Appl. Phys.* **43** L1038
[73] Hatae T. 2006 *J. Korean Phys. Soc.* **49** S160
[74] Hatae T. *et al* 2006 *Rev. Sci. Instrum.* **77** 10E508
[75] Kawano Y., Chiba S. and Inoue A. 2001 *Rev. Sci. Instrum.* **72** 1068
[76] Carlstrom T.N. *et al* 1998 *Diagnostics for Experimental Thermonuclear Fusion Reactors 2* ed P.E. Stott *et al* (New York: Plenum) p 193
[77] Kawano Y. *et al* 1997 *J. Plasma Fusion Res.* **73** 870
[78] Kondoh T. *et al* 2004 Rev. Sci. Instrum. **75** 3420
[79] Segre S.E. and Zanza V. 2002 *Phys. Plasmas* **9** 2919
[80] Petrov A. and Petrov V.G. 2003 *Rev. Sci. Instrum.* **74** 1465
[81] Manso M.E. *et al* 2001 *Plasma Phys. Control. Fusion* **43** A73
[82] Varela P. *et al* 2001 *Rev. Sci. Instrum.* **72** 315
[83] Varela P. *et al* 2003 *Rev. Sci. Instrum.* **74** 1493
[84] Doyle E.J. *et al* 1999 *Rev. Sci. Instrum.* **70** 1064
[85] Wang G. *et al* 2003 *Rev. Sci. Instrum.* **74** 1525
[86] Clairet F. *et al* 2003 *Rev. Sci. Instrum.* **74** 1481
[87] Estrada T. *et al* 2001 *Plasma Phys. Control. Fusion* **43** 1535
[88] Santos J. *et al* 2003 *Rev. Sci. Instrum.* **74** 1489
[89] Vershkov V.A. *et al* 2004 *Instrum. Exp. Tech.* **47** 54
[90] Prentice R *et al* 1995 *Rev. Sci. Instrum.* **66** 1154
[91] Takenaga H *et al* 1998 *Rev. Sci. Instrum.* **69** 3181
[92] Proschek M. *et al* 2000 *Proc. 18th Int. Conf. on Fusion Energy 2000 (Sorrento, 2000)* (Vienna: IAEA) CD-ROM file (Exp5/34) and http://www.iaea.org/programmes/ripc/physics/fec2000/html/node1.htm
[93] Kubo H. *et al* 1999 *J. Plasma Fusion Res.* **75** 945
[94] von Hellermann M.G. *et al* 2001 *Proc. Int. Conf. on Advanced Diagnostics for Magnetic and Inertial Fusion (Varenna, Italy)* ed P.E. Stott *et al* (New York: Plenum) p 205
[95] Di Pietro E. *et al* 2001 *Fusion Eng. Design* **56-7** 929
[96] von Hellermann M. 1996 *Diagnostics for Experimental Fusion Reactors 1* ed P.E. Stott *et al* (New York: Plenum) p 321
[97] König R.W.T. *et al* 1998 *Diagnostic for Experimental Fusion Reactors 2* ed P.E. Stott *et al* (New York: Plenum) p 371
[98] von Hellermann M. *et al* 2004 *Rev. Sci. Instrum.* **75** 3458.
[99] von Hellermann M. *et al* 2006 *Rev. Sci. Instrum.* **77** 10F516
[100] von Hellermann M. *et al* 2006 *Proc. 21st Int. Conf. on Fusion Energy 2006 (Chengdu, 2006)* (Vienna: IAEA) CD-ROM file (IT/P1-26)
[101] Ida K. 2006 private communication (NIFS, Japan)
[102] Bitter M. *et al* 2004 *Rev. Sci. Instrum.* **75** 3660
[103] Lee S.G. *et al* 2004 *Rev. Sci. Instrum.* **75** 3693
[104] Bertschinger G. *et al* 2004 *Rev. Sci. Instrum.* **75** 3727
[105] Nelson M. *et al* 2004 *Rev. Sci. Instrum.* **75** 3734
[106] Mikulec B. *et al* 2003 *Nucl. Instrum. Methods* A **511** 282
[107] Sauli F. 2002 *Nucl. Instrum. Methods.* A **477** 1
[108] Barnsley R. 2002 private communication (UKAEA, Culham)
[109] Summers H.P. 2001 Atomic data and analysis structure, manual. Available http://adas.phys.strath.ac.uk
[110] Lauro-Taroni L. *et al* 1994 *Proc 21st EPS Conf. on Controlled Fusion and Plasma Physics (Montpellier)* vol 1 p 102
[111] Widmann K. *et al* 1996 *Phys. Rev.* A **53** 2200
[112] Bitter M. *et al* 1993 *Phys. Rev. Lett.* **71** 1007
[113] Barnsley R. *et al* 2004 *Rev. Sci. Instrum.* **75** 3743
[114] Coffey I.H., Barnsley R. and JET EFDA Contributors 2004 *Rev. Sci. Instrum.* **75** 3737
[115] Ingesson L.C. *et al* 2004 *Rev. Sci. Instrum.* **75** 3696
[116] Nakano T. *et al* 2004 *J. Plasma Fusion Res.* **80** 500
[117] Mandl W. *et al* 1993 *Plasma Phys. Control. Fusion* **35** 1373
[118] Bettella D. *et al* 2003 *Plasma Phys. Control. Fusion* **45** 1893
[119] ITER EDA documentation series No. 24 2002 *2.6 Plasma Diagnostic System in ITER Technical Basis* (Vienna: IAEA)

[120] Kadota K. *et al* 1980 *Nucl. Fusion* **20** 209
[121] Schissel D.P. *et al* 1988 *Phys. Fluids* **31** 3738
[122] Hollmann E.M. *et al* 2003 *Rev. Sci. Instrum.* **74** 3984
[123] Schunke B., Huysmans G. and Thomas P. 2004 *Proc. 31st EPS Conf. on Controlled Fusion and Plasma Physics (London, UK)* vol 28G (ECA) paper P-4.111 http://epsppd.epfl.ch/London/pdf/P4_111.pdf
[124] Pospieszczyk A. *et al* 1989 Spectroscopic studies of carbon containing molecules and their breakup in PISCES-A *University of California at Los Angeles Report No. UCLA-PPG-1251*
[125] Tugarinov S. *et al* 2003 *Rev. Sci. Instrum.* **74** 2075
[126] ITER Design Description Document 1998 Final Design Report *(ITER EDA Documentation Series)* (Vienna: IAEA)
[127] Edmonds P.H. *et al* 1998 *Diagnostics for Experimental Thermonuclear Fusion Reactors 2* ed P.E. Stott *et al* (New York: Plenum) p 79
[128] Hawkes N.C. *et al* 1998 *Diagnostics for Experimental Thermonuclear Fusion Reactors 2* ed P.E. Stott *et al* (New York: Plenum) p 297
[129] Barnsley R. *et al* 2003 *Rev. Sci. Instrum.* **74** 1969
[130] Biel W. 2004 *Rev. Sci. Instrum.* **75** 3268
[131] Biel W. 2004 private communication (Forschungszentrum Jülich, Germany)
[132] Barnsley R. *et al* 1986 *Rev Sci Instrum.* **57** 2159
[133] Barnsley R. *et al* 1992 *Rev. Sci. Instrum.* **63** 5023
[134] Bitter M. *et al* 1986 *Rev. Sci. Instrum.* **57** 2145
[135] Bitter M. *et al* 1999 *Rev. Sci. Instrum.* **70** 292
[136] Sugie T. *et al* 2003 *Proc. 30th EPS Conf. on Controlled Fusion and Plasma Physics (St Petersburg, Russia)* vol 27A (ECA) paper P-4.63 http://epsppd.epfl.ch/StPetersburg/PDF/P4_063.PDF
[137] Ogawa H. *et al* 2006 *Design of Impurity Influx Monitor (Divertor) for ITER* JAEA Report, JAEA-Technology 2006-015 http://jolissrch-inter.tokai-sc.jaea.go.jp/pdfdata/JAEA-Technology-2006-015.pdf
[138] Sugie T. *et al* 2003 *J. Plasma Fusion Res.* **79** 1051
[139] Moskalenko I. *et al* 2004 *Plasma Phys. Rep.* **30** 432
[140] Leonard A.W *et al* 1996 Bolometry for divertor characterization and control *Diagnostics for Experimental Thermonuclear Fusion Reactors* ed P.E. Stott *et al* (New York: Plenum) p 549
[141] Ingesson L.C., Rapp J., Matthews G.F. and Contributors to the EFDA-JET Workprogramme 2003 *J. Nucl. Mater.* **313–316** 1173
[142] Konoshima S. *et al* 2003 *J. Nucl. Mater.* **313–316** 888
[143] Rapp J. *et al* 2002 *Plasma Phys. Control. Fusion* **44** 639
[144] Fuchs J.C. *et al* 2001 *J. Nucl. Mater.* **290–293** 525
[145] Jackson G.L. *et al* 1997 *J. Nucl. Mater.* **241-243** 618
[146] Reichle R., Di Maio M. and Ingesson L.C. 1998 Progress of the reference design for ITER bolometers and development of a high performance alternative *Diagnostics for Experimental Thermonuclear Fusion Reactors 2* ed P.E. Stott *et al* (New York: Plenum) p 389
[147] Ingesson L.C. and Reichle R. 1998 Lines of sight for ITER bolometers *Report JET-R(98)03* (JET Joint Undertaking, Abingdon)
[148] Kálvin S. 2005 private communication (KFKI-RMKI, Hungary)
[149] Fuchs J.C. *et al* 1994 *Proc. of the 21sts Conf. on Plasma Physics and Controlled Fusion (Montpellier, France)* ed E. Joffrin *et al* vol 18B (ECA) Part III p 1308
[150] Konoshima S. *et al* 2001 *Plasma Phys. Control. Fusion* **43** 959
[151] Vallet J.-C. *et al* 1997 *Proc. 24th EPS Conf. on Controlled Fusion and Plasma Physics (Berchtesgaden, Germany)* ed M. Schnittenhelm *et al* vol 21A (ECA) Part I pp 233
[152] Ingesson L.C. *et al* 1997 *Proc. 24th EPS Conf. on Controlled Fusion and Plasma Physics (Berchtesgaden, Germany)* ed M. Schnittenhelm *et al* vol 21A (ECA) Part I pp 113
[153] Barana O. *et al* 2002 *Rev. Sci. Instrum.* **73** 2038
[154] Reichle R. *et al* 1996 Bolometer for ITER *Diagnostics for Experimental Thermonuclear Fusion Reactors* ed P.E. Stott *et al* (New York: Plenum) pp 559
[155] Mast K.F. *et al* 1991 *Rev. Sci. Instrum.* **62** 744
[156] Reichle R. *et al* 2001 *Proc. 28th EPS Conf. on Controlled Fusion and Plasma Physics (Funchal, Portugal)* vol 25A (ECA) paper P3.103 http://epsppd.epfl.ch/Madeira/html/authors/nav/AutR01fr.html
[157] Nishitani T. *et al* 2002 *Fusion Eng. Des.* **63–64** 437
[158] Gonzalez M. and Hodgson E.R. 2003 *Fusion Eng. Des.* **66–68** 881
[159] Gonzalez M. and Hodgson E.R. 2005 *Fusion Eng. Des.* **74** 875
[160] Gusarov A. 2005 private communication (SCK/CEN, Belgium)
[161] Giannone L. *et al* 2005 *Plasma Phys. Control. Fusion* **47** 2123
[162] Mast K.F. 2004 private communication (IPP, Garching, Germany)
[163] Alekseyev A.G. 2003 *Proc. 30th EPS Conf. on Controlled Fusion and Plasma Physics (St Petersburg, Russia)* vol 27A (ECA) paper P-1.70 http://epsppd.epfl.ch/StPetersburg/PDF/P1_070.PDF
[164] Di Maio M., Reichle R. and Giannella R. 1998 *17th IEEE/NPSS Symp. Fusion Engineering (San Diego, USA)* (IEEE: Piscataway) vol 2 pp 775
[165] Bittner R. *et al* 2003 *Integr. Ferroelectr.* **47** 143
[166] Kulikov D.V. *et al* 2002 *Tech. Phys. Lett.* **28** 628
[167] Bittner R. *et al* 2003 *Fus. Eng. Des.* C **66–68** 833
[168] Sternberg A. *et al* 2004 *J. Eur. Ceram. Soc.* **24** 1653
[169] Hodgson E.R. (ed) 2004 *14th IEA Workshop on Radiation Effects in Ceramic Insulators EUR-CIEMAT 96 (September 2004)*
[170] Wurden G.A. and Peterson B.J. 1999 *Rev. Sci. Instrum.* **70** 255
[171] Ashikawa N. *et al* 2000 *J. Plasma Fusion Res.* **3** 436
[172] Peterson B.J. 2000 *Rev. Sci. Instrum.* **71** 3696
[173] Peterson B.J. *et al* 2003 *Rev. Sci. Instrum.* **74** 2040
[174] Peterson B.J. *et al* 2003 *Plasma Phys. Control. Fusion* **45** 1167
[175] Peterson B.J. *et al* 2003 *Proc. 30th EPS Conf. on Controlled Fusion and Plasma Physics (St Petersburg, Russia)* vol 27A (ECA) paper P-4.67 http://epsppd.epfl.ch/StPetersburg/PDF/P4_067.PDF
[176] Konoshima S. *et al* 2005 *Proc. 32nd EPS Conf. on Controlled Fusion and Plasma Physics (Tarragona, Spain)* vol 29C (ECA) paper P-4.92 http://epsppd.epfl.ch/Tarragona/pdf/P4_092.pdf
[177] Alekseyev A.G., Portnov D.V. and Cecil F.E. 2003 *Proc. 30th EPS Conf. on Controlled Fusion and Plasma Physics (St Petersburg, Russia)* vol 27A (ECA) paper P-1.71 http://epsppd.epfl.ch/StPetersburg/PDF/P1_071.PDF
[178] Donné A.J.H. *et al* 2004 *Rev. Sci. Instrum.* **75** 4694
[179] Donné A.J.H. *et al* 1999 *Rev. Sci. Instrum.* **70** 726
[180] Voitsenya V.S. *et al* 2005 *Rev. Sci. Instrum.* **76** 083502
[181] Fuchs Ch. And Hartfuss H.J. 1999 *Rev. Sci. Instrum.* **70** 722
[182] Guenter K. 2004 *Plasma Phys. Control. Fusion.* **46** 1423
[183] Rommers J.H. and Howard J. 1996 *Plasma Phys. Control. Fusion* **38** 1805
[184] Ding W.X. *et al* 2004 *Rev. Sci. Instrum.* **75** 3387
[185] Park H.K. *et al* 1999 *Rev. Sci. Instrum.* **70** 710
[186] Segre S.E. 1999 *Plasma Phys. Control. Fusion* **41** R57
[187] Giudicotti L. *et al* 2004 *Plasma Phys. Control. Fusion* **46** 681
[188] Stratton B.C. *et al* 1999 *Rev. Sci. Instrum.* **70** 898
[189] Hawkes N.C. *et al* 1999 *Rev. Sci. Instrum.* **70** 894
[190] Hobirk J. *et al* 2001 *Proc. Int. Conf. on Advanced Diagnostics for Magnetic and Inertial Fusion (Varenna, Italy)* (New York: Plenum) ed P.E. Stott *et al* p 197
[191] Jayakumar R.J. *et al* 2005 *Fusion Sci. Technol.* **48** 852
[192] Kuldkepp M. *et al* 2005 *Appl. Opt.* **44** 5899
[193] Fujita T. *et al* 1997*Fusion Eng. Des.* **34–35** 289

[194] Jaspers R. *et al* 2001 *Rev. Sci. Instrum.* **72** 1018
[195] Jakubowska K. *et al* 2004 *Rev. Sci. Instrum.* **75** 3475
[196] Levinton F. 2004 *Rev. Sci. Instrum.* **75** 4162
[197] Foley E. and Levinton F. 2004 *Rev. Sci. Instrum.* **75** 3463
[198] Malaquias A. *et al* 2004 *Rev. Sci. Instrum.* **75** 3393
[199] Suzuki T. *et al* 2004 *J. Plasma Fusion Res.* **80** 362
[200] Jayakumar R.J. *et al* 2004 *Rev. Sci. Instrum.* **75** 2995
[201] Suzuki T. *et al* 2006 *Rev. Sci. Instrum.* **77** 10E914
[202] Kuldkepp M. *et al* 2004 *Rev. Sci. Instrum.* **75** 3446
[203] Hawkes N.C. and Brix M. 2006 *Rev. Sci. Instrum.* **77** 10E509
[204] Maddaluno G. and Greco V. *Proc. 30th EPS Conf. on Controlled Fusion and Plasma Physics (St Petersburg, Russia)* vol 27A (ECA) paper P-1.69 http://epsppd.epfl.ch/StPetersburg/PDF/P1_069.PDF
[205] Jaspers R. *et al* 2001 *Rev. Sci. Instrum.* **72** 466
[206] Entrop I. *et al* 1999 *Plasma Phys. Control. Fusion* **41** 377
[207] Gill R.D. *et al* 2000 *Nucl. Fusion* **40** 163
[208] Gott Yu. 2003 private communication (Kurchatov Institute, Moscow) (refer to gott@nfi.kiae.ru)
[209] Séguin F.H., Petrasso R.D. and Li C.K. 1997 *Rev. Sci. Instrum.* **68** 753
[210] Barykov I.A., Gott Yu.V. and Stepanenko M.M. 2004 *Instrum. and Exp. Tech.* (Russian Transl.) **47** 242
[211] Eich T. *et al* 2003 *Phys. Rev. Lett.* **91** 195003
[212] Itami K., Sugie T., Vayakis G. and Walker C. 2004 *Rev. Sci. Instrum.* **75** 4124
[213] Riccardo V., Fundamenski W. and Matthews G.F. 2001 *Plasma Phys. Control. Fusion* **43** 881
[214] Matthews G.F., Davies S.J. and Monk R. 1995 *Proc. 2nd Int. Workshop on Electrical Probes in Magnetized Plasmas (Berlin, Germany, 4–6 October 1995)* (Berlin: The Harnack-House) ed M. Laux
[215] Haas G. and Bosch H.-S. 1998 *Vacuum* **51** 39
[216] Boivin R.L. *et al* 2002 *Advanced Diagnostics for Magnetic and Inertial Fusion* ed P.E. Stott *et al* (Dordrecht New York: Kluwer/Plenum) p 423
[217] Hodgson E.R. 2003 Ceramics for heating and current drive and diagnostic systems *EUR-CIEMAT 95*
[218] Morgan P.D. and Kuma V. 1997 Prospects for Determining the D-T Isotopic Ratio in the JET Plasma by Spectroscopic Observation of a Penning Discharge JET–R(97)08
[219] Jones R. and Wykes C. 1989 *Holographic and Speckle Interferometry* 2nd edn (Cambridge: Cambridge University Press)
[220] Gauthier E. and Roupillard G. 2003 *J. Nucl. Mater.* **313–316** 70
[221] Coletti A. *et al* 2003 *Fusion Eng. Des.* **69** 169
[222] Matsumoto H., Minoshima K. and Telada S. 2003 *Recent Developments in Traceable Dimensional Measurements II* ed J.E. Decker and N. Brown *Proc. SPIE* **5190** 308
[223] Menon M.M. and Slotwinski A. 2004 *Rev. Sci. Instrum.* **75** 4100
[224] Rubel M.J *et al* 2004 *J. Nucl. Mater.* **329–333** 795
[225] Kuteev B *et al* 2006 *Proc. 21st Int. Conf. on Fusion Energy 2006 (Chengdu, 2006)* (Vienna: IAEA) CD-ROM file (EX/P4-13)
[226] Counsell G.F. and Wu C.H. 2001 *Phys. Scr.* T **91** 70
[227] Counsell G.F. *et al* 2006 *Rev. Sci. Instrum.* **77** 093501
[228] Bader A. *et al* 2004 *Rev. Sci. Instrum.* **75** 370
[229] Bonheure G. *et al* 2004 *Rev. Sci. Instrum.* **75** 3540
[230] Conway G.D. *et al* 2004 *Plasma Phys. Control. Fusion* **46** 951
[231] Hirsch M. *et al* 2001 *Plasma Phys. Control. Fusion* **43** 1641
[232] Hennequin P. *et al* 2004 *Rev. Sci. Instrum.* **75** 3881
[233] Bulanin V.V. *et al* 2000 *Plasma Phys. Rep.* **26** 813
[234] Conway G.D. *et al* 2005 *Plasma Phys. Control. Fusion* **47** 1165
[235] Heidbrink W., Watson G.W. and Burrell K.H. 2004 *Rev. Sci. Instrum.* **75** 3862
[236] Watson G.W. *et al* 2004 *Plasma Phys. Control. Fusion* **46** 471
[237] Heidbrink W.W. 2006 private communication (University of Irvine, USA)
[238] Kawano Y., Kondoh T. and Hatae T. 2005 Generation and diagnostics of relativistic electron beam in a torus plasma *Proc. Plasma Science Symp. 2005/22nd Symp. on Plasma Processing (Nagoya, Japan, 26–28 January 2005)* pp 93–4
[239] Kawano Y., Kondoh T. and Hatae T. 2006 Diagnostics of relativistic electron beam in a torus plasma *Technical Meeting on Pulsed Power Technology (Wajima, Japan, 6 February 2006)* (Japan: IEE) p 95
[240] Kawano Y. *et al* 2006 *Proc. 33rd EPS Conf. on Controlled Fusion and Plasma Physics (Rome, Italy)* paper P-4.138
[241] Howard J. 2006 *Plasma Phys. Control. Fusion* **48** 777
[242] Bitteker L. J. *et al* 2000 *Rev. Sci. Instrum.* **71** 3677
[243] Heidbrink W.W. *et al* 2004 *Plasma Phys. Control. Fusion* **46** 1855
[244] Kawano Y., Chiba S. and Inoue A. 2004 *Rev. Sci. Instrum.* **75** 279
[245] Hodgson E.R. 2002 *Plasma Phys.* **7** 76
[246] Ibarra A. and Hodgson E.R. 2004 *Nucl. Instrum. Methods Phys. Res.* B **218** 29
[247] Decreton M., Shikama T. and Hodgson E.R. 2004 *J. Nucl. Mater.* **329–333** 125
[248] Shikama T. *et al* 2003 *Nucl. Fusion* **43** 517
[249] E.R. Hodgson 2003 private communication (CIEMAT, Spain)
[250] Krasilnikov A., Nishitani T. and Vukulov K. 2004 *6th Meeting of the ITPA Topical Group on Diagnostics (Naka, Japan)*
[251] Gusarov A. *et al* 2005 *Fusion Eng. Des.* **75–79** 819
[252] Nagata S. *et al* 2004 *Proc. 50th Annual Meeting of the Int. Society for Optical Engineering (San Diego, USA) Proc. SPIE* **5199** 132
[253] Brichard B. *et al* 2004 *J. Nucl. Mater.* **329–333** 1456
[254] Brichard B. 2004 private communication (SCK/CEN, Belgium)
[255] Okamoto K. *et al* 2004 *J. Nucl. Mater.* **329–333** 1503
[256] Plaksin O.A., Kishimoto N. and Shikama T. 2004 *J. Nucl. Mater.* **329–333** 1490
[257] Toh K. *et al* 2004 *J. Nucl. Mater.* **329–333** 1495
[258] Sporea D., Sporea A. and Constantinescu B. 2005 *Fusion Eng. Des.* **74** 763
[259] Sugie T. *et al* 2002 *J. Nucl. Mater.* **307–311** 1264
[260] Moroño A., Vila R. and Hodgson E.R. 2004 *J. Nucl. Mater.* **329–333** 1438
[261] Nishitani T., Sugie T., Morishita N. and Yokoo N. 2005 *Fusion Eng.* **74** 871
[262] Martin P., Moroño A. and Hodgson E.R. 2004 *J. Nucl. Mater.* **307–311** 1260
[263] Martin P., Moroño A. and Hodgson E.R. 2004 *J. Nucl. Mater.* **329–333** 1442
[264] Gorbunov A.V. *et al* 2005 *Fusion Eng. Des.* **74** 815
[265] Gonzalez S.M., Moroño A. and Hodgson E.R. 2005 *Fusion Eng. Des.* **74** 831
[266] Bender S.E. *et al* 2001 *Fusion Eng. Design* **56–57** 911
[267] Van Nieuwenhove R. and Vermeeren L. 2003 *Rev. Sci. Instrum.* **74** 4675
[268] Vermeeren L. and Van Nieuwenhove R. 2003 *Rev. Sci. Instrum.* **74** 4667
[269] Bender S.E. *et al* 2003 *Plasma Devices Oper.* **11** 185
[270] Bender S.E. *et al* 2004 *Instrum. Exp. Tech.* **47** 163
[271] Vila R. and Hodgson E.R. 2004 *J. Nucl. Mater.* **329–333** 1524
[272] Vila R. 2004 private communication CIEMAT, Spain
[273] Nishitani T. *et al* 2004 *J. Nucl. Mater.* **329–333** 1461
[274] Vermeeren L. 2005 *Fusion Eng. Des.* **74** 885
[275] Vila R. And Hodgson E.R. 2005 *Proc. 12th Int. Conf. On Fusion Reactor Materials (ICFRM-12) (Santa Barbara, USA) J. Nucl. Mater.* submitted
[276] Van Nieuwenhove R. 2003 private communication (SCK/CEN, Belgium)
[277] ITER Team 2001 *Required plasma and first wall measurements* (ITER-FEAT) *Final Design Report, ITER EDA Documentation Series* (Vienna: IAEA)

[278] Litnovsky *et al* 2006 *Proc. 21st Int. Conf. on Fusion Energy 2006 (Chengdu, 2006)* (Vienna: IAEA) CD-ROM file (IT/P1-22)
[279] Voitsenya V. *et al* 2001 *Rev. Sci. Instrum.* **72** 475
[280] Litnovsky A. *et al* 2007 *Fus. Eng. Des.* **82** 123
[281] Lipa M. *et al* 2006 *Fus. Eng Des.* **81** 221
[282] Wienhold P. *et al* 2005 *J. Nucl. Mater.* **337–339** 1116
[283] Litnovsky A. *et al* 2005 Exposures of diagnostic mirrors in DIII-D divertor *9th Meeting of the ITPA Topical Group on Diagnostics (Daejeon, Korea)* (refer to a.litnovsky@fz-juelich.de)
[284] Rudakov D. *et al* 2006 *Rev. Sci. Instrum.* **77** 10F126
[285] Rubel M. *et al* 2006 *Rev. Sci. Instrum.* **77** 063501
[286] Kreter A. *et al* 2006 *Plasma Phys. Control. Fusion* **48** 1401
[287] Droste S. *et al* 2006 *Contrib. Plasma Phys.* **46** 628
[288] De Temmerman G. *et al* 2005 *Proc. 32nd EPS Conf. on Controlled Fusion and Plasma Physics (Tarragona, Spain)* vol 29C (ECA) paper P-1.076 http://epsppd.epfl.ch/Tarragona/pdf/P1_076.pdf
[289] Kochergin M.M. *et al* 2006 *Plasma Dev. Oper.* **14** 171
[290] Vukolov K. *et al* 2001 Experimental study of first mirror degradation under influence of ITER relevant conditions *Advanced Diagnostics for Magnetic and Inertial Fusion* ed P.E. Stott *et al* (New York: Kluwer/Plenum) p 299
[291] Vukolov K.Yu. *et al* 2003 *Proc. 30th EPS Conf. on Controlled Fusion and Plasma Physics (St Petersburg, Russia)* vol 27A (ECA) paper P-2.76 http://epsppd.epfl.ch/StPetersburg/PDF/P2_076.PDF
[292] Vukolov K. *et al* 2004 Deposition of contaminants, in-vessel mirror tests *6th Meeting of the ITPA Topical Group on Diagnostics (Naka, Japan)*
[293] Brown B.W., Gowers C.W., Nielsen P. and Schunke B. 1995 *Rev. Sci. Instrum.* **66** 3077
[294] Narihara K. *et al* 1992 *Rev. Sci. Instrum.* **63** 3527
[295] Federici G. *et al* 2001 *J. Nucl. Mater.* **290–293** 260
[296] Behrisch R *et al* 2003 *J. Nucl. Mater.* **313–316** 388
[297] Bardamid A.F. *et al* 2003 *J. Nucl. Mater.* **313–316** 112
[298] Ye M. Fukuta *et al* 2000 *J. Plasma Fusion Res. Ser.* **3** 265
[299] Yoshida N. *et al* Irradiation effects of low energy helium ions on optical reflectivity of metallic mirror *J. Nucl. Mater* submitted
[300] Yoshida N. *et al* 2006 Effects of He irradiation on optical reflectivity and He damage of in-vessel materials in LHD *11th Meeting of the ITPA Topical Group on Diagnostics (Sendai, Japan)* (refer to yoshida@riam.kyushu-u.ac.jp)
[301] Gorshkov A. *et al* 2005 *Fus. Eng. Des.* **74** 859
[302] Voitsenya V.S. *et al* 2005 *Plasma Devices Oper.* **5** 291
[303] Skinner C.H. *et al* 2005 *J Nucl. Mater.* **337-339** 129
[304] Voitsenya V.S. *et al* 2006 The properties of contaminated films deposited on in-vessel mirrors in Large Helical Device, Tore Supra, TCV and TRIAM-1M *Proc. 33th EPS Conf. (Roma, Italy)* Paper P5.134
[305] Meno M.M. *et al* 2001 *Fusion Eng. Des.* **58–59** 495
[306] Itami K. 2005 Updates in the study of the divertor erosion monitor for ITER *9th ITPA Topical Group Meeting on Diagnostics (Daejeon, Korea)* (refer to Kiyoshi.Itami@iter.org)
[307] Bolshakova I. 2005 Radiation-hard galvanomagnetic devices for ITER magnetic diagnostic *8th ITPA Topical Group Meeting on Diagnostics (Culham, UK)* (refer to inessa@mail.lviv.ua)
[308] Melnikov A. and Eliseev L. 1999 *Rev. Sci. Instrum.* **70** 951
[309] West W.P. *et al* 2006 *Plasma Phys. Control. Fusion* **48** 1661